IEA Bioenergy

IEA Bioenergy Task 32

BIOMASS IMPACTS ON SCR CATALYST PERFORMANCE

Technical Report

October 2005

Larry Baxter
Brigham Young University
Provo, UT, USA

Table of Contents

Chapter 1: Introduction

NO_x, defined as the sum of NO and NO_2, represents a major source of environmental pollution. According to the Environment Protection Agency (EPA), US national annual NO_x emissions in 2001 were estimated at about 4.70 million tons for all boilers subject to Clean Air Act Title IV [1]. Selective catalytic reduction (SCR) of NO_x with NH_3 catalyzed by the vanadia catalyst represents a promising post-combustion technique to reduce NO_x emissions from stationary sources and to meet ever-more stringent emission limits imposed by the EPA. Those limits require existing plants impacted by the NO_x CAIR to reduce NO_x emissions to 0.125 lb/MM Btu (6.45×10^{-6} kg/MJ) on an annual basis [2].

The most common SCR process for coal-fired power plants in the US is the high-dust (HD) configuration, in which the SCR catalyst is upstream of the precipitator or other particle collection devices and processes the full dust loading leaving the boiler. HD configuration may cause serious catalyst deactivation problems, especially for low-rank coals and biomass that contain both high alkali (mainly sodium and potassium) and alkaline earth (mainly calcium) concentrations. Alkali and alkaline earth materials contribute to both fouling and possibly chemical poisoning of catalysts.

In spite of many investigations, mechanisms of vanadia/titania catalysis and deactivation during SCR applications remain uncertain. The consensus opinion indicates that vanadium catalytic activity correlates with acid site concentration on the catalyst surface. However, it is not clear which of the two principal types of acid sites on the catalyst surface, Lewis or Brønsted sites, provides the catalytic properties. Furthermore, much of the laboratory analysis on such catalysts uses SO_2-free gases, representing most situations of natural gas firing, even though SCR catalysts are known to at least partially sulfate and to actively promote SO_2 to SO_3 reactions. As for catalyst deactivation, Siemens [3] and Mitsubishi [4], among others, investigated different deactivation mechanisms. This previous work indicates that minerals from fly ash may cause fouling, masking, and poisoning to the catalysts. The relative importance of these different mechanisms for different coal and biomass fly ash streams is unclear. The present work focuses on poisoning of SCR catalysts by fly ash minerals and the effects of SO_2 interactions with the catalysts. The results of this work will present an improved understanding of poisoning, deactivation, and sulfation that provides new information needed to understand and manage commercial SCR systems.

Chapter 2: Literature Review

The literature review below first briefly summarizes the background of SCR, and then discusses current studies of the effects of SO_2 interaction with catalysts and catalyst deactivation.

I Background of SCR and SCR catalysts

I.A SCR Chemistry

In the SCR process, ammonia, the reductant, is injected into the flue gas to reduce NO_x and form N_2 and water at 300-400 ˚C, near atmospheric pressure, with high selectivity. Two overall stoichiometric reactions of NO_x reduced by NH_3 are [5]:

$$4NH_3 + 4NO + O_2 \rightarrow 4N_2 + 6H_2O \quad (1)$$

$$4NH_3 + 2NO_2 + O2 \rightarrow 3N_2 + 6H_2O \quad (2)$$

More water is produced than molecular nitrogen in each of these reactions. Janssen et al. [6] conducted isotopic labeling experiments with $^{15}NH_3$, NO and $^{18}O_2$ confirming that the two atoms in the product N_2 are from NH_3 and NO separately.

Side reactions also occur and produce the highly undesirable products N_2O and SO_3, as follows.

$$4NH_3 + 4NO + 3O_2 \rightarrow 4N_2O + 6H_2O \quad (3)$$

$$SO_2 + \tfrac{1}{2}O_2 \rightarrow SO_3 \quad (4)$$

Moreover, when the temperature increases above about 350 °C, NH_3 reacts with oxygen rather than NO to form nitrogen and nitrogen oxides [5].

$$2NH_3 + \tfrac{3}{2}O_2 \rightarrow N_2 + 3H_2O \quad (5)$$

$$2NH_3 + 2O_2 \rightarrow N_2O + 3H_2O \quad (6)$$

$$2NH_3 + \tfrac{5}{2}O_2 \rightarrow 2NO + 3H_2O \quad (7)$$

I.B Reaction Kinetics

Reaction kinetics is important in modeling catalyst deactivation. A general global rate expression for the SCR reaction is $r = K_c C_{NO}^{\alpha} C_{NH3}^{\beta} C_{O2}^{\gamma} C_{H2O}^{\delta}$ [5]. The reaction order, α with respect to NO is usually found to be 0.5~1.0, depending on reaction temperature and NH_3/NO ratio. Most authors report that ammonia concentration has no effect on reaction rate, $\beta = 0$, at near stoichiometric conditions, $\beta \approx 0.2$ when with a sub-stoichiometric NH_3/NO ratio, and $\beta = 1$ when the ammonia concentration is low [7]. During industrial vanadia catalysis, where H_2O concentration is generally greater than 5 mole %, water negligibly impacts the kinetics, although there are reports of inhibiting effects of water [7]. Under practical conditions, oxygen is in excess; therefore γ is usually taken as 0. In general, the kinetics of SCR can be

modeled with a simple rate expression $-r = K_C C_{NO}$, where the reaction rate is first order in NO and zero order in ammonia, water, and oxygen.

I.C V_2O_5—WO_3 (MoO_3) /TiO_2 catalyst

Vanadia catalytic activity in reducing NO was discovered in the 1960s, and its high activity when supported on TiO_2 was recognized in the 1970s [8]. The original shapes for vanadia catalysts are pellets or spheres. Current technologies use honeycomb monoliths, plates and coated metal monoliths because of low pressure drop, higher geometric surface area, attrition resistance, and low plugging tendency from fly ash [9]. Unfortunately, vanadia also catalyzes SO_2 oxidation to SO_3, the latter of which is a pollutant, highly corrosive, and can cause catalyst deactivation. TiO_2, however, only weakly and reversibly sulfates under SCR conditions. Also, TiO_2 promotion of vanadia catalytic activity makes titania a preferred support in comparison to other materials such as Al_2O_3 and ZrO_2. Tungsten or molybdenum is commonly added to SCR catalysts in quantities significantly higher than vanadium to increase acidity, which is directly related to the activity, to increase the thermal stability of the catalyst and suppress SO_2 oxidation [8]. In addition, Molybdenum is used to decrease arsenic poisoning from the exhaust gas [8].

Typically, commercial V_2O_5-WO_3/TiO_2 catalysts guarantee NO_x reduction efficiencies close to or over 80%, with an ammonia slip (excess ammonia in the flue gas) of 1-5 ppm and SO_2 conversion to SO_3 lower than 1-2%. Therefore, commercial vanadia catalysts usually contain ~1% vanadia and ~9% tungsten/molybdenum on a titanium (anatase) substrate. The operating temperature for V_2O_5-WO_3/TiO_2 catalysis varies from 550 K to 700 K. In some coal- and biomass-fired power plant applications, deactivation is a major problem for vanadia catalysts.

I.D Surface analysis of vanadia catalysts

Vanadia catalyst surface chemistry provides some critical information to understand SCR reaction and deactivation mechanisms. The current project focuses on further developing this understanding through surface analysis and identification of surface components and structures.

I.D.1. Surface structure of vanadia/titania

Vanadia species exist on catalyst surfaces in three phases: isolated monomeric vanadyl (V=O) species, polymeric vanadate species (polymeric chain of isolated vanadyl species), and crystalline vanadia V_2O_5. Went proposed structures of monomeric and polymeric vanadia species based on Raman and NMR studies as are shown in Figure 1 [10].

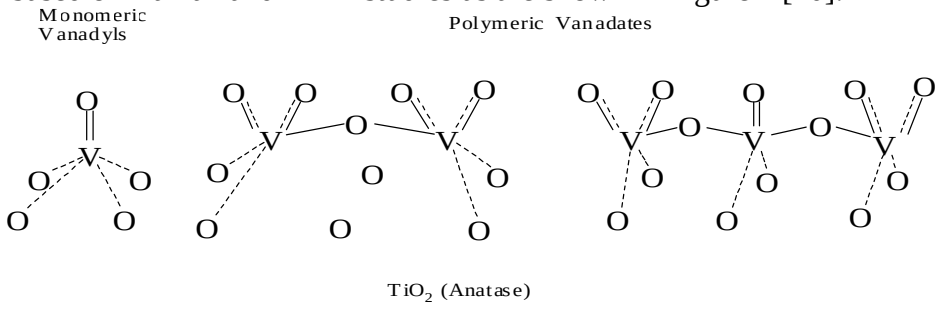

Figure 1 Schematic depicting structure of the monomeric vanadyl and polymeric vanadate species on anatase TiO_2 [10]

Under monolayer coverage (the maximum amount of amorphous or two-dimensional vanadia in contact with the oxide support [11]), both monomeric vanadyl and polymeric vanadate species appear on the catalyst surface, with monomeric vanadyl species dominant on lightly loaded (e.g. 1.3%) catalyst surfaces [12, 13]. Monomeric vanadyl species could transform to polymeric vanadate species with increasing vanadia content (up to 6%) by breaking M-O-V bonds to form V-O-V bonds [14]. Crystalline vanadia species form from polymeric vanadate species only when the loading exceeds the monolayer capacity (about 6%) [10, 14].

I.D.2. Active sites identification

a. Active sites investigation based on structures

Polyvanadate species reportedly have higher activity than monomeric vanadyl species [13, 15, 16]. The group of V-O-support may also provide the active center [17]. Crystalline V_2O_5 oxidizes NH_3 at high temperatures [18, 19]. A dual-site mechanism involving a surface vanadia redox site and an adjacent surface non-reducible metal oxide site has been suggested as well [7, 12].

b. Active sites investigation based acid sites

Both Lewis and Brønsted acid sites exist on vanadia/titania catalyst surfaces. The V-OH bond appears to be directly related to Brønsted acid sites [12], while the V=O bond forms a Lewis acid site that can convert to V-OH by water adsorption [5]. Therefore monomeric vanadyl and polymeric vanadate species (Figure 1) could provide both Lewis and Brønsted acid sites. No acidity assignment for the V-O-site appears in the literature thus far. Both Brønsted acid sites [12, 20] and Lewis acid sites [13, 15, 21] reportedly form active centers for SCR catalysis. Convincing evidence supports each argument as will be discussed later in the reaction mechanism section.

There is no general consensus regarding the identity of the active sites on vanadium-based SCR catalysts from the view of either vanadia surface structures or the acid sites. The NH_3, NO, and NH_3/NO surface adsorption and spectroscopy investigations planned as part of this investigation may resolve some of the confusion on this issue. Related investigations recorded in the literature are reviewed here.

I.D.3. NH3 adsorption

NH_3, the reductant of NO_x in the SCR reaction, demonstrates strong adsorption - desorption behaviors on both titania and vanadia catalysts observed by Fourier-transformed infrared (FTIR) spectroscopy, laser Raman spectroscopy (LRS), temperature programmed desorption (TPD), and transient response studies.

a. FTIR and Raman study summaries

The following lists generally accepted results from FTIR spectroscopy and LRS appear in the literature:

1. Ammonia adsorbs on both support titania and vanadia/titania catalysts at room temperature, with major associated adsorption bands on Brønsted acid sites at 1430 and 1670 cm^{-1} and on Lewis acid sites at 1220 and 1605 cm^{-1} [10, 12, 20, 22].

2. Pure titania possesses only Lewis acid sites [23, 24].
3. Vanadia/titania catalysts provide both Lewis and Brønsted acid sites, vanadia species introduce Brønsted acid sites on the catalyst surface [12].
4. Sulfate species enhance Lewis acid sites on pure titania, introduce Brønsted acid sites onto the sulfated titania surface [23], and may enhance the number and strength of acid sites on vanadia catalyst surfaces [25].
5. Ammonia adsorbs on Lewis acid sites as coordinated ammonia and on Brønsted acid sites as protonated ammonia. NH_3 absorption is stronger on Lewis acid sites than on Brønsted acid sites [12].
6. NH_3 desorbs from SCR surfaces with increasing temperature and is practically removed above 300 ˚C [26].
7. Poisons (Li_2O, Na_2O, K_2O) interact primarily with Brønsted acid sties [20].

The following issues remain controversial or have not been thoroughly investigated:

1. The extent to which ammonia adsorbs on the SCR surface at reaction temperature, and
2. Whether sulfation of the surface increases the number of acid sites or strengthens the acidity of existing sites on SCR catalysts.

b. TPD study summaries

The following lists generally accepted results from TPD literature analyses:

1. Ammonia adsorbs on both titania and vanadia/titania catalyst surfaces [10, 16, 27, 28], consistent with the spectroscopic results.
2. Ammonia adsorbs stronger on Lewis acid sites than on Brønsted acid sites [10, 27, 28], again consistent with the spectroscopic results.
3. Ammonia adsorption energy is about 18~26 kcal/mol [27].
4. Multiple ammonia adsorption species exist on vanadia/titania catalyst surfaces but are not distinguishable from TPD profiles.
5. Poisons occupy strong acid sites on vanadia catalysts [25, 29]. This disagrees with spectroscopy studies since FITR spectroscopy analysis indicates poisons occupy Brønsted acid sites, which are weak acid sites relative to Lewis acid sites.

The following issues remain controversial or have not been thoroughly investigated:

1. Whether different peak temperatures observed in ammonia TPD profiles arise from different vanadia catalyst sites or are artifacts of preparation methods,
2. The effects of sulfate species on ammonia TPD profiles on titania and vanadia catalysts, and
3. The correlation between total acidity and SCR activity.

I.D.4. NO adsorption

The following are generally accepted results from FTIR spectroscopy analyses of NO adsorption:

1. NO adsorption occurs on both non-sulfated [18, 23, 30] and sulfated titania [23], and on reduced vanadia catalyst at room temperature [26, 31].

2. NO adsorption does not occur on fully oxidized or NH_3 pre-adsorbed vanadia catalyst [26, 31].
3. Vanadium ions with a lower oxidation state and Ti-OH sites represent possible adsorption centers for NO [26, 31].
4. NO adsorption reversibility increases on sulfated TiO_2 compared to bare TiO_2 [23].

The Following issues have not been investigated:

1. The effect of alkali and alkali earth metals on NO adsorption on either titania or vanadia catalyst.
2. The effect of sulfate on NO adsorption on vanadia catalysts.
3. NO TPD study on titania and vanadia catalysts.

In summary, ammonia adsorption and NO adsorption are well studied on sulfur- and poison-free titania and vanadia catalysts, whereas investigations regarding the effects of sulfate and poisons on ammonia and NO adsorption are inconclusive.

I.D.5. NH3 and NO coadsorption

Several investigators document the behavior of NH_3 and NO coadsorption, which can elucidate the active center, structures of the active site, and the intermediate species.

The following generally accepted conclusions arise primarily from different responses of NO and NH_3 during coadsorption studies.

a. An Eley-Rideal mechanism reasonably represents the SCR reaction involving a strongly adsorbed NH_3 and a gas-phase or weakly adsorbed NO molecule [15].
b. Lietti et al. observed that more coordinated adsorbed ammonia is consumed than protonated NH^{4+} during NO and NH_3 coadsorption [15].
c. Centeno et al. found V=O has a redox property, and suggested a redox mechanism with V=O, a Lewis acid sites, as the active center for the SCR reaction [21].
d. Topsoe et al observed both V-OH and V=O play an important role in the SCR catalytic cycle, and Brønsted acid site concentration directly correlates to NO conversion for a range of vanadia concentrations (0-6 wt %) [12]. However, Topsoe's approach only measured protonated ammonia bands, not the coordinately-adsorbed ammonia bands which occur at 1300 cm^{-1} as reported by Lietti et al [15].

Thus, both Lewis and Brønsted acid sites have been reported to be the active center based on convincing evidence from various IR investigations. The disagreement upon the properties of active sites may arise from different sample preparation methods and materials applied, as well as different IR regions investigated. The effects of surface sulfate and alkali and alkali earth metals on NH_3 and NO coadsorption behavior on titania and vanadia/titania acid site concentrations have not been reported.

I.E Proposed reaction mechanism

Based on the above investigations, different mechanisms appear in the literature with some points of agreement: the active sites are acidic, a redox reaction involves in the mechanism,

Eley-Rideal type reaction mechanisms appear important with NH_3 as the adsorbed species and NO as the gas-phase or weakly adsorbed species, and V sites provide the active centers.

The disagreements are: the nature of the acid sites: Lewis or Brønsted acids, and the number of vanadia atoms involved: single or multiple atoms with reaction either on the vanadia or at the interface/terminal vanadia atom. Busca et al. provided a review of these suggested active sites and intermediates, as shown in Table 1 [5].

Table 1 Proposed reactant species, intermediates and active sites in different mechanism from Busca [5]

Reactant species		Intermediate	Catalyst	Supposed active site	Reference
From NH_3	From NO				
NH_4^+	O-N-O |		V_2O_5		Takagi et al.
NH_4^+	NO gas	H-bonded complex	V_2O_5	O OH || | -O-V-O-V-O	Inomata et al.
O-NH_2 | V	NO gas		V_2O_5/supp	O O || || -O-V-O-V-O	Janssen et al.
NH_4^+	NO gas		V_2O_5	OH | V + V-O-V	Gasior et al.
NH_2 | V	NO gas	NH_2NO | V	V_2O_5/TiO_2	O || V	Ramis et al.
NH_3ads NH_2	N_2Oads adsorbed NO		V_2O_5/supp V_2O_5/TiO_2	Lewis sites	Maragonzis et al. Went et al.
O^- H_3N^+ HO | | V V	NO gas	O^-H_3N-N=O HO | | V V	V_2O_5/TiO_2	O HO || | -V- -V-	Topsøe et al. 1993
NH_4^+	O-NO_2 | V^{4+}	NH_4NO_2	V_2O_5/TiO_2	O || V^{5+}	Kantcheva et al.
NH_4^+	NO_3^-		V_2O_5/ZrO_2		Indovina et al.

The $DeNO_x$ catalytic cycle suggested by Topsøe based on *in situ* FTIR combined with on-line mass spectrometry investigations, as shown in Figure 2, is among the most accepted pathways for SCR catalysis [32]. In this mechanism, NH_3 first adsorbs on V-OH, the Brønsted acid site, and then reduces gas phase NO with the V=O site involved in the redox cycle.

In another mechanism scheme proposed by Ramis et al., shown in Figure 3, Lewis acid sites act as the active center [5]. Ammonia first adsorbs on V=O sites by interacting with V instead of O in the V=O bond. The adsorbed ammonia species then reacts with gas-phase NO on V=O sites and produces N_2 and H_2O. Gas-phase oxygen then oxidizes the V=O site, preparing the site for another cycle of SCR reaction.

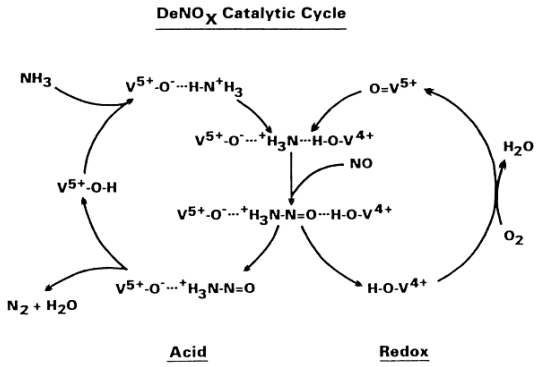

Figure 2 **Scheme illustrating the cycle of the SCR reaction over vanadia/titania catalyst by Topsoe et al. [32].**

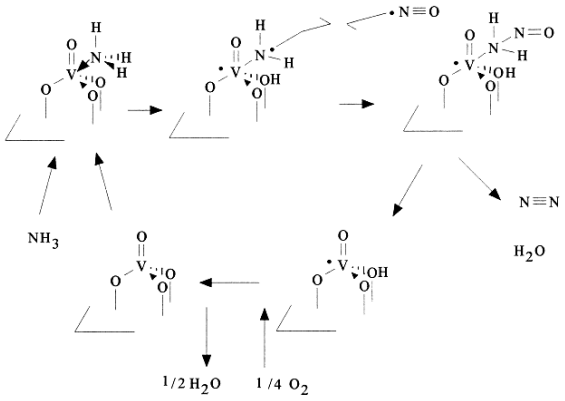

Figure 3 **Mechanism of the NO-NH_3 reaction on supported vanadium oxide catalyst proposed by Ramis et al. [15].**

Both mechanisms involve similar steps during the catalytic cycle. The difference is that Topsøe's mechanism involves two active sites, with Brønsted acid sites as the active center, while Ramis's mechanism only involves a single active site (V=O), which is a Lewis acid. Neither mechanism clarifies the role of the V-O-support during the SCR reaction, which has been suggested as the active center by Wachs [7]. Therefore, there is no general agreement about the identity of the active center either from a structural perspective – whether V=O, V-OH, or V-O-support or some combination represents the active center – or from the acidity perspective – whether Lewis or Brønsted acid sites provide the active center.

Furthermore, most surface investigations involved non-sulfated surfaces. At least some of the surface sites sulfate under commercial SCR catalysis conditions with SO_2 in the gas phase, which would include essentially all coal-related applications. Such sulfation has a high likelihood of impacting surface reactions, activity, and poisoning.

II Interaction with sulfur dioxide

Sulfur dioxide appears in the effluent from the power plant and plays a dramatic role in the SCR process. It can increase SCR catalyst activity by increasing the number and strength of Brønsted acid sites [25]. On the other hand, sulfur trioxide, formed during oxidation of SO_2 catalyzed by the same vanadia catalysts, reacts with ammonia to form ammonia sulfate and ammonia bisulfate at temperatures lower than typical SCR reactions. Moreover, SO_2 can

react with free CaO or alkali earth compounds in the flue gas to produce $CaSO_4$ and alkali earth metal sulfates. These products introduce potentially serious deactivation, corrosion, and related problems for both the catalyst and other equipment.

Yang et al. indicate that the sulfate species on titania is probably SO_4^{-2}, since the observed peak in XPS spectra is 168.5 eV, which is typical of S^{+6} [33]. This agrees with the analysis of Soo Tae Choo et al.[19]. TPD analyses show that sulfate species start to decompose thermally at about 800 K and are completely removed around 1073 K on both titania and vanadia catalysts [15, 19]. In addition, R.T. Yang et al. propose two types of sulfate on the titania surface: bridge bindenlate and chelating bidentate SO_4^{-2}, with bridged bidentate as the most prevalent form [23].

However, there is no general agreement about the site where sulfates form on vanadia catalysts. Orsenigo compared catalyst conditioning between NO_x reduction and SO_2 oxidation and suggested that sulfation occurs first at vanadia sites, then on titania and tungsten sites [34]. But no further verification data were provided. Choo et al. pointed out from FTIR spectroscopy analysis that both vanadia and sulfate species compete for hydroxyl group sites on the catalyst surface [19]. FTIR spectra from Dunn et al. [35] and Amiridis et al. [24] show that the concentration of surface sulfate species (centered at 1373 cm^{-1}) decreases with increasing vanadia coverage on the catalyst supported on TiO_2, ZrO_2, or Al_2O_3.

To date, only a few investigations of sulfation have been conducted, and no *in situ* studies appear in the literature. The sulfation mechanism on the vanadia/titania surface is still uncertain. In addition, the effects of surface sulfates on catalyst BET surface area, NO adsorption-desorption, NH_3 TPD behavior, and the extent that sulfates influence vanadia catalytic activity have not been reported. The effect of sulfate on catalyst deactivation by alkali and alkali earth metals is still under debate. Conditions involving sulfur dioxide are common in industrial practice, including essentially all systems that involve coal combustion. Investigations of the sulfate effect on vanadia catalyst performance will provide additional critical information on the SCR reaction and deactivation mechanism.

III Deactivation of Vanadia catalysts

Deactivation is a major problem for vanadia catalysts in SCR applications. For example, the typical design lifetime of vanadia catalyst for coal-fired power plants is 3-5 years [36]. Existing anecdotal evidence indicates that catalysts may deactivate 3-4 times faster in low-rank coal-fired and biomass-coal co-fired boilers [25]. Poisoning, fouling, and thermal sintering are common categories of catalyst deactivation, and different mechanisms dominate in different SCR applications. For instance, sintering and rutilization (rutile formation) of titania after long-term operation is one of the major deactivation mechanisms during natural gas firing, while poisoning of the catalyst active sites by alkali metals is significant in oil firing [4]. In the case of coal firing and bio-fuel applications, plugging, fouling and poisoning are probable deactivation mechanisms. Table 2 summarizes different major deactivation mechanisms for different fuels. Table 3 identifies some of the major differences between commercially important coals and biomass in the US. The great majority of SCR experience available is from bituminous coals. These fuels pose the fewest deactivation risks to vanadium-based catalysts. Figure 4 illustrates several general mechanisms of poisoning, fouling, and plugging.

Table 2 Deactivation mechanism related to fuel types

Fuel type	Main deactivation reason	Deactivation substance
Coal	Fouling	Sub-micron ash particle
Biomass	Poisoning	Soluble Alkali(K) compounds
Oil	Poisoning	Soluble Alkali (K, Na) compounds
Gas	Sintering	
Waste incineration	Poisoning	Lead compounds

Table 3 Difference between different coals in US

Constituent	Bituminous coal	Sub-bituminous coal	PRB coal	Biomass
Sulfur	High	Intermediate	Low	Low
Arsenic	Intermediate	Intermediate	Low	Varies
Active Alkali Compounds	Low	High, especially Na	High Na	High, especially K.
Active Alkaline Earth Compounds	Low	High, especially Ca	Very high Ca	Intermediate, generally Ca

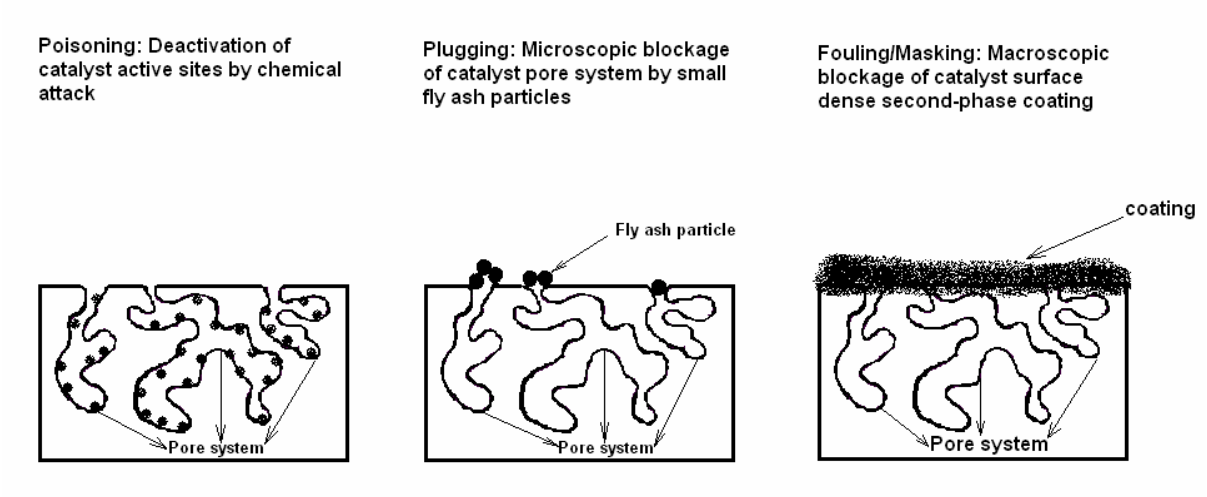

Figure 4 Overview of general mechanism which can contribute to SCR catalyst deactivation

A. Poisoning can be caused by arsenic, alkali-metal-containing compounds, alkaline-earth-containing compounds, lead, and hydrochloric acid (HCl).

1. Arsenic in the coal may vaporize into arsenic oxides, generally As (III), which nucleates to submicron particles that penetrate the catalyst fine structure and react with vanadia to form stable vanadia-arsenate compounds. Thus, poisoning by arsenic is irreversible. Arsenic concentration in the flue gas is usually low. It is most significant in wet-bottom (high-temperature) boilers where arsenic is built up through flue-gas recirculation [37].
2. Water soluble alkali- and alkaline-earth-containing compounds, especially K and Na, react directly with active sites which are acid sites, resulting in acidity neutralization and subsequent deactivation. This is a major deactivation problem in oil-fired applications [4].

3. Lead poisoning is significant in waste incineration application [38-40]. Lead is preferentially deposited on the fly ash by either volatilization or entrainment in three forms: elemental lead, lead oxide, and lead chloride [39, 41]. The poisoning of catalyst is more likely due to chemisorption of lead onto the active sites instead of pore blocking because of little change of catalyst BET surface area and pore volume before and after lead addition [39].
4. HCl deactivates vanadia catalyst by either forming NH_4Cl, which consumes ammonia and blocks the active surface area, or reacting with vanadate to form VCl_4 and VCl_2 [37].

As to deactivation caused by alkali-containing compounds, many complications exist: (1) physical form: alkali-containing compounds exit as alkali salts in fly ash, or as aerosol (particle, liquid or gas), (2) location: IR results show alkali metals occupy Brønsted acid sites (weaker acid sites), while TPD results show alkali metals first occupy strong acid sites (Lewis acid sites). Reports indicate that Lewis acid sites are stronger than Brønsted acid sites on vanadia catalyst surface [10, 12, 27, 28]. (3) Mechanism: Alkali metal compounds deactivate vanadia catalysts by poisoning or by pore blockage. (4) Transformations: Alkali metal oxides may reduce catalyst BET surface area, pore volume, and average pore diameter. One general agreement is that poisoning by alkali metals does not change the underlying reaction mechanism so much as its rate. *In situ* and post fly ash property characterization is critical to resolve these issues.

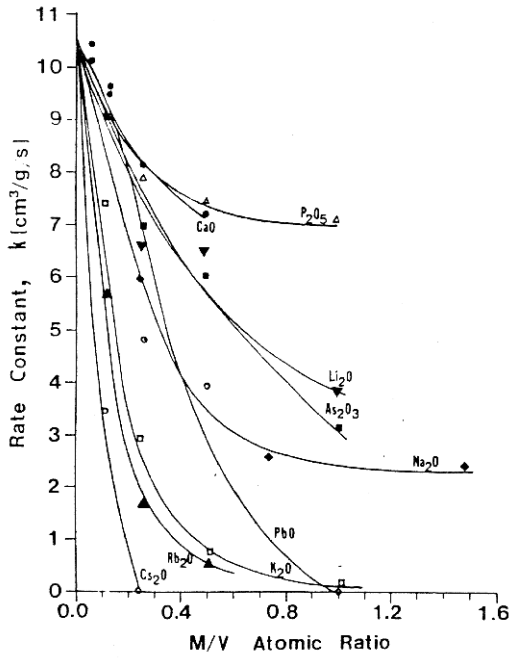

Figure 5 Activities of 5% V2O5/TiO2 doped with different amount of metal oxide poisons, M=metal, 300 C, O_2= 2%, NO=NH_3=1000 ppm, N_2= balance, GHSV=15000hr^{-1} [20]

Yang did a thorough investigation on the poisoning mechanism of alkali- and alkaline-earth-containing oxides, and found that the deactivation directly relates to the basicity of metals, as shown in Figure 5. The strength of the poison oxide is as follows: Cs_2O > Rb_2O > K_2O > PbO > Na_2O > LiO > CaO > P_2O_5

A great deal of the evidence for chemical poisoning of SCR catalysts is either anecdotal or contained within company reports that commonly are proprietary. The quality of this information varies, resulting in a weak case for chemical deactivation despite relatively widespread suspicion that poisoning is a significant deactivation mechanism. The proposed investigation intends to provide scientifically credible information on poisoning from systems of commercial interest and will make a significant contribution in this regard.

B. Fouling and masking may prevent NO_x and ammonia from reaching active catalyst sites and may deactivate catalysts. Free CaO in the flue gas reacts with SO_3 adsorbed on the catalyst surface to form $CaSO_4$, potentially masking the catalyst surface. This mechanism is potentially related to the chemical deactivation mechanism in that $CaSO_4$ is basic and could neutralize the acidic catalyst sites in addition to fouling the surface. This problem is especially significant in boilers burning Powder River Basin (PRB) coals, since PRB coals have almost 3 times more free CaO than US bituminous coals [3]. In addition, fly ash accumulation on surfaces (fouling) even in the absence of chemical reactions may present physical barriers to gas reaction with the catalyst.
C. Plugging caused by ammonia salt and fine fly ash particles represents a third potential mechanism. Ammonia salt refers to ammonium sulfate and bisulfate, which are small (< 10μm [42]) sticky particles that cause major plugging problems in the air heater and on the catalyst surface. Small fly ash particles lodge in the large pores on the catalyst surface, blocking the entrance to the pores. Possibly the single most significant cause of poor SCR catalyst performance is plugging of monolith channels by rogue large particles called popcorn ash. This completely mechanical mechanism is difficult to distinguish from surface fouling or chemical deactivation based on commonly available field measurements. However, channel plugging leads to larger increases in pressure drop than to any of the other mechanisms. While this mechanism substantially affects SCR performance, its prevention is largely a matter of separating large fly ash particles from the gases prior to their entrance into the SCR reactor and there is little chemical- or reaction-related research needed for this activity.
D. There are also deactivation mechanisms involving catalyst erosion by abrasive fly ash. The catalyst is sensitive to the flue gas constituents, which are determined by the fuel properties (main and trace elements) and method of firing. When system design, catalyst durability, and catalyst edge hardening are proper, erosion is not a significant deactivation factor [4].

Clogging by ammonia sulfate and poisoning by arsenic may be the main deactivation mechanisms for bituminous coals. Since strict SO_2 emission limits have led to an increase in the number of US utilities burning sub-bituminous coals, where poisoning by alkali metals and masking by calcium sulfate may be more important for sub-bituminous (PRB) coals and biomass. Thus, understanding poisoning mechanisms by alkali- and alkaline-earth containing compounds could become a critical issue in vanadia/titania catalysts for SCR applications in coal and biomass combustion.

IV Summary of Literature Review

Surface vanadia species are the active sites with several suggested structures, while is no general agreement appears on the active structures and the role of acidity. The SCR reaction is a redox reaction following an Eley-Rideal mechanism that involves reaction of adsorbed ammonia and gas phase NO. The presence of sulfur changes the chemical composition of

both the active and inactive surface sites and measurably increases specific activity. However, no convincing evidence indicates the site sulfur interacts with or the mechanism of activity enhancement by sulfur species. Alkali- and alkaline-earth-containing compounds can potentially deactivate SCR catalysts by fouling and chemical poisoning. Current available studies of vanadia catalyst surface chemistry and reaction kinetics variation caused by addition of alkali and alkaline earth metals do not provide definitive data, especially in the areas of NH_3 and NO adsorption/desorption, SO_2 impact on catalyst activity and mechanisms, and poisoning impact in SO_2 laden environments on catalyst mechanisms. There is a need to develop a better understanding of SCR reaction mechanisms and rates relevant to coal and biomass combustion conditions, with a particular emphasis on the role of sulfur, alkali metals, and alkaline earth metals on catalyst activity and deactivation, and provide contributions to deactivation modeling.

The current boundaries of established knowledge with respect to SCR application in coal-based systems are illustrated in Figure 6 in several areas of relevance to this proposed body of work. The ordinate represents increasing knowledge while the abscissa represents various aspects of SCR reactions, with those most closely related arranged next to each other. The bottom row represents the status of current studies, and the envelope illustrates how this proposed work contributes to the ultimate goal of developing enough information about SCR processes to make fundamentally based contributions in complex practical applications such as coal combustion systems.

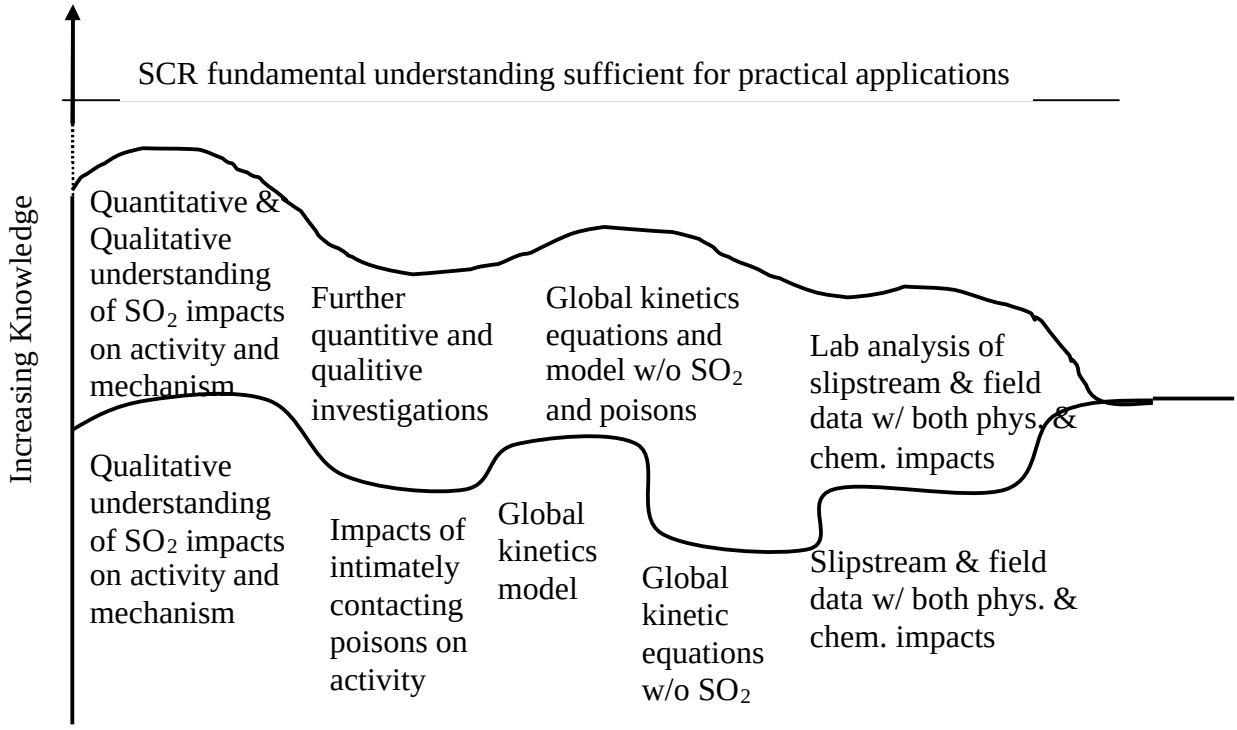

Figure 6 Overview of SCR research field and Xiaoyu's contribution (within the envelope)

Chapter 3: Objective

I SCR Catalyst Performance under Biomass Co-Firing

The cost and effectiveness of NOx control strategies for coal-fired boilers have received considerable attention over the last two decades and a number of successful approaches have been applied. Utilities weigh a number of issues when determining the best strategy for their specific units. Comparisons routinely include cost and the amount of NOx reduction, with selective catalytic reduction (SCR) often used as a standard for comparison. However, to make this comparison meaningful, the total cost of combustion modifications must be considered (carbon-in ash levels, waterwall wastage, etc.). Industry is developing experience evaluating many of these costs and it is one of the tasks of this program to better understand two such areas – waterwall corrosion and soot formation. For SCR, the "real" cost for coal-fired boilers using US coals and coal/biomass blends is uncertain.

The economics of SCR are closely tied to catalyst costs, including initial investment cost and the cost of regeneration or replacement. The need for data and models that enable assessment of such costs is emphasized.

The purpose of this task is to develop databases and a model for assessing catalyst deactivation and its effects on SCR catalyst life and cost.

Within this task there are for principal sub-tasks:

1. technology assessment and fundamental analysis of chemical poisoning of SCR catalysts by alkali and alkaline earth materials;
2. evaluation of commercial catalysts in a continuous flow system that simulates commercial operation;
3. evaluating the effectiveness of catalyst regeneration; and
4. develop a model of deactivation of SCR catalysts suitable for use in a CFD code.

Items 1 and 3 are principally performed at Brigham Young University (BYU) under the direction of Profs. Larry Baxter, Calvin Bartholomew, and William Hecker. The work effort for items 2 and 4 is being performed by REI, with assistance from the University of Utah and BYU. Progress during the last performance period on this task is described below.

II Technology Assessment/Fundamental Analysis

The objectives of this subtask are (1) to supplement the SCR-catalyst-deactivation literature with results from new laboratory-scale, experimental investigations conducted under well-controlled and commercially relevant conditions in the presence of SO2, and (2) to provide a laboratory-based catalyst test reactor useful for characterization and analysis of SCR deactivation suitable for samples from commercial facilities, slipstream reactors, and laboratory experiments. Two catalysts flow reactors and several additional characterization systems provide the analytical tools required to achieve these objectives. The flow reactors include the in situ surface spectroscopy reactor (ISSR) and the catalyst characterization system (CCS), both of which are described in more detail in previous reports. Additional

characterization systems include a temperature-programmable surface area and pore size distribution analyzer, scanning electron microscopes and microprobes.

The sample test matrix includes two classes of catalysts: commercial, vendor-supplied SCR catalysts and research catalysts synthesized at BYU. The commercial catalysts provide immediate relevance to practical application while the research catalysts provide unfettered ability to publish details of catalyst properties. The five commercial catalysts selected for use come from most commercially significant catalyst manufacturers (Cormetech, Haldor-Topsoe, Hitachi, and Siemens) and provide a wide range of catalyst designs and compositions. The in-house catalysts will be subjected to detailed analysis, activity testing, and characterization, thus providing a comprehensive test and analysis platform from which to determine rates and mechanisms of catalyst deactivation. The result of this task will be a mathematical model capable of describing rates and mechanisms of deactivation.

Within the last performance period, in situ, spectroscopic experiments partially reported last quarter were completed. The most significant finding of these investigations is a consistent indication that vanadium does not sulfate during SCR activity in the presence of gas-phase SO2 while both the substrate (anatase) and modifiers (molybdenum) do. In addition, mass-spectroscopy-based analyses of product gases from this reactor system help elucidate fundamental kinetics and deactivation mechanisms.

Chapter 4: Experimental Design

This investigation requires substantial mechanistic and kinetic experimentation. The intention is to supplement the existing literature by investigation of sulfur-laden gases using the equipment and techniques describe below. The effort to understand vanadia catalyst reaction and deactivation mechanisms in typical coal and coal-biomass co-combustion is approached in three directions:

1. Catalyst activity characterization system measures the NO reduction activity of both home-made and commercial vanadia catalysts.
2. *In situ* FTIR surface spectroscopic studies of vanadia catalysts to provide mechanistic information, such as definite indications of surface-active species, and if possible surface-active sites coverage (ratio of the number of active sites to the total number of sites on the catalyst surface),
3. MS reactivity investigation to provide global kinetic parameters, such as activity and activation energy of NO_x reduction of fresh, sulfated, and poisoned catalysts,
4. Other surface characterization tests to provide information such as the effects of sulfate and poisons on BET surface area, pore-size distribution, geometry changes observed from SEM (scanning electron microscopy), and surface elemental compositions by XPS (x-ray photon spectroscopy), and standard (bulk) analyses that supplement the reactor data. All of the above experiments should provide sufficient data to develop a deactivation sub-model for incorporation into a CFD model.

Samples: Two types of catalyst samples will be investigated and are summarized below:

- Commercial catalysts installed in a slip-stream reactor with various exposure times, as a partial accomplishment of the contract with sponsors. Detailed sample information is listed the results section (CCS).

- Laboratory-prepared catalysts

    1. One fresh sample of each of four vanadia-based catalysts (4 samples total) with total vanadia concentrations of 0, 1, 2, and 5 % (by mass).
    2. One deliberately contaminated sample of each of three vanadia-based catalysts (3 samples total) using each of three contaminants (K, Na, and Ca, details is in session B). All deliberately contaminated samples will be based on 1% vanadia catalyst preparations.
    3. One sample of each of the fresh and deliberately contaminated samples (7 additional samples in total) after complete sulfation of surface.

Laboratory-prepared catalysts use an incipient wetness impregnation method for preparation. The procedure results in intimate association of catalyst and contaminant. All contaminants dissolve in solution in nitrate form but eventually form oxides. Two categories of catalysts (field-exposed and laboratory-prepared) are chosen for comparison, especially in cases of contaminated catalysts, to indicate differences between field-exposed and laboratory-prepared catalysts with similar contaminants since there are no reports dealing with these differences.

Details of the experimental equipment and procedure appear in the task statements below.

I Vanadia catalyst in situ surface chemistry investigation

The purpose of this task is to gain knowledge of surface chemistry of vanadia catalysts. Intentions include identification of acid sites, interaction pattern between reactant gases (NH_3, NO, and SO_2) and surface sites before and after contamination, and the extent of sulfation on poisoned and fresh SCR catalyst surfaces. These investigations will provide indicators of how poisons impact vanadia catalyst surface chemistry.

The experimental apparatus includes the ISSR (*in situ* surface spectroscopy reactor system) and the TPD (temperature-programmed desorption) systems. ISSR provides *in situ* transmission FTIR spectra of adsorbed SO_2, NH_3, and NO_x, among other species, and the TPD provides quantitative measures of behavior with lower detection limits, but with no direct surface-adsorption information.

This task includes the following specific activities.

A. NH_3 transient adsorption and NO transient adsorption (each 1000 ppm in helium) at temperatures from 25-380 ˚C are conducted by monitoring *in situ* FTIR spectra of adsorbed species on laboratory-prepared catalyst surfaces exposed to a variety of laboratory and field conditions. This study should provide qualitative and relative quantitative critical parameters, including Brønsted and Lewis acid site densities, their relative acidities, and changes of acidities induced by surface sulfation and poisoning. Another intent is to acquire NH_3 adsorption site coverage on the catalyst surface by correlating the change of NH_3 adsorption IR peak areas with the MS signal of desorbed NH_3.
B. Interaction among surface species. The objective of this activity is to identify the surface active sites (surface titania or vanadia or sulfated species) for each reactant gas (NH_3, NO, SO_2) and interacting surface species (vanadia and sulfate species) to help elucidate SCR reaction mechanisms and specifically the impact of sulfur on such mechanisms. Tests will be based on laboratory-prepared catalysts. Hypotheses are already established and will be tested with different experiments as shown in follow schemes:

   1. NO adsorption site identification

   Possibilities: A: NO adsorbs on titania sites (A)

   B: NO adsorbs on vanadia sites. We probably will not be able to identify which vanadia sites (1, 2, 3, or 4 as labeled on the drawing) NO adsorbs on if NO does adsorb on vanadia sites.

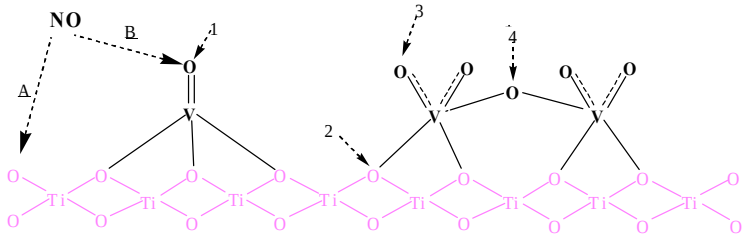

Expected experimental outcomes:

Hypothesis	Observations
A	NO adsorption intensity↓ vs. V% ↑
B	NO adsorption intensity ↑ vs. V% ↑

2. Sulfate adsorption site identification:

Possibilities: A: Sulfate interacts with titania surface

B: Sulfate interacts with vanadia surface

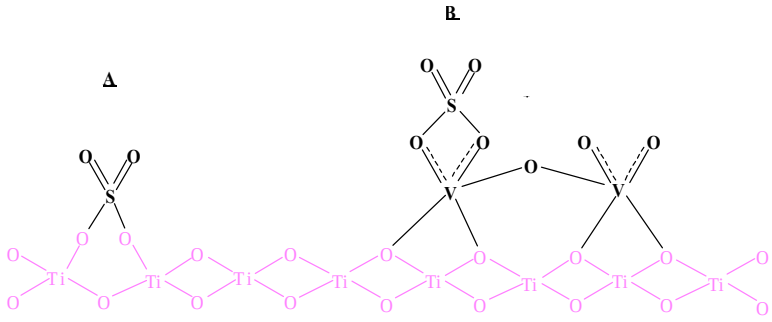

Expected experimental outcomes:

Hypothesis	Observation
A	Sulfate IR adsorption intensity or Sulfur % ↓ vs. V% ↑
B	Sulfate IR adsorption intensity or Sulfur % ↑ vs. V% ↑

3. NH_3 adsorption sites identification:

Possibilities A: NH_3 adsorbs on titania site

B: NH_3 adsorbs on vanadia site

C: NH_3 adsorbs on sulfate site

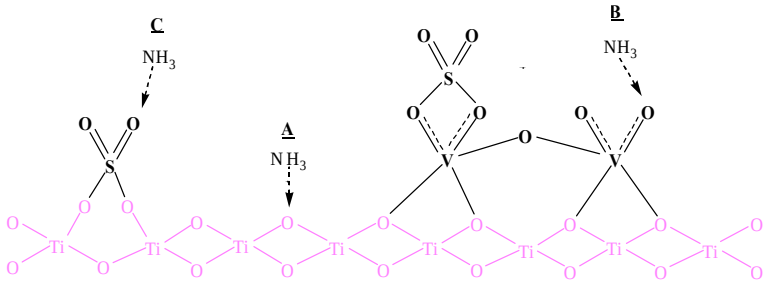

Expected experimental outcome

Hypothesis	Observation
A	NH_3 IR adsorption peak on pure TiO_2
B	NH_3 IR adsorption intensity ↑ vs. V% ↑
C	NH_3 IR adsorption intensity ↑ vs. S % ↑

Identification of active adsorption sites for NO, NH_3, and SO_2 provides additional information to SCR reaction and poisoning mechanism.

C. Co-adsorption tests involving NH_3 and NO_x help elucidate mechanisms and rates of both reaction and deactivation by monitoring variation of NH_3 and NO adsorption IR peak during co-adsorption on laboratory-prepared catalysts, where temperature is increased from 25-380˚C. From these co-adsorption tests we hope to determine which are the active sites for adsorption and the effect of surface sulfates and poisons on active sites coverage and reactivity.
D. Surface sulfation represents a critical issue in this investigation since the practical applications of low-rank coal combustion and coal-biomass co-firing involve SO_2-laden gases. As discussed earlier, literature opinion regarding the impacts of SO_2 on SCR surface sulfation differ and the majority of the literature comes to conclusions different from those indicated by our preliminary results. This test used *in situ* FTIR spectra obtained during 24-hour sulfation of each fresh laboratory-prepared catalyst. IR spectra of fresh, sulfated vanadia catalyst, and vanadyl sulfate indicate with which site sulfate interacts and where it forms. Subsequent XPS surface chemistry analyses of both fresh and sulfated vanadia catalysts should provide evidence for identifying sulfate species oxidation state and concentration. Also, the extent to which each field-exposed catalyst is sulfated will be determined.

II NOx reduction kinetic investigation

NO reduction kinetic investigation was conducted in two characterization systems, the catalyst characterization system CCS and ISSR.

II.A CCS Overview

The catalyst characterization system (CCS) provides capabilities for long-term catalyst exposure tests required for ascertaining deactivation rates and mechanisms and a

characterization facility for samples from the slipstream reactor to determine changes in reactivity and responses to well-controlled environments. This system simulates industrial flows by providing a test gas with the following nominal composition: NO, 0.1%; NH_3, 0.1%; SO_2, 0.1%; O_2, 2%; H_2O, 10%; and He, 87.7%. Both custom and commercial catalysts are tested as fresh samples and after a variety of laboratory and field exposures under steady conditions.

II.B ISSR Overview

The purpose of the FTIR-ISSR is to provide definitive indication of surface-active species through *in situ* monitoring of infrared spectra from catalytic surfaces exposed to a variety of laboratory and field conditions. The ISSR provides *in situ* transmission FTIR spectra of SO_2, NH_3, and NO_x, among other species. Absorption and desorption behaviors of these and other species are monitored. Quantitative indications of critical parameters, including Brønsted and Lewis acidities on fresh and exposed catalysts, are included. Indications of coadsorption of NH_3 and NO_x help elucidate mechanisms and rates of both reactions and deactivation.

Mass-spectrometry-based kinetics (activity in steady state) investigations compare reactivity of the various SCR catalysts under overall nominal gas-phase conditions of: 0.1% NH_3, 0.1% NO, 5% O_2, and helium. All reactivity will be based on relatively simple reaction mechanisms, such as mechanisms assumed to be first order in NO and zero order in ammonia, water, oxygen, and all other reactants. The details of the assumed mechanism may change, but in any case the detailed mechanism will not include elementary or completely fundamental descriptions. These tests will involve temperatures relevant to commercial operation but in differential mode. This will probably be about 300 °C, but some experimentation will be required to establish a specific temperature.

A statistical experiment will determine effects of poisons and sulfates on catalyst activity as well as interactions among sulfates and poisons, since no previously published investigation clarifies whether interactions among poisons and sulfates exist, and how important interactions are if they do exist. Table 4 summarizes factors and factor levels to be investigated. Four factors will be studied including 3 poisons (K, Na, and Ca) and 1 sulfate on a 1% vanadia catalyst surface, each with two levels. NO_x reduction activity will be chosen as the response.

Table 4 Statistic experiment design of interactions between poisons

Runs	Poison types with 2 concentration				Response-X_{NO}	Runs	Poison types with 2 concentration				Response-X_{NO}
	K	Na	Ca	SO_4			K	Na	Ca	SO_4	
1	0.5	0	0	0		8	0.5	0	0	1	
2	0	0.5	0	0		9	0	0.5	0	1	
3	0	0	0.5	0		10	0	0	0.5	1	
4	0.5	0.5	0	0		11	0.5	0.5	0	1	
5	0.5	0	0.5	0		12	0.5	0	0.5	1	
6	0	0.5	0.5	0		13	0	0.5	0.5	1	
7	0.5	0.5	0.5	0		14	0.5	0.5	0.5	1	

III Other surface characterization investigations

BET surface area and pore size distribution analyses for all samples provide physical and structural information about the catalysts. A Micromeritics Tri-star Instrument (Model 3000) using the N_2 surface area method provides all data for these measurements. The test matrix includes all samples, that is, fresh and exposed commercial samples, sulfated and non-sulfated laboratory samples, and contaminated and uncontaminated laboratory samples. Several other surface-sensitive laboratory diagnostics such as XPS and ToFSIMS (time-of-flight-secondary-ion mass spectroscopy) as well as standard (bulk) analyses supplement the reactor data collected in our laboratory.

The above experiments involve comparisons of sulfated and non-sulfated samples of uncontaminated and contaminated laboratory-prepared catalysts with known amounts and forms of contaminants and catalyst. Uncontaminated SCR material and at least one sample of the same material contaminated with each poison provide a database with which to compare commercially exposed materials (discussed next). The completion of this activity occurs when a database of FTIR-MS and TPD results describing surface spectra, reactor effluent compositions, and transient concentration profiles for contaminated and uncontaminated catalysts is completed for both sulfated and non-sulfated catalyst surfaces. The experimental design is shown in Table 5.

Table 5 Experiment design for sulfation and poison tests of catalyst samples

	$V\%/TiO_2$	Samples Poisons	sulfation	Adsorption (FTIR)	Reactivity (MS)	Surface Characterization (BET, XPS, SEM, ToFSIMS)
BYU- prepared	0	0	×	2	2	2
	0	0		2	2	2
	1	0	×	2	2	2
	1	0		2	2	2
	5	0	×	2	2	2
	5	0		2	2	2
	1	K	×	2	2	2
	1	K		2	2	2
	1	Na	×	2	2	2
	1	Na		2	2	2
	1	Ca	×	2	2	2
	1	Ca		2	2	2
Commercial	Fresh ×6				2	2
	Front – exposed × 6				2	2
	Tail – exposed × 6				2	2

Based on the above designed experiments, the effect of sulfur and poison addition on vanadia catalyst surface chemistry and kinetics should be acquired to supplement the existing literature, to help elucidate the mechanism of SCR catalysts deactivation, and to support developing deactivation modeling in Task 2.

Chapter 5: Results and Discussion

A series of experiments were designed to investigate the kinetics and deactivation mechanisms of commercial SCR catalysts after exposure in coal and biomass effluent. To accomplish this part of the project, two classes of catalysts were tested: commercial, vendor-supplied SCR catalysts and BYU-manufactured, research catalysts. The commercial catalysts

provide immediate relevance to practical application while the research catalyst provides less fettered ability to publish details of catalyst properties. The five commercial catalysts selected for use come from most commercially significant catalyst manufacturers (Cormetech, Haldor Topsoe, Hitachi, and Siemens) and provided a wide range of catalyst designs and compositions. The in-house catalyst allows detailed analysis and publication of results that may be more difficult with the commercial systems. This catalyst suite provides a comprehensive test and analysis platform from which to determine rates and mechanisms of catalyst deactivation. The experimental design and setup, test samples, and current results are described below.

I Catalyst Characterization System (CCS)

The Catalyst Characterization System (CCS) quantitatively determines deactivation mechanisms by measuring specific, intrinsic catalyst reactivity of custom (laboratory) and commercial catalysts under a variety of conditions. These catalysts are impregnated with a variety of contaminants, including Ca, Na, and K. In addition, the CCS characterizes samples of catalyst from slipstream field tests to determine similar data and changes in characteristics with exposure. Advanced surface and composition analyses are used to determine composition, pore size distribution, surface area, and surface properties (acidity, extent of sulfation, etc.).

I.A Powder catalyst tests

We have assumed first-order reaction kinetics (Eq.(1)) and computed first-order rate constants by performing a material balance across the packed bed and integrating the resulting expression (Eq. (2)), as did Chen *et al.* In this way, our results are directly comparable to the literature results.

In our analysis, r_{NO} is the rate of reaction of NO, C_{NO} and $C_{NO,0}$ are local and *inlet* NO concentrations, respectively [moles/volume], k is the rate constant [$cm^3/g/s$], $F_{NO,0}$ is inlet feed rate of NO [moles/time], X_{NO} is NO outlet conversion, and W is weight of catalyst [g]. Eq. (2) contains variables that are known or measurable and thus the observed first-order rate constant, k_{obs}, may be determined from experiment.

$$-r_{NO} = kC_{NO} \tag{1}$$

$$k_{obs} = \frac{F_{NO,0}}{C_{NO,0}W}\ln(1 - X_{NO}) \tag{2}$$

It should be emphasized that Eq. (2) rests on several assumptions, which are listed below.

1. The gas flow through the bed is uniform with no significant radial or angular flow or concentration gradients.
2. The catalyst bed is isothermal.
3. Expansion effects due to reaction stoichiometry or pressure changes across the bed are negligible.
4. The rate can be modeled according to a first-order model.

After a series study of particle size effect on the kinetics regime, we feel comfortable running tests with powders in the 90-106 micron range since they do not appear to be significantly affected by mass transfer or pore diffusion limitations until the reactor temperature exceeds 375 °C, at which point the effectiveness factor drops below 0.9 (see Figure 7).

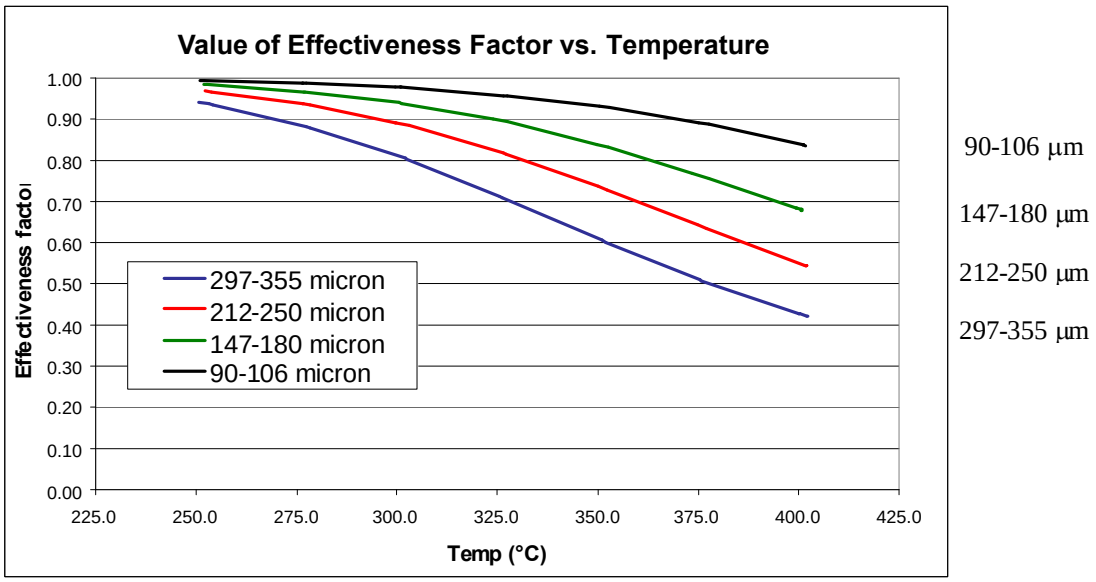

Figure 7 Plot of effectiveness factor, η, versus temperature for various pellet sizes

Thus we are comfortable to make the last assumption, which is

5. Film mass transfer and catalyst pore diffusion effects are nonexistent (i.e. the gas composition at any axial position through bed, including inside the pellets, is uniform).

I.A.1. Poisoning study

A poisoning study similar to that reported by Chen, Buzanowski, *et al.* was conducted on the BYU SCR catalyst in the 90-106 micron particle range that had been poisoned at various levels with Ca and Na by a previous student. In our study, 50 mg of catalyst was used. Prior to reaction, the catalyst was "steam treated" overnight at around 400 °C with 10% water, 2% O_2, and balance He at 150 sccm flow (as described above). The reaction conditions of the two studies are compared in Table 2.

Data obtained from running the catalyst both wet and dry are shown in Figure 8. In this figure, it can be seen that addition of water vapor appears to inhibit the reaction (i.e. reduces the value of the observed first order rate constant), while it can also be seen that Na is a stronger poison than Ca, resulting in almost complete deactivation when the Na:V ratio is 1. Ca is not as strong of a poison at the same poison-to-vanadium atom ratio. This is consistent with the fact that Na is more strongly basic and thus has a greater effect on the surface Brønsted acidity.

Table 6 Comparison of conditions in poisoning study by BYU to those of Chen, Buzanowski, et al.

	BYU	**Chen, Buzanowski, *et al.***
Catalyst Composition	1% V_2O_5-9% WO_3/TiO_2	5% V_2O_5/TiO_2
Poisons	Ca, Na	Ca, Na, K, Li, P, As, Pb, Rb, Cs
Reaction Conditions	340 °C NO = NH_3 = 900 ppm 2% O_2 10% H_2O (when used) balance He flowrate = 380 sccm (estimated ~1,000,000 hr^{-1} based on solid catalyst volume (!) with 0.022 cm^3-50 mg-catalyst)	300 °C NO = NH_3 = 1000 ppm 2% O_2 no H_2O balance N_2 space velocity = 15,000 hr^{-1} (500 sccm with 2 cm^3 of pellets)
Pellet/granule sizes	90-106 μm (170-140 mesh)	500-812 μm (32-20 mesh)
BET surface area	~32 m^2/g	30.6 m^2/g

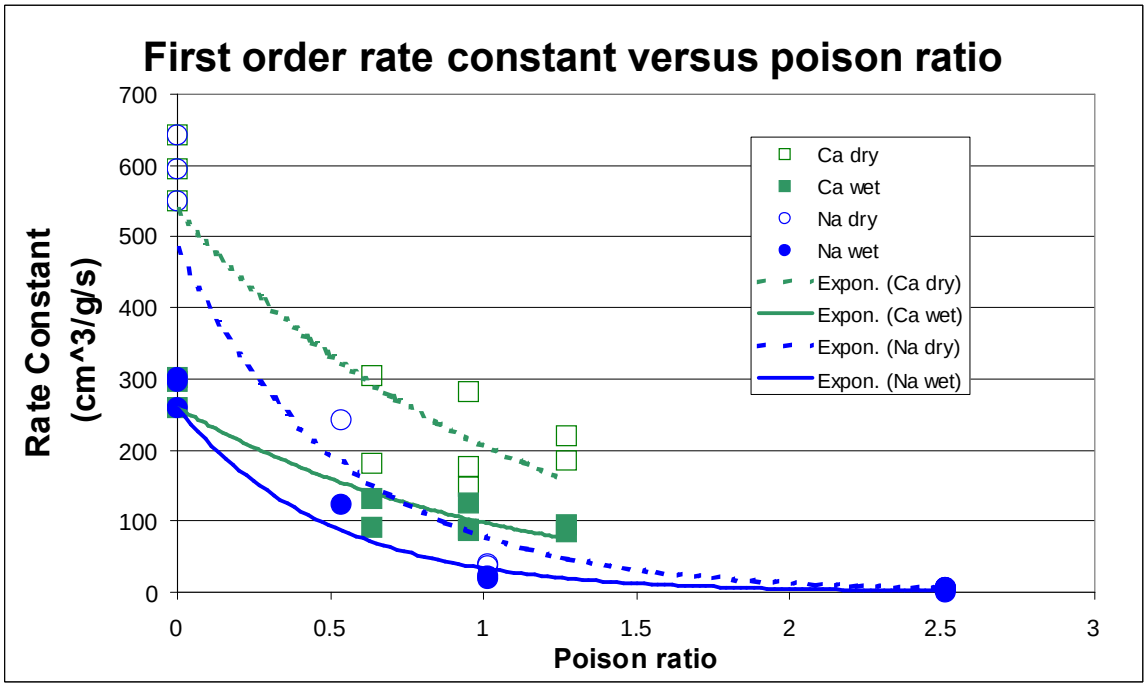

Figure 8 Plot of observed rate constants at various poison levels for Na, Ca with and without water.

Normalized catalytic *activity* as a function of poison level is shown for Ca (Figure 9) and for Na (Figure 10). Normalized activity is defined here as the observed rate constant at any given poison level divided by the observed rate constant for the fresh catalyst. Data obtained on the same poisons by Chen, Buzanowski, *et al.* are also plotted in these figures for easy comparison.

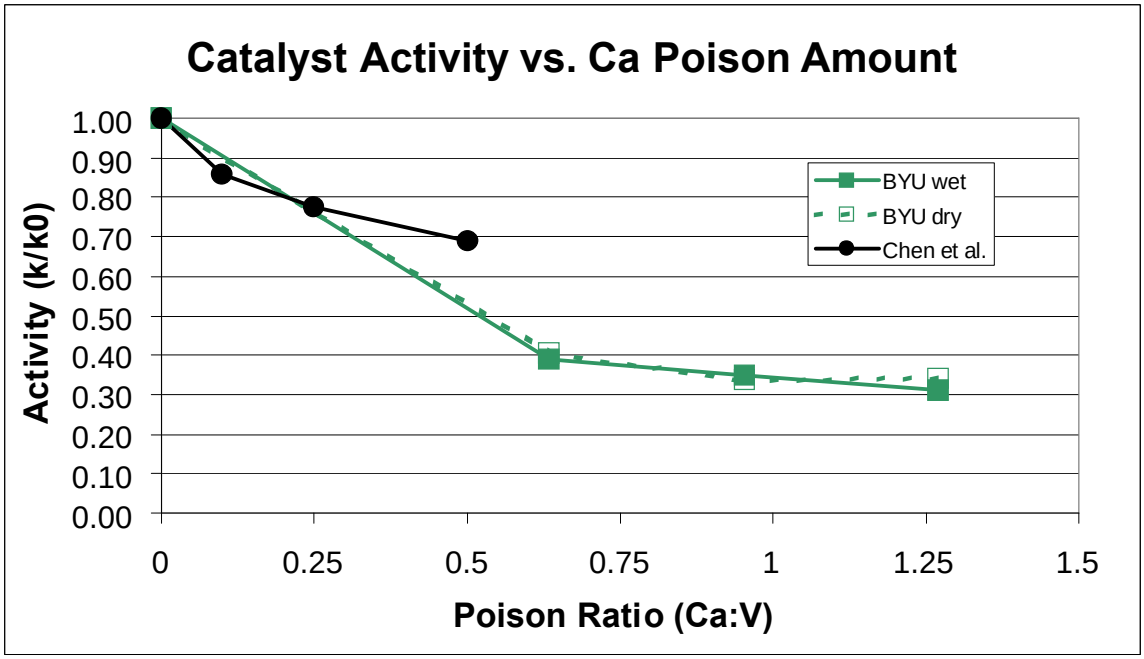

Figure 9 Catalyst activity versus Ca:V ratio.

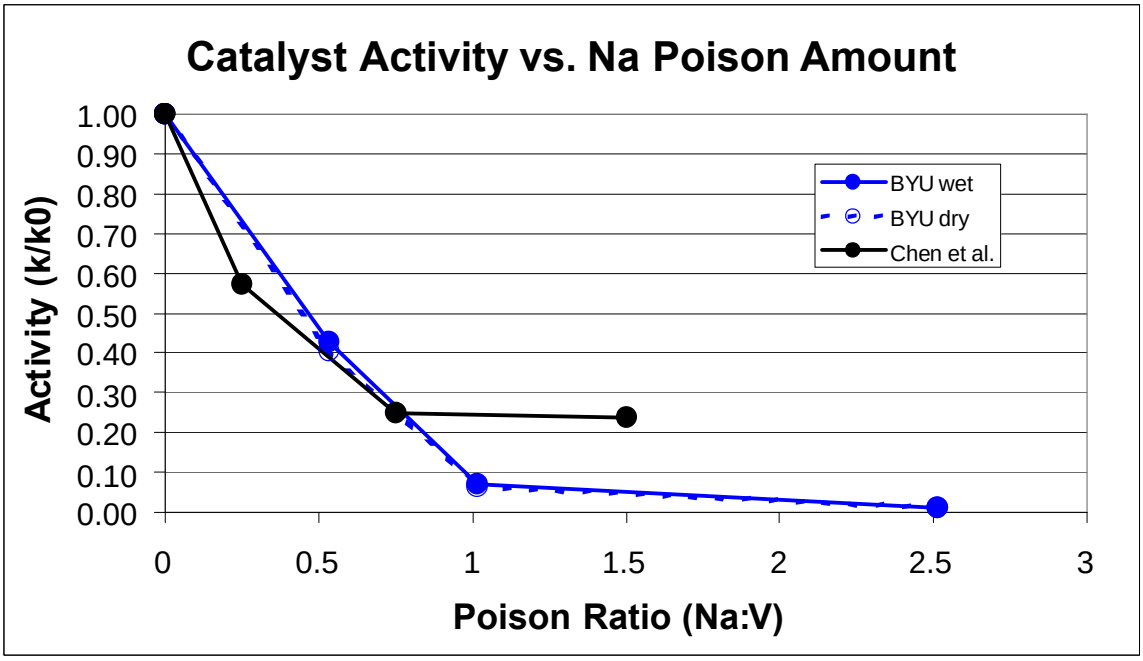

Figure 10 Catalyst activity versus Ca:V ratio.

Two observations are important at this point. First, although addition of water vapor does lower the observed rate constant, it does not affect normalized activity. Second, the same trends in activity loss with poison ratio are observed in the two studies for both poisons, i.e., the activity levels off at a higher value for Ca-doped catalysts relative to Na-doped catalysts. The Na-doped catalysts of this study were essentially completely poisoned at Na:V = 1, in contrast to the Ca-poisoned samples, which appeared to level off at around 30% of original

activity. Activity results from higher Ca:V ratios would reveal whether activity truly levels off.

Therefore at this point, we realized that alkali metals Na, and alkaline earth metals Ca are poisons to vanadia catalyst. The following question is whether the deactivation of commercial monolith catalyst is caused by the poisoning of alkali and alkaline earth metals deposition. Thus, a series NO reduction activity tests were conducted on commercial and home-made monolith and plate vanaida catalysts which had been tested in a slipstream reactor.

I.B Monolith and Plate Catalyst Tests

Five vendor-supplied commercial catalysts, three of which are of monolith form and two are of plate form, and a BYU prepared monolith are being analyzed in order to help characterize the deactivation that occurs in coal-boiler flue gas over time. Of each catalyst type a fresh, unused sample is available, a sample that has been exposed in the flue gas of a slipstream reactor for about 2063 hours, and a sample that has been exposed for 3800 hours the flue gas of a slipstream reactor are available for testing. The catalysts will now be described:

I.B.1. Physical Dimensions

Physical dimensions of the catalyst samples from vendors and BYU were measured as accurately as possible with calipers and a tape measure. A summary of this information is contained in Table 7. Table 8 presents other geometric properties of the catalyst, including area open to flow, total cross sectional areas, total geometric surface area available to reaction, and total volume available to gas flow. In the case of Monolith 3, the calculations reported are approximate because of the irregularity of the shape of its channels.

Table 7 Physical Dimensions of the Six Catalyst Samples under Investigation

Catalyst	Length (in/cm)	Width 1 (in/cm)	Width 2 (in/cm)	Cell width (in/mm)[1]	Wall Thickness (in/mm)[1]	Pitch (in/mm)[1]
M1	19.75/50.17	2.09/5.32	2.063/5.24	0.24/6.2	0.047/1.2	0.29/7.4
M2	21.63/54.93 (BYU = 20.25/51.4)[2]	2.0/5.08	2.0/5.08	0.25/6.3	0.030/0.77	0.28/7.07
M3	19.31/49.054	2.13/5.40	2.13/5.40	NA	~1mm flat piece, ~0.9mm curved	NA
M3 (stainless case)	20.06/50.96	2.25/5.72	2.25/5.72	NA	~1mm thick	NA
M4 (BYU)	6.0/15.24 (x4 = 24.0/60.96)[3]	2.0/5.08 (1.82/4.62 for 7x7 cell cross-section)[4]	2.0/5.08 (1.82/4.62 for 7x7 cell cross-section)[4]	0.20/5.0	0.055/1.4	0.25/6.4
P1	21.5/54.61[5] (BYU = 19.75/50.2)[2]	3.875/9.84	NA	NA	0.039/01.0	0.2231/5.667
P2	19.75/50.17[5] (BYU = 18.75/47.6)[2]	4.375/11.11	NA	NA	0.035/0.90	0.2231/5.667

[1] Note: metric measurements more accurate than inches on cell width, wall thickness, and pitch.
[2] In order to test methods of cutting catalysts, these fresh catalyst samples were cut at BYU and the lengths reported next to this footnote subscript are the cut lengths.
[3] Four 6-inch M4 catalysts are placed in series in the slipstream reactor, making 24" total length.
[4] See 4. Monolith 4 section below.
[5] Because two plate sections are installed in series, twice the plate length (2*21.5" = 43.0" for P1 and 2*19.75" = 39.50" for P2) should be used in calculating space velocities.

Table 8 **Exterior surface area and open flow area information for catalysts in the slipstream reactor.**

Catalyst	Total Cells	Single-cell Open Area (in^2/cm^2)	Total Open Area (in^2/cm^2)	Total Frontal Area (in^2/cm^2)	% Open Frontal Area	Total surface area for reaction[6] (in^2/cm^2)	Total open volume[6] (in^3/cm^3)
M1	49	0.0596/0.384	2.92/18.84	4.32/27.9	67.61	995/6096	57.7/945
M2	49	0.0615/0.397	3.01/19.45	4.0/25.8	75.36	1051/6782	65.2/1068
M3	~45	~0.070/~0.45	~3.1/~20	4.52/29.1	~70	~925/~5970	~61/~993
M4 (BYU)	49	0.0388/0.250	1.90/12.25	3.31/21.3	57.4	231/1493-6” 926/5974-24”	11.4/187-6” 45.6/747-24”
	64	0.0388/0.250	2.48/16.0	4.29/27.7	57.8	302/1951-6” 1209/7803-24”	14.9/244-6” 59.5/975-24”
P1	21[7]	NA	14.86/95.87	17.81/114.92	83.42	6450/41613	639/10470[8]
P2	21[7]	NA	17.18/110.81	20.19/130.24	85.08	6715/43323	678/11118[8]

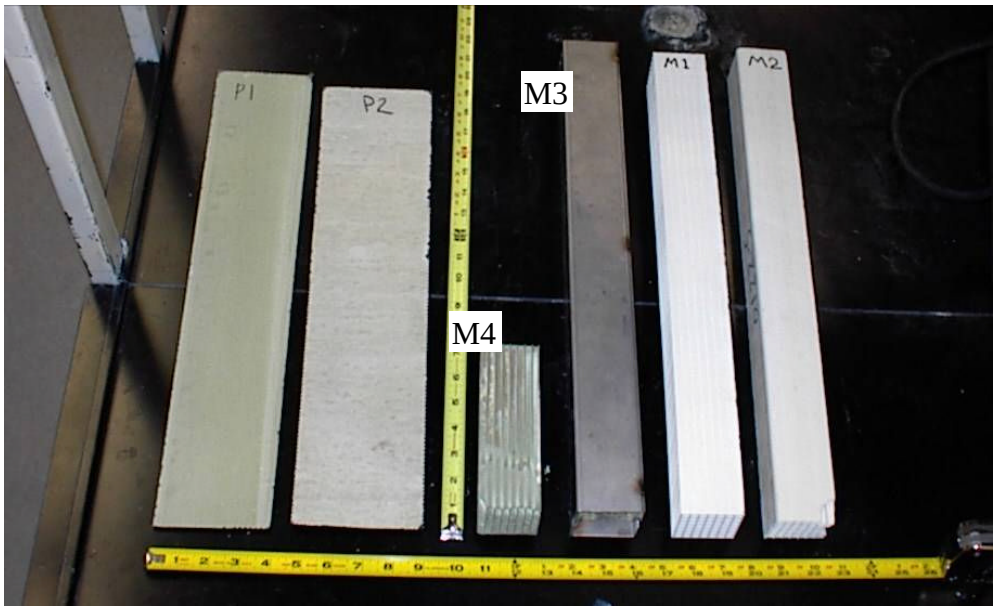

Figure 11 **Photograph showing all 6 catalyst samples alongside one another [order from left to right = P1, P2, M4 (BYU), M3 (SS-encased), M1, M2].**

[6] Total surface areas and volumes for monolith catalysts are ¼ what they are for the entire catalyst in the reactor since there are four monolith pieces in the slipstream reactor (see Figure 24).
[7] 19 cells of one equal size are between the plates and 2 of another equal size on either side of the end plates between the plates and the chamber wall.
[8] Important note: the volumes reported for the plate catalysts include only the volume where there is catalyst material, not the dead volume between the top and bottom sections of catalyst.

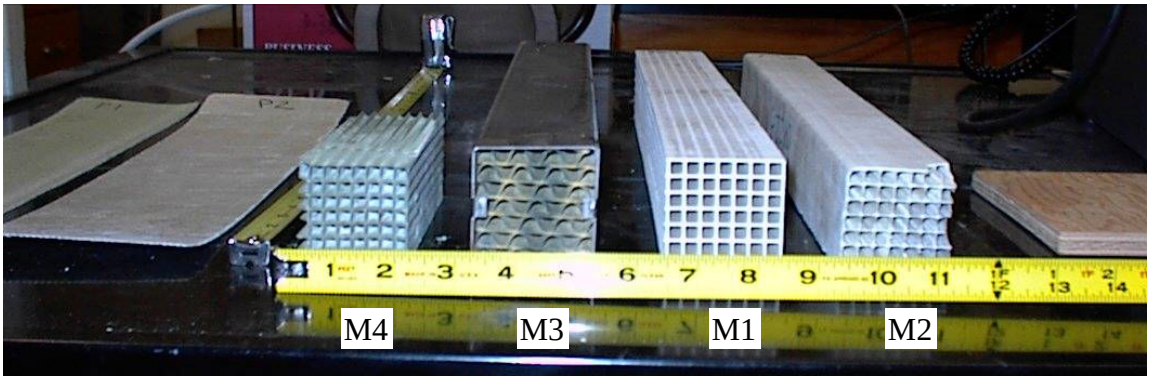

Figure 12 **Photograph showing all 6 catalyst sample faces [order from left to right = P1, P2, M4 (BYU), M3 (SS-encased), M1, M2.**

1. Monolith 1 (M1)

Monolith 1 is extruded monolith. The wall pitch is the thicker of the two square commercial monoliths, and is thus the more robust of the two commercial square-channel monoliths. Scheme of M1 is shown in Figure 13; Figure 14 shows the photos of M1.

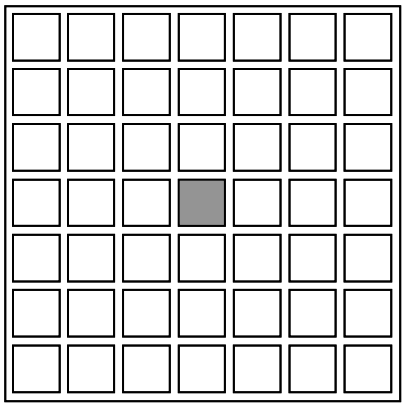

Figure 13 To-scale Schematic of Monolith 1.

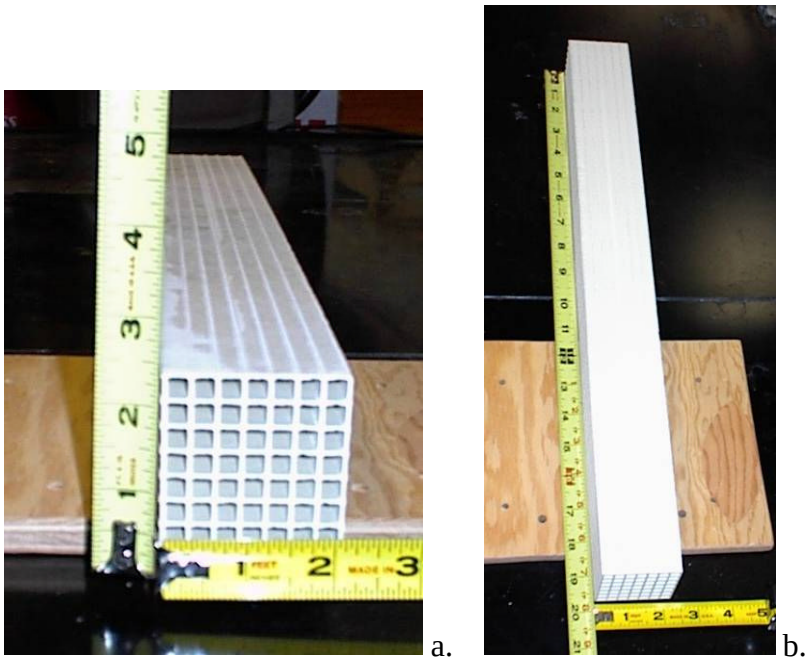

a. b.

Figure 14 Photos of (a) the face and (b) the length of Monolith 1.

2. Monolith 2 (M2)

Monolith 2 is also extruded monolith. The wall pitch is thinner than Monolith 1, while the channel width is essentially the same. M2 scheme is shown in Figure 15, and photos are shown in Figure 16.

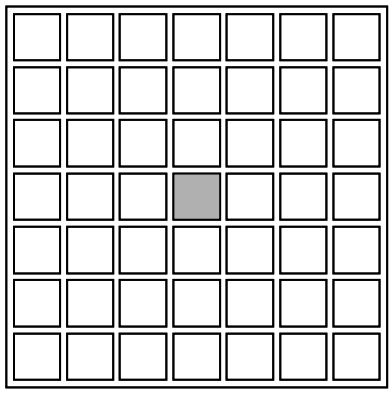

Figure 15 To-scale Schematic of Monolith 2.

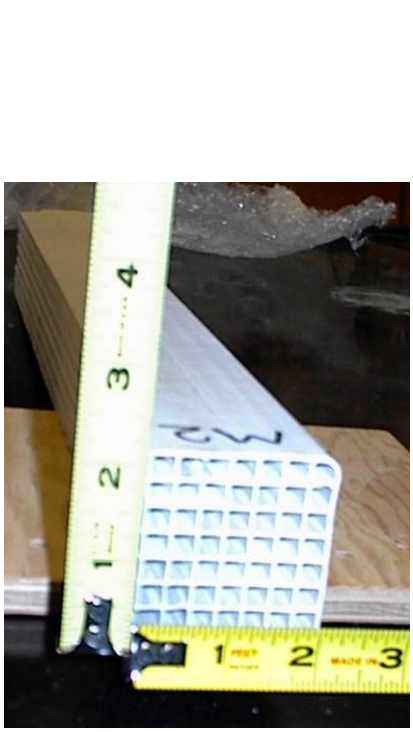

a.

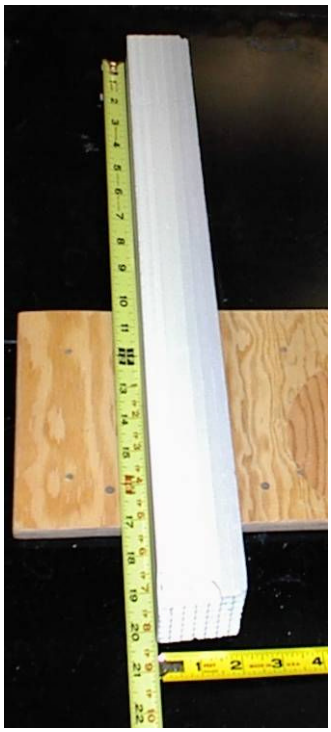

b.

Figure 16 Photos of (a) the face and (b) the length of Monolith 2.

3. Monolith 3 (M3)

Monolith 3 is placed inside a rectangular stainless steel jacket, and the catalyst consists of a stiffened cardboard-like material that alternates between corrugated and flat layers (See Figure 17).

Distance between “peaks” of corrugated part (i.e. wavelength): 15.0 mm (0.59 in)

Distance between flat layers (i.e. amplitude): ~7.5 mm (0.30 in)

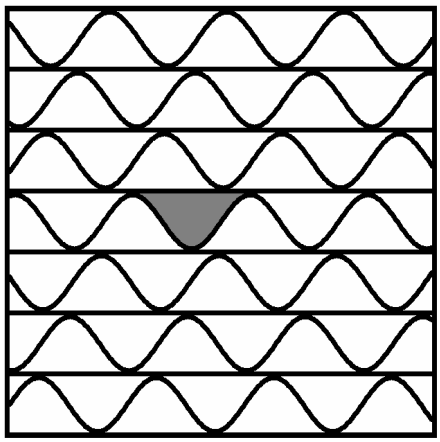

Figure 17 To-scale schematic of Monolith 3.

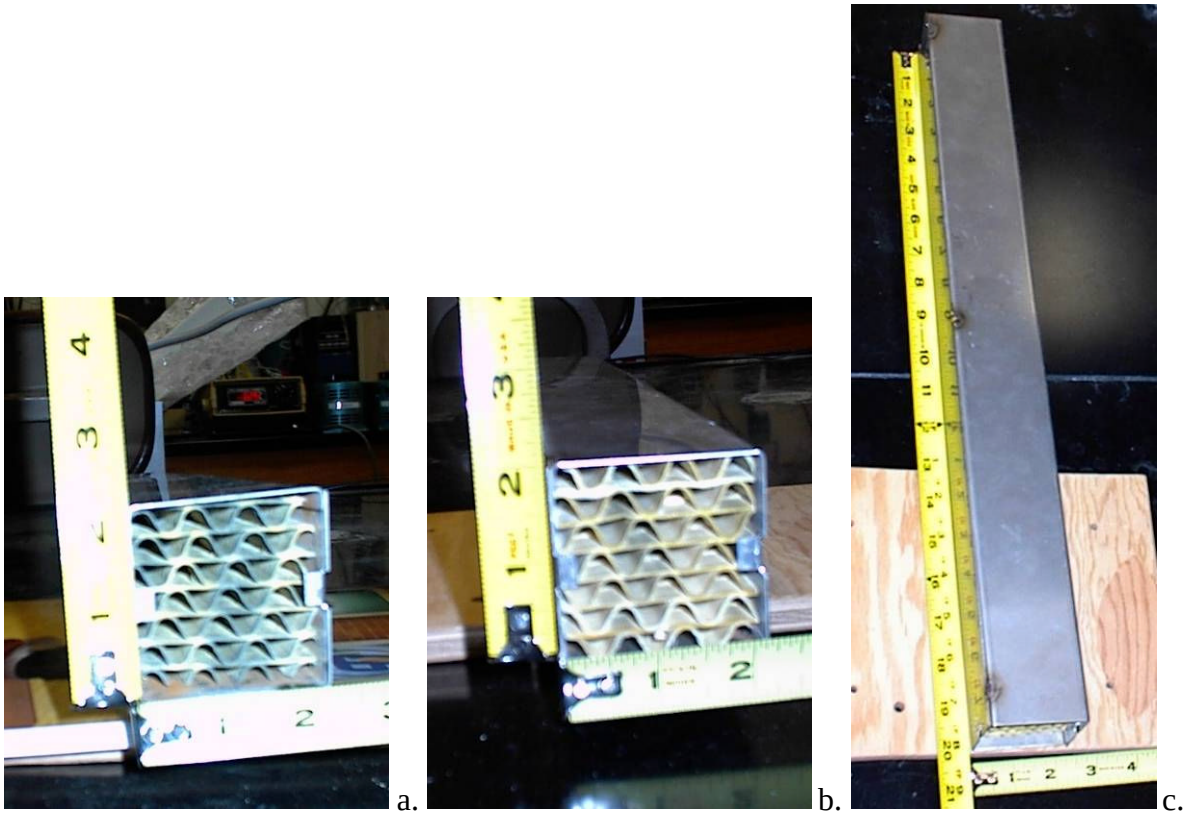

a. b. c.

Figure 18 Photos of (a) and (b) the face and (c) the length of Monolith 2.

4. Monolith 4 (M4)

Monolith 4 was prepared at BYU by cutting an extruded 4”x 4” cordierite support lengthwise into four pieces (see Figure 19; ideal cuts would be along the dotted lines). The resulting pieces are in the form shown in Figure 20a, the breakage of the top and right edges resulting from cutting the catalyst into four equal pieces. Some wall pieces may be intact (or partially intact) where the cuts were made, as shown in Figure 20b. These monolith pieces were cut approximately 6” long.

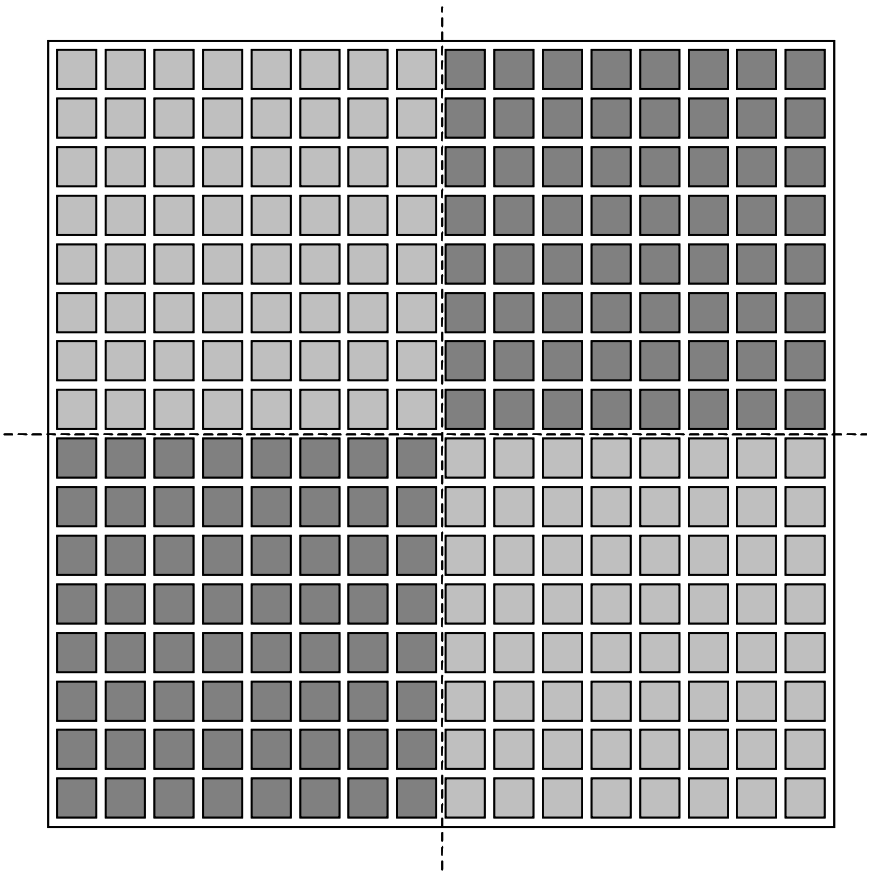

Figure 19 **To-scale schematic of cordierite support with regions corresponding to smaller monolith pieces highlighted in different shades of gray.**

Note that the channels in Figure 20 are slightly rounded at the corners. This is the result of dipping the cordierite pieces in a slurry consisting of the active catalytic phase supported on titania.

The preparation method of BYU made monolith catalyst is listed in Appendix A.

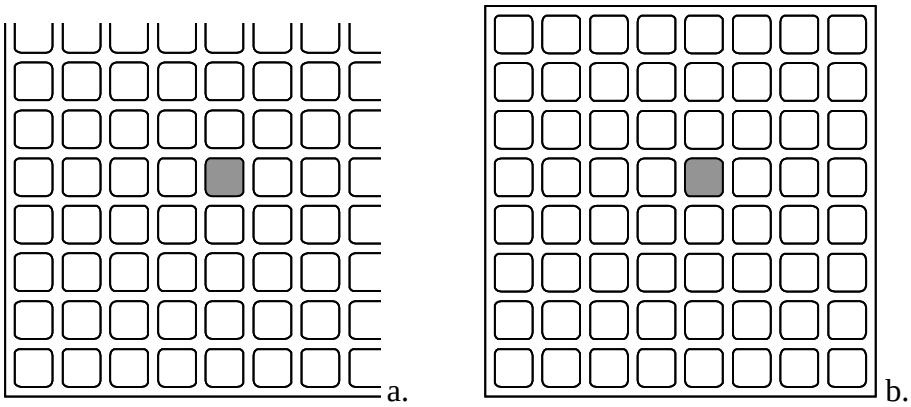

a. b.

Figure 20 **To-scale schematic of Monolith 4 (BYU) after cutting (a) and as it would have turned out ideally without cutting effects (b).**

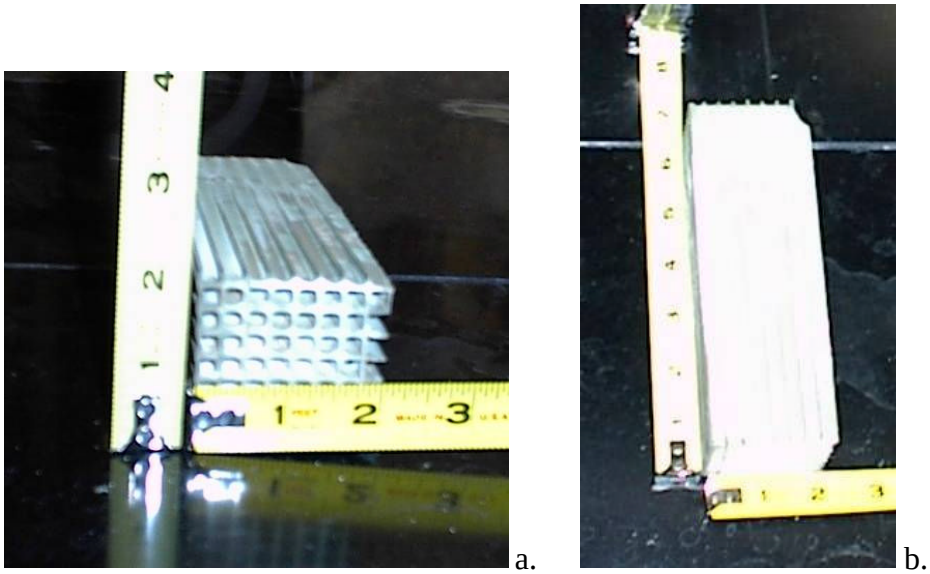

a. b.

Figure 21 **Photos of (a) the face and (b) the length of Monolith 4 (BYU).**

5. Plates 1 and 2 (P1 and P2)

The plate samples geometrically simple rectangular pieces, consisting of a perforated steel wire screen that has been coated with catalytic material. The plates are thin (<1mm thickness). The wire on Plate 1 is finer than on Plate 2, but both contain holes of similar diamond-like shape.

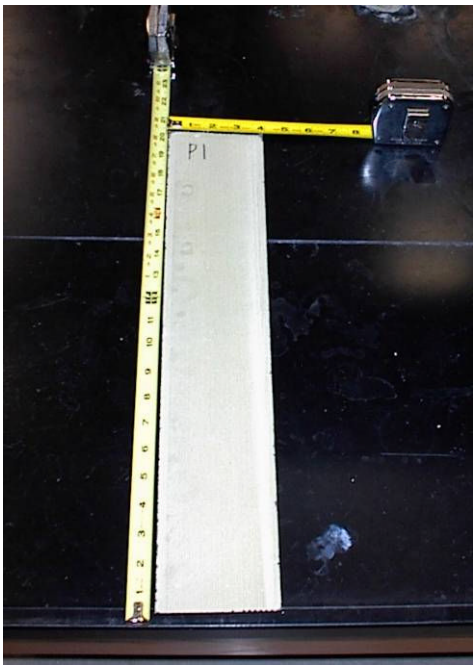

a.


b.

Figure 22. Photographs of Plate 1 (a) and Plate 2 (b).

The plate catalysts offer the advantage of being flexible and may be bent considerably without the catalyst coating flaking off (See Figure 23).

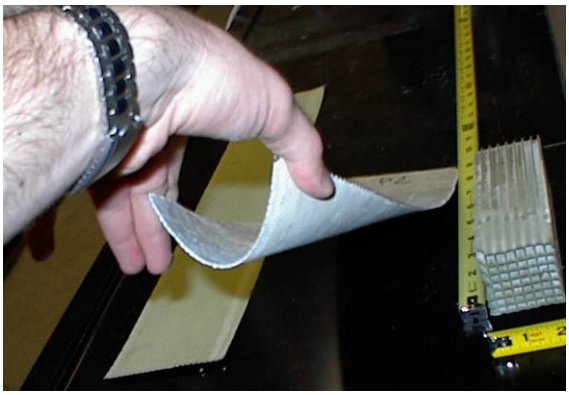
a.
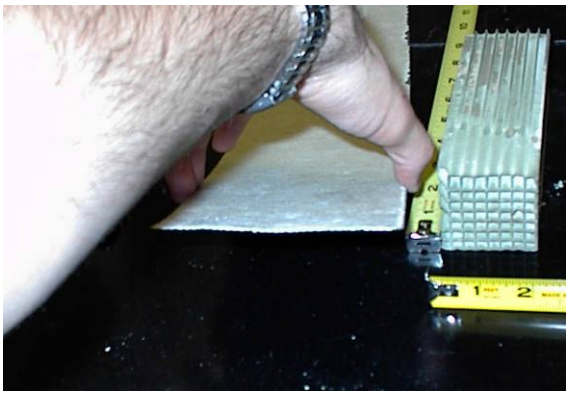
b.

Figure 23 Plate 2 can be bent (a) and will return to its original shape (b).

6. Housing in Slipstream Reactor

Catalysts were placed in the slipstream reactor according to Figure 24. The monolith catalysts were arranged in groups of four and are placed at the corner sections of the slipstream reactor casing. The plate catalysts were located in the middle sections. The placement of the plate catalysts is now discussed.

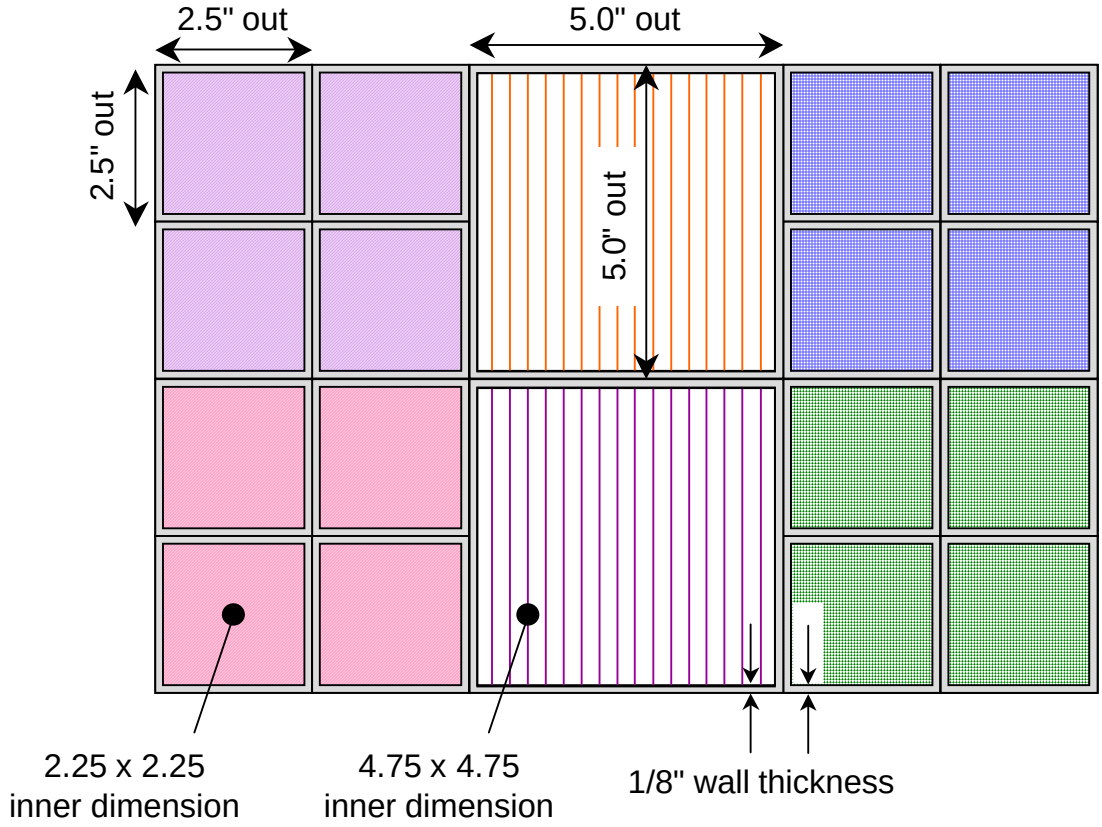

Figure 24 Layout of catalysts in slipstream reactor (picture courtesy of Connie Senior).

There were 40 plates in each chamber--20 on top and 20 on bottom, with the bottom plates installed transverse (or perpendicular) to the top plates. To illustrate, the plate holders for the top catalysts would be on the north and south sides, while the holders for the bottom catalysts would be on the east and west sides.

The top set of plates was installed such that the top edge of the plate was flush with (or perhaps 2-3 mm below) the top edge of the 4.75x4.75 inch square chamber tube holding the plates. The plate holders were 23 inch long, 1/4" thick aluminum plates with twenty 0.06" wide grooves machined the length of the plate (0.2231” pitch). All eight plate holders (2 top, 2 bottom in each of the 2 plate chambers) were identical. Another 1/4" thick, 1/2" high "block" was screwed onto the front side of these holders to keep the catalysts from sliding downwards. This block was positioned such that the top of the catalysts was just about flush (perhaps 2-3mm below) the top of the chamber.

The bottom edge of the bottom plate holders was just about flush with the bottom of the aluminum tube, and the "block" was about 1 inch above the bottom. Consequently, there was

a space between the upper and lower set of plates. This space is estimated to be 3.5 inches for plates P1 and 7.5 inches for plates P2.

The plate holders for P2 were attached directly to the chamber tube. With two 0.25" thick plate holders secured to two sides of this, the actual inner dimensions are 4.25x4.75 inches. The grooves in the plate holders were about 0.125" deep, so the total spacing for the plate was about 4.50". The 4.375" plates slide into this nicely.

Because P1 are narrower, 0.25” thick backing plates were placed behind the catalyst holders to move them closer together. This results in a smaller chamber of dimensions 3.75x4.75 inches, allowing 4.0 inches of total spacing for the 3.875 inch wide P1.

I.B.2. Sample Preparation

Small samples of catalysts cut from the monoliths/plates exposed in the field tests provided localized measures of catalyst activity and deactivation. This not only allows position-sensitive measures for performance, but avoids the very large gas supplies and controllers that would be required for calibrated tests of entire monoliths.

A scroll saw cut sections out of the monolith catalysts (Figure 25). These sections were then sanded around the sides and on the ends to yield samples of four channels, in a two by two arrangement. M3, which doesn’t have square channels, was cut in a shape shown in Figure 26. When preparing the exposed catalyst samples, some ash was dislodged due to movement and vibrations caused by the scroll saw and sanding. Care was taken to dislodge as little ash as possible.

Metal snips were used to cut rectangular-shaped samples from the plate catalyst.

All samples taken from catalysts that had been exposed in the slipstream reactor were taken from the upstream end of the catalyst. Table 9 summarizes the dimensions of test samples for each catalyst.

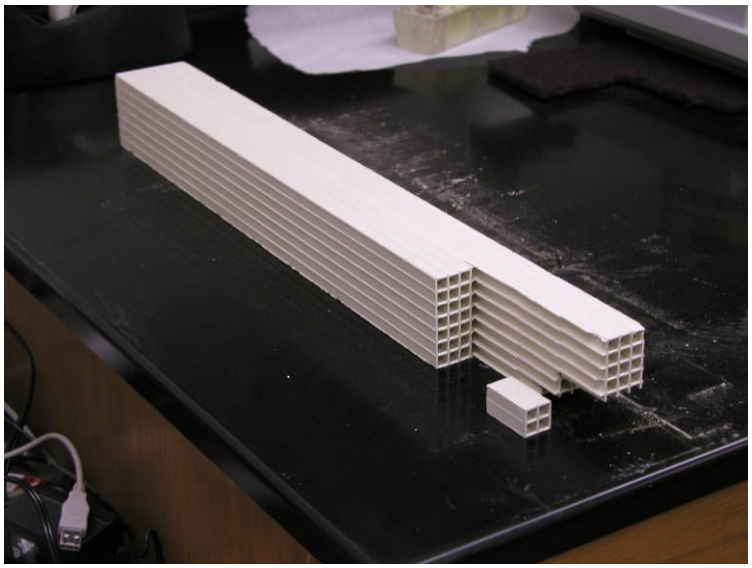

Figure 25 Picture of a Section cut out of the Fresh M1 Catalyst.

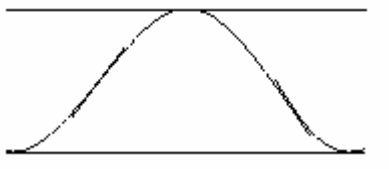

Figure 26 Face of M3 Test Sample

Table 9 Dimensions of Test Samples

CATALYST	LENGTH (cm)	WIDTH (cm)	HEIGHT (cm)
M1	3.1	1.5	1.5
M2	2.9	1.4	1.4
M3	3.2	1.7	0.9
M4	2.8	1.3	1.3
P1	2.9	---	1.8
P2	3.0	---	1.8

I.B.3. Results and Discussion

Table 10 summarizes how many samples were run for each type of catalyst. Figure 27 to Figure 30 show a comparison of NO conversion for the fresh catalysts versus the exposed catalysts. The 95% confidence intervals were found by fitting the data to a second order polynomial using Igor Pro®. For M1 and M2, the 2063-hour exposed catalysts exhibited the same activity as the fresh catalyst and the 3800-hour exposed catalysts exhibited less activity than the fresh catalyst. For P1 and P2, the exposed catalysts exhibited less activity than that of the fresh catalyst, while the 3800-hour exposed catalysts exhibited less activity than the 2063-hour exposed catalyst.

Table 10 Samples Run for Each Catalyst

Catalyst	Fresh	2063 hr Exposure	3800 hr Exposure
M1	3	3	2
M2	3	3	2
P1	3	3	6
P2	3	3	3

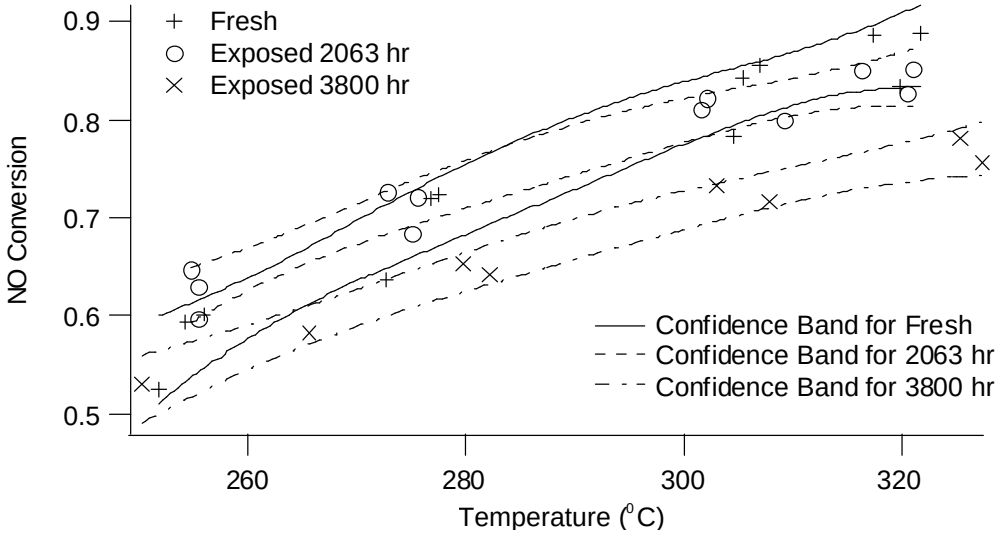

Figure 27 M1 Results with 95% Confidence Bands.

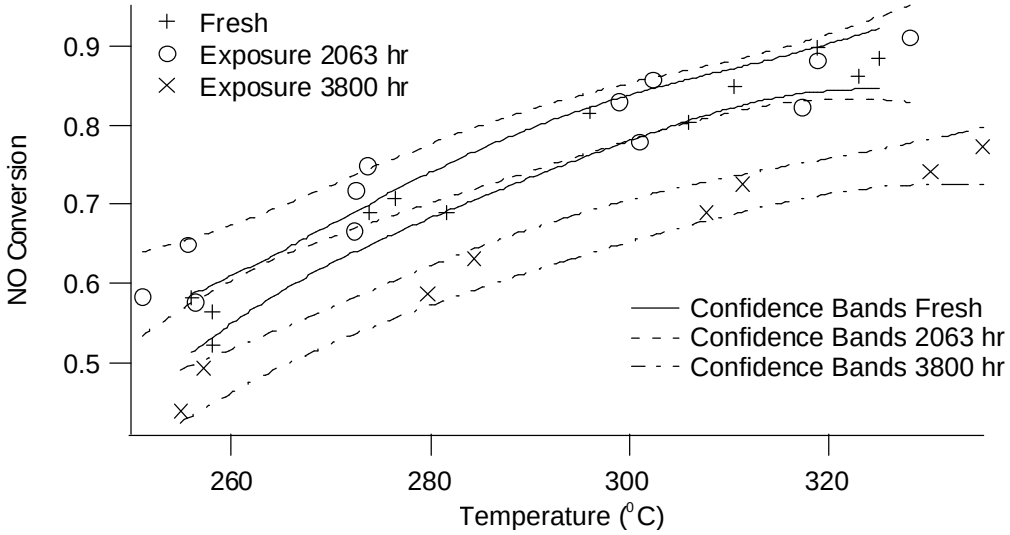

Figure 28 M2 Results with 95% Confidence Bands.

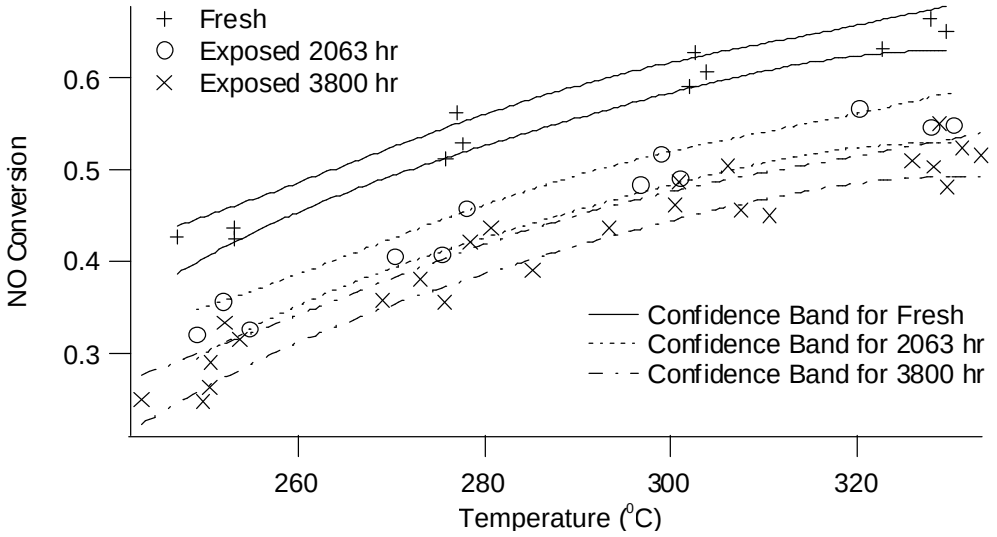

Figure 29 P1 Results with 95% Confidence Bands.

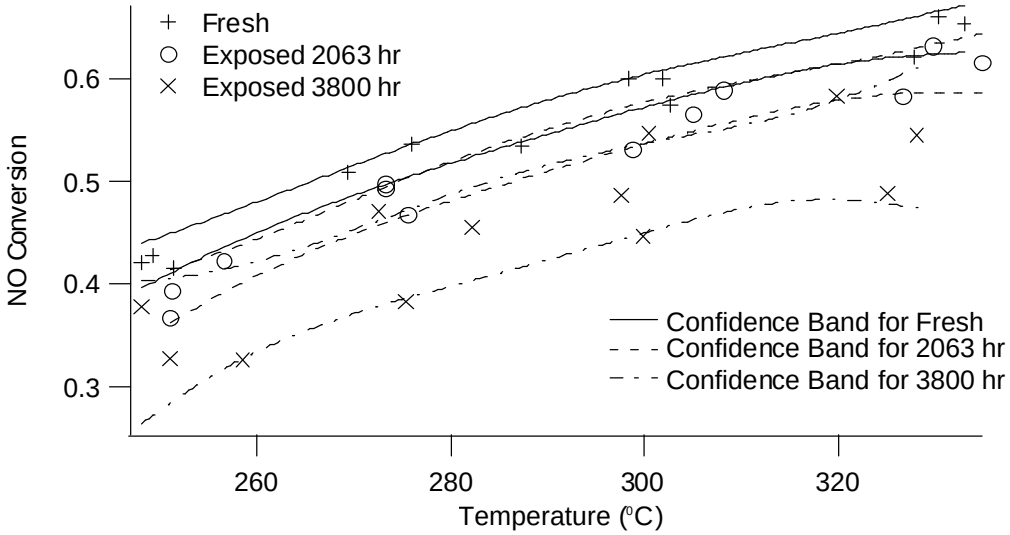

Figure 30 P2 Results with 95% Confidence Bands.

The 3800-hour exposed P1 and P2 were taken from both the top and bottom sections in the slipstream reactor. The 3800-hour exposed P1 samples taken from the top of the slipstream-reactor chamber were compared to those taken from the bottom of the chamber. Figure 31 indicates that samples taken from both positions exhibit similar activities.

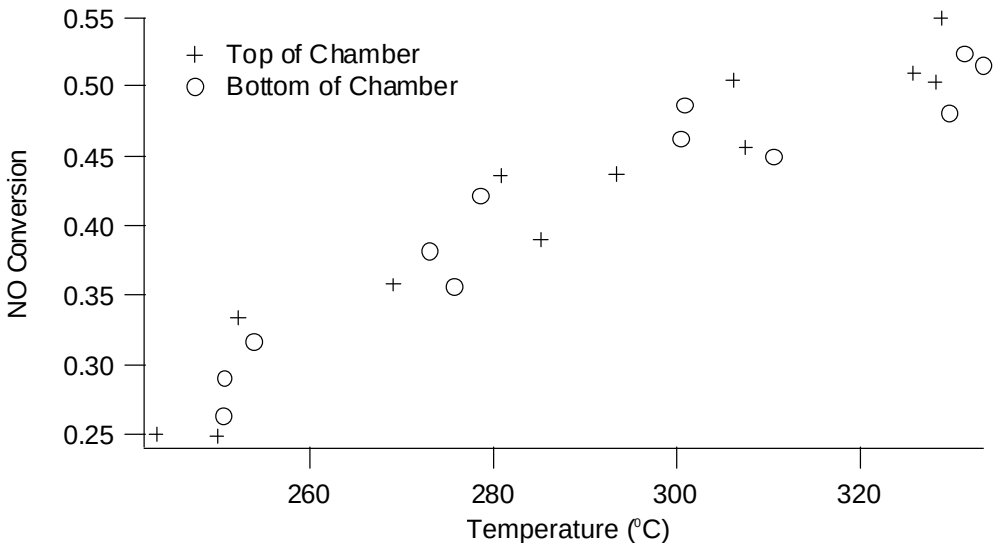

Figure 31 **Top of Chamber versus Bottom of Chamber for P1 Exposed 3800 hr Catalyst.**

Some tests have been run on M3 samples. The results, shown in Figure 32, show that the sample behavior varies widely. This is probably due to sample size variability caused by the shape of the channels that are characteristic of the M3 catalyst. The M1 and M2 catalysts have defined square channels in which sample size is more easily reproducible. Consistently reproducible characterization of the M3 samples has thus far not been possible because of its wave-shaped channels and an inability to cut identical and representative samples from this form of material.

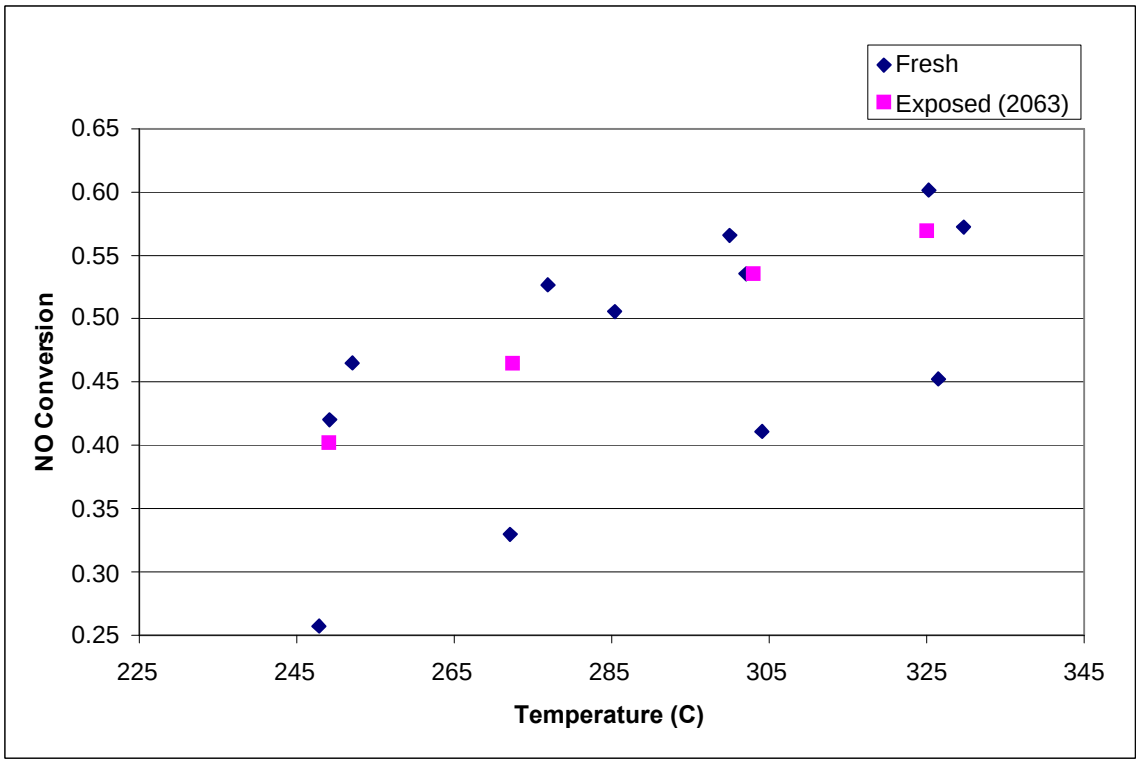

Figure 32 **M3 Preliminary Results.**

Samples of the commercial catalysts that have been exposed in co-coal-biomass-combustion flue gas have been received and will be tested.

I.B.4. Reaction Rate Constant, Activation Energy, and Activity of M1 and M2 Catalysts

The Chen model (Chen), developed to describe monolith catalyst deactivation in SCR**,** provides a quantitative means of tracking deactivation and a potential means of incorporating such deactivation in a combustion simulation code. The model comparisons between the activity of the exposed catalysts and the fresh M1 and M2 catalysts appear below. The Chen model predicts NO conversion (X_{NO}) of an exposed catalyst through the equations (see subsequent section for the derivation of the Chen model):

$$X_{NO} = 1 - \exp\left(-\frac{\sigma_{cat} L}{u A_{cs}} \frac{1}{\frac{1}{k_m} - \frac{1}{(D_e k a)^{1/2}} \frac{\exp(-2\phi)+1}{\exp(-2\phi)-1}} \right) \quad (1)$$

where

$$\phi = \left(\frac{h^2 k a}{D_e} \right)^{1/2} \quad (2)$$

σ_{cat} = perimeter length of a monolith cell
L = monolith length
u = linear gas velocity in cell
A_{cs} = cross-sectional area of a cell
k_m = mass-transfer coefficient
D_e = effective diffusivity of NO
k = first order reaction rate constant
a = activity
Φ = Thiele modulus
h = wall half-thickness

To compare the activities, the reaction rate constants ($\underline{K}$) were found over a range of temperatures for each of the fresh catalysts by setting activity (a) equal to one. The pseudo-first-order Arrhenius' reaction rate pre-exponential factor (A) and activation energy (E_a) for each sample resulted from non-linear least-squares analyses of the measured reaction rate coefficients and temperatures. (Igor Pro® was used to fit the data):

$$k = A \exp\left(-\frac{E_a}{RT} \right) \quad (3)$$

R = ideal gas constant
T = temperature

The results appear in Table 11 and the fit is appears in Figure 33.

Table 11 k_0 and E_a Values.

Catalyst	A ($cm^3/(g*s)$)	E_a (kJ/mol)
M1	$1.06 * 10^{10}$	87.7
M2	$2.65 * 10^{10}$	97.4

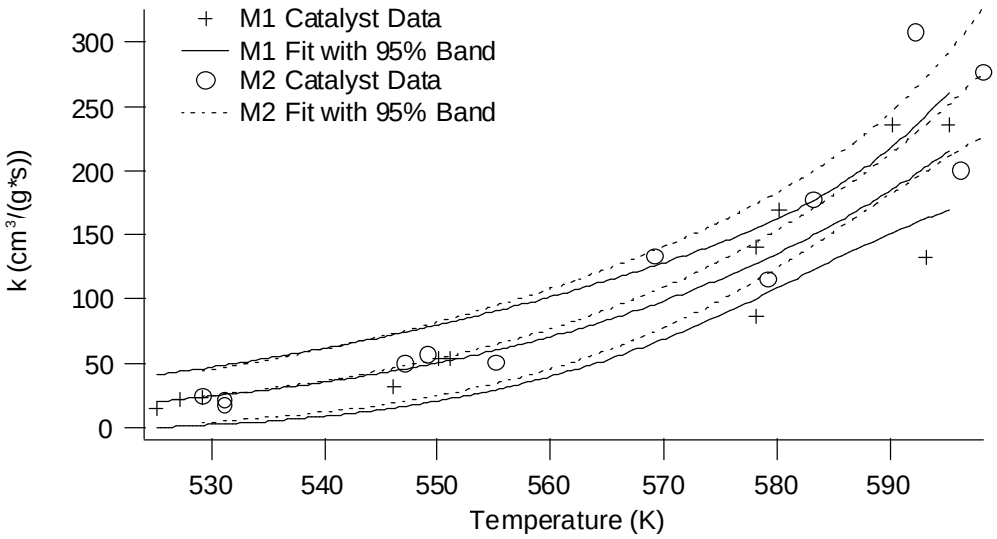

Figure 33 Arrhenius Law Fit for M1 and M2.

By holding the reaction rate coefficients constant, conversion data from the exposed catalysts determine values of the activity factor (a) in the Chen model. These values appear in Table 11. Figure 34 and Figure 35 compare the Chen model fits to the actual data.

Table 12 Activity Factor Fits for Exposed Catalysts.

Catalyst	2063 hr Exposure	3800 hr Exposure
M1	1.029	0.533
M2	1.152	0.413

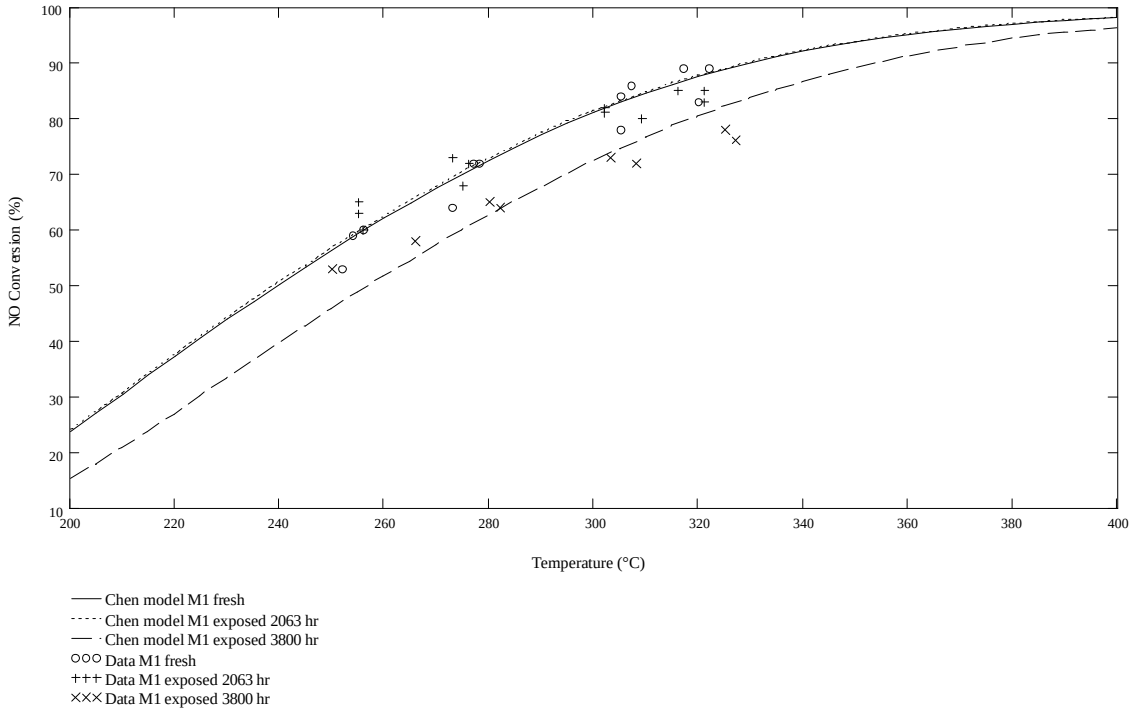

,k

Figure 34 M1 Comparison of Data to Chen Model Prediction.

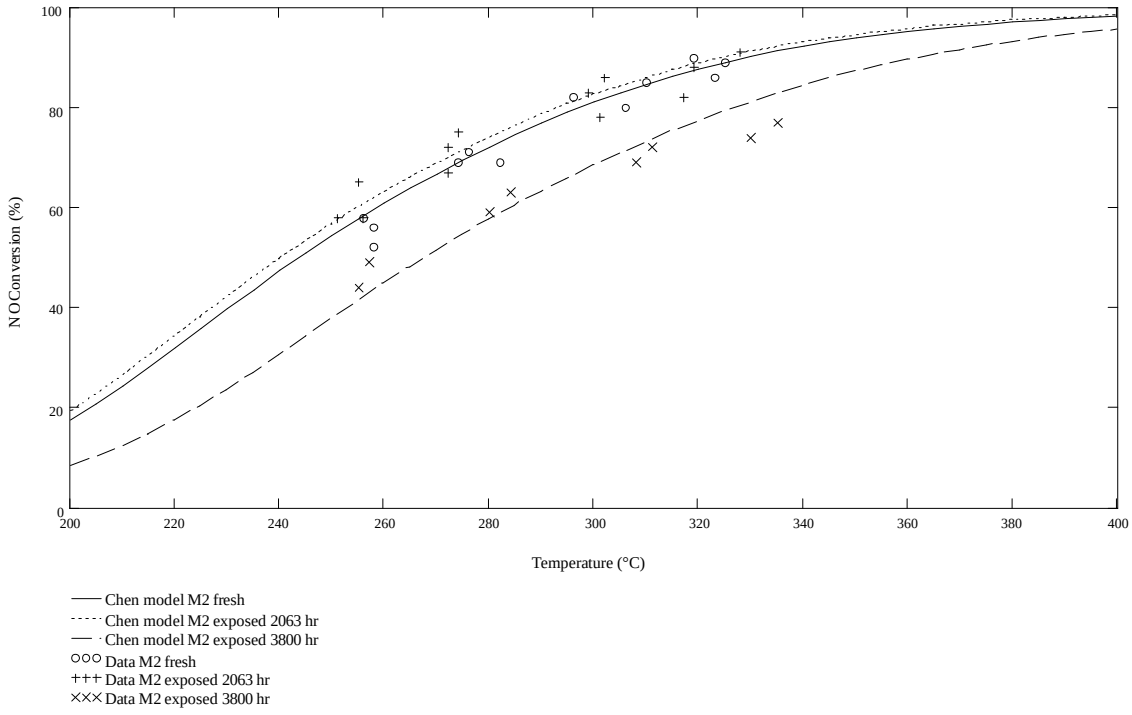

Figure 35 M1 Comparison of Data to Chen Model Prediction.

Values of the activity factor, *a*, from the Chen model, indicate that activity increases slightly after 2063 hours of exposure, presumably due to catalyst sulfation. However, after 3800 hours of exposure the activity decreases significantly. It is as yet unknown if this deactivation is caused by plugging, masking, poisoning, or a combination (see Figure 36).

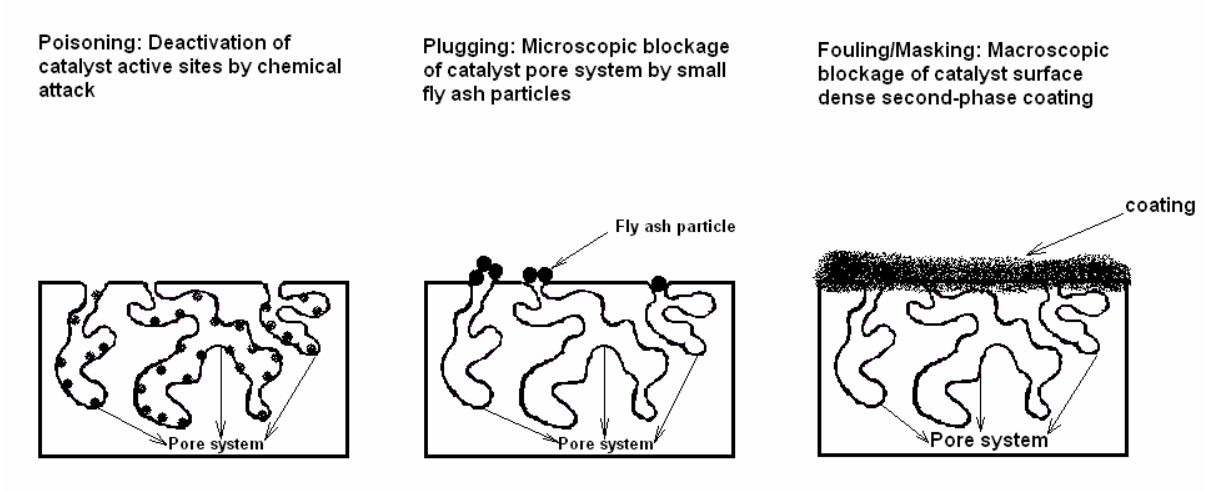

Figure 36 Comparison of Plugging, Masking and Poisoning.

Preliminary comparisons of estimated kinetic activity parameters from the field samples and the laboratory-prepared catalysts indicate that the field samples are approximately 3 times more active than the laboratory samples. However, these results do not account for (a) film resistance in the analysis of the field samples which is almost certainly present, (b) differences in chemical composition between the field and the laboratory samples (field samples contained tungsten whereas the lab samples with which comparisons were made did not), and (c) differences in physical structures (porosity, specific surface areas, etc.).

The derivation of Chen's model is listed in Appendix 3.

The 2063 hour exposed M1 and M2 exhibited slightly higher NO reduction activity than the corresponding fresh catalysts M1 and M2, one explanation is that sulfate species built up on the catalyst surface during the exposure, and brought higher activity to the catalyst. To verify this presumption, the effect of sulfation on titania and vanadia catalyst surface chemistry and NO reduction activity were conducted with an in situ FTIR-MS system. Besides, the effect of poisons including potassium, sodium, and calcium were also investigated. The results were summarized in the following section ISSR.

II ISSR

The purpose of the FTIR-ISSR is to provide definitive indication of surface-active species through *in situ* monitoring of infrared spectra from catalytic surfaces exposed to a variety of laboratory and field conditions. The ISSR provides *in situ* transmission FTIR spectra of SO_2, NH_3, and NO_x, among other species. Adsorption and desorption behaviors of these and other species are monitored. Quantitative indications of critical parameters, including Brønsted and Lewis acidities on fresh and exposed catalysts, are included. Indications of coadsorption of NH_3 and NO_x help elucidate mechanisms and rates of both reactions and deactivation. Much of the existing literature focuses on SCR reactions in SO_2-free environments. A significant effort in the ISSR laboratory relates to analyzing SCR reactions under coal-relevant conditions (SO_2 laden flows).

1. Most ash-derived contaminants and oxide components of the catalyst are exposed to relatively high concentrations of SO_2 under conditions where coals high in sulfur content

are burned (such is the case at many utility boilers in the United States). Sulfates thus formed or deposited on the catalyst surface may profoundly affect surface acidity and hence activity (since the active sites for SCR are thought to include acid functions).

2. Most studies have been conducted either in the absence of SO_2 or under conditions and/or during short periods unfavorable for sulfate formation. Accordingly, it is questionable if these studies are relevant to "realistic" industrial conditions involving long exposures to SO_2 in the presence of water.
3. There are conflicting views in the literature as to whether vanadium species on the catalyst surface are sulfated or not.

This work thus far has focused on the effect of sulfation and poisoning on the vanadia catalyst surface chemistry and NO reduction activity. The objective of the sulfation investigation is to identify the surface sites with which sulfate species interact and the effect of sulfate species on vanadia catalyst activity. Addition of poisons to the catalysts is designed to explore the poisoning mechanism of the vanadia catalyst exposed to similar commercial combustion situations. The accomplishments of previous work are shown in Table 13.

Table 13 Previous finished work as part of the general experiment design

×: work that has been accomplished

	Samples			Adsorption (FTIR)	Reactivity (MS)	Surface Characterization (BET, XPS, SEM, ToFSIMS)
	V%/TiO_2	Poisons	sulfation			
B	0	0	×	2	2	2
Y	0	0		2	2	2
U	1	0	×	2	2	2
|	1	0		2	2	2
P	5	0	×	2	2	2
R	5	0		2	2	2
E	1	K	×	2	2	2
P	1	K		2	2	2
A	1	Na	×	2	2	2
R	1	Na		2	2	2
E	1	Ca	×	2	2	2
D	1	Ca		2	2	2
	Fresh ×6				2	2
Commercial	Front – exposed × 6				2	2
	Tail – exposed × 6				2	2

II.A FTIR quality confirmation

To obtain accurate and detailed information from FTIR, the quality control tests involving comparing system performance with known standards were performed first. NO adsorption on Rh/ZSM5 provides data to compare with previous research results that were obtained with the same FTIR apparatus. The main peaks of NO adsorption on the Rh/ZSM5 catalyst appear at the same spectral position as those observed in the previous experiments, as illustrated in Figure 37 and Figure 38. The new data report results over a wavenumber range shifted somewhat toward the visible compared with the previous results. The two characteristic NO adsorption peaks at 1869 and 1783 cm^{-1} are even clearer than those in the former results.

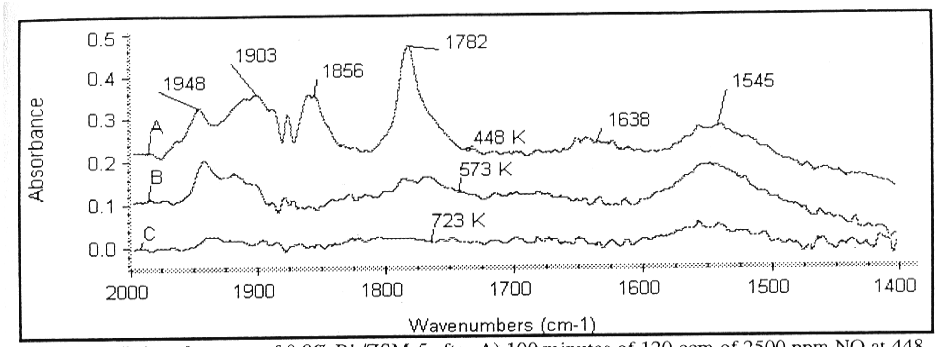

Figure 37 NO adsorption from previous experiment

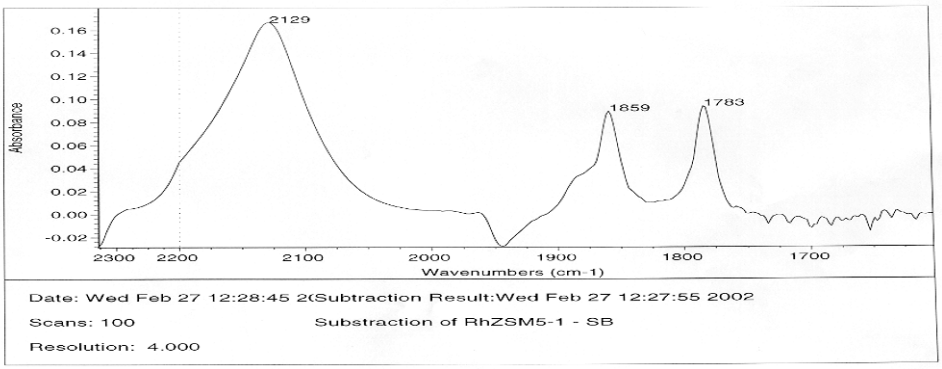

Figure 38 NO adsorption with current FTIR system, total flow = 20 ccm, 1000 ppm NO at 448K.

II.B Sulfation study

With confirmed good detection quality of the current FTIR system, sulfation investigation on titania support and vanadia catalysts was conducted, which involves 24-hour sulfation tests under both dry and wet conditions on TiO_2, 2% V_2O_5/TiO_2, and 5% V_2O_5/TiO_2. *In situ* IR spectra were collected during the sulfation of each sample. Surface chemical compositions of fresh, dry and wet sulfated TiO_2, 2% V_2O_5/TiO_2, and 5% V_2O_5/TiO_2 were obtained from XPS analyses. As results, FTIR spectra indicate that intensities of sulfate peak on vanadia catalysts, an indication of surface sulfate contents, decrease with increasing vanadia content on catalyst surfaces. The XPS surface elemental concentration analysis agrees with FTIR results. Furthermore, XPS analyses indicate that the vanadia oxidation state is 5+ and remains unchanged upon sulfate species addition. This indicates no vanadyl sulfate, the product of sulfated vanadia species with vanadia oxidation state of 4+, forms on the vanadia catalyst surface.

II.B.1. In situ FTIR investigation

Many sulfation tests have been conducted and knowledge about sulfation was gained (for example, CaF_2 window should be used during sulfation which won't be sulfated as KCl or NaCl windows did. For XPS analysis, the original pellet sample should be tested instead of grinded powder catalyst from the original pellet). After a large amount of preliminary sulfation tests were conducted and data collected, final sulfation conditions were determined, as summarized in Table 14.

Table 14 Sulfation conditions for TiO_2, 2 and 5% V_2O_5/TiO_2 under both wet and dry conditions

Sample Name	Sample Details	Notes	Gas Stream Composition, %				Flow (sccm)	Temp (°C)
			He	O_2	SO_2	H_2O		
VTOD	5% V_2O_5/TiO_2	Preoxidation	88.2	11.8		0	56.7	380
		24 Hours Sulfation	89.01	10.72	0.27	0	62.3	380
VTOF	2% V_2O_5/TiO_2	Preoxidation	88.2	11.8		0	56.7	380
		24 Hours Sulfation	89.01	10.72	0.27	0	62.3	380
TiO8	TiO_2	Preoxidation	88.2	11.8		0	56.7	380
		24 Hours Sulfation	89.01	10.72	0.27	0	62.3	380
VTHF	5% V_2O_5/TiO_2	Preoxidation	88.2	11.8		0	56.7	380
		24 Hours Sulfation	87.33	10.51	0.267	1.88	63.54	380
VTHG	2% V_2O_5/TiO_2	Preoxidation	88.2	11.8		0	56.7	380
		24 Hours Sulfation	87.33	10.51	0.267	1.88	63.54	380
TiO9	TiO_2	Preoxidation	88.2	11.8		0	56.7	380
		24 Hours Sulfation	87.33	10.51	0.267	1.88	63.54	380

a. Sulfate peak identification

During the sulfation, only one peak located at around 1370 cm^{-1} appears in the IR spectrum for all the samples including 0, 2, and 5% V_2O_5/TiO_2. Figure 39 illustrates the IR confirmation of this only peak formed during the sulfation. Literature has designated this peak originated from S=O stretching mode of the surface sulfate, therefore, sulfate species formed on 5% vanadia catalyst during the sulfation. This sulfate species formation has been observed on TiO_2, 2 and 5% V_2O_5/TiO_2 under both dry and wet sulfation.

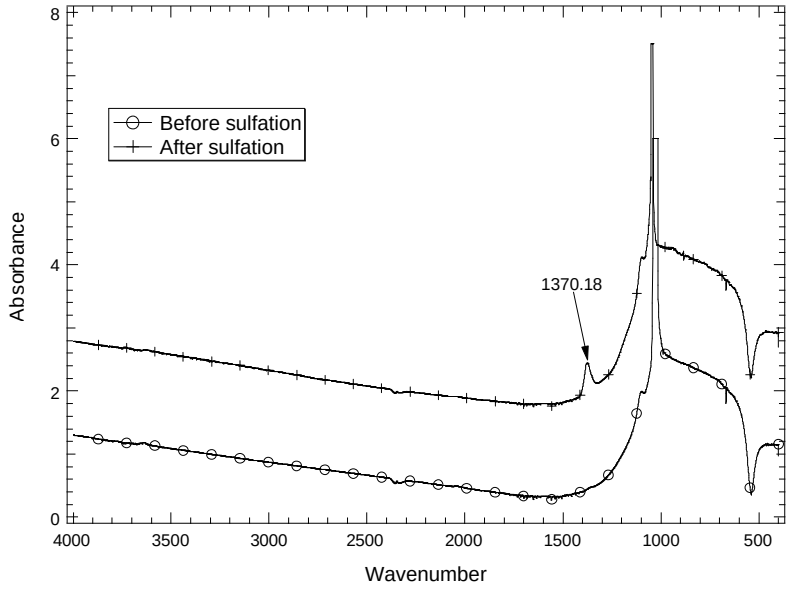

Figure 39 IR spectra comparison of 5% V_2O_5/TiO_2 before and after sulfation

Figure 40-Figure 45 summarize the *in situ* IR spectra collected during the sulfation of each sample.

b. Dry sulfation of 5 and 2% V_2O_5/TiO_2, and TiO_2

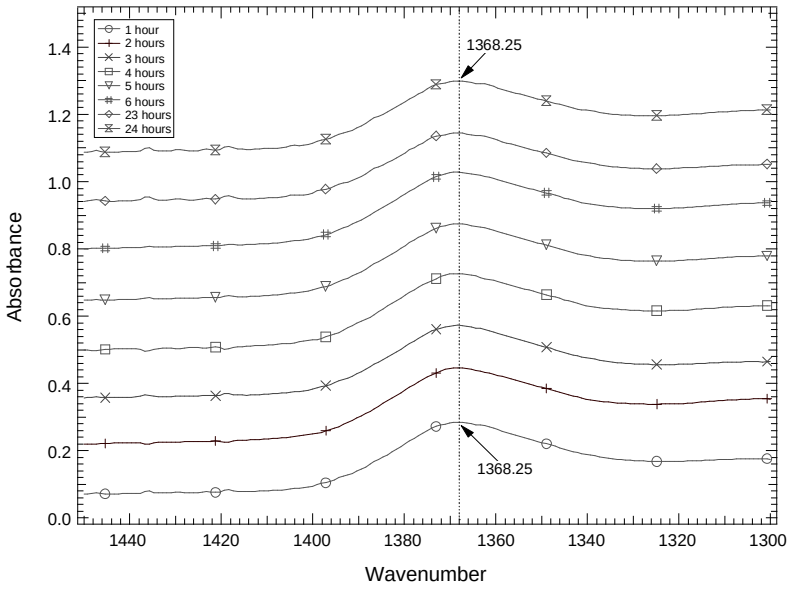

Figure 40 ***In situ*** **IR spectra of dry sulfation on 5% V_2O_5/TiO_2. (VTOD)**

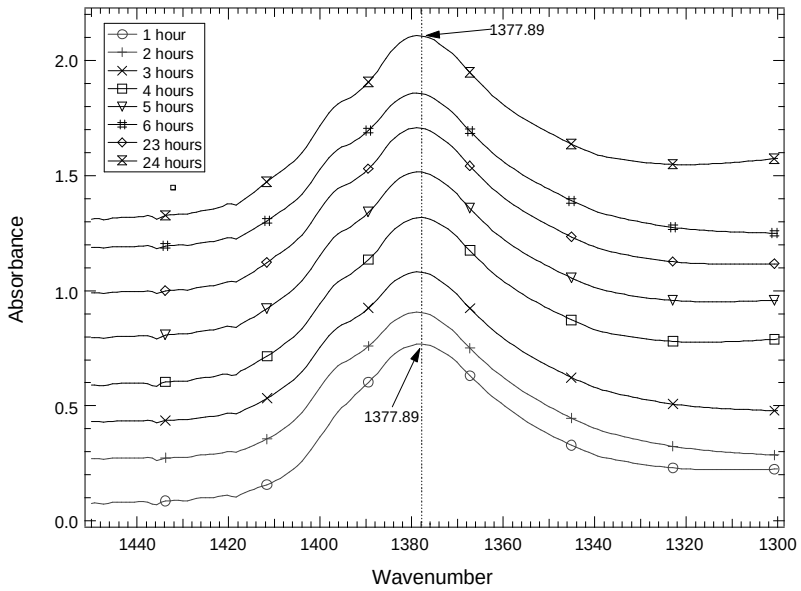

Figure 41 ***In situ*** **IR spectra of dry sulfation on 2% V_2O_5/TiO_2. (VTOF)**

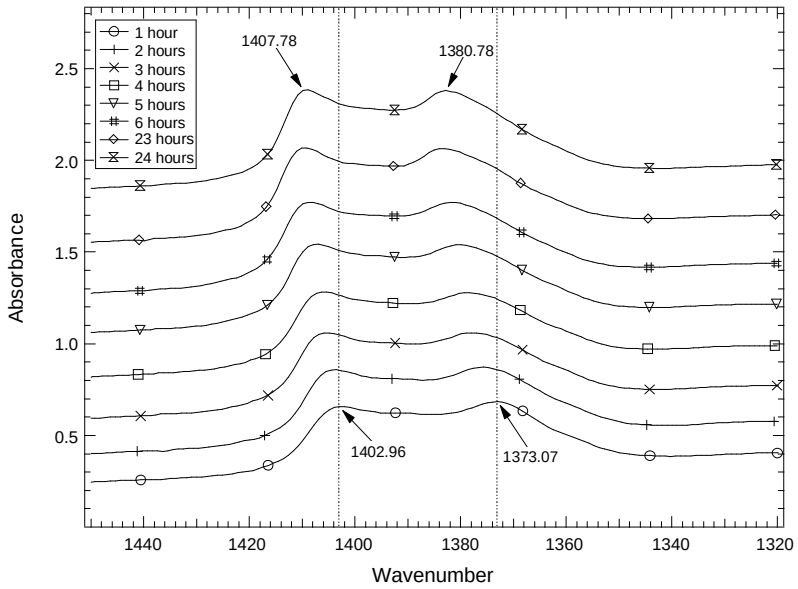

Figure 42 ***In situ*** **IR spectra of dry sulfation on TiO_2. (TiO7B)**

c. Wet sulfation of 5 and 2% V_2O_5/TiO_2, and TiO_2

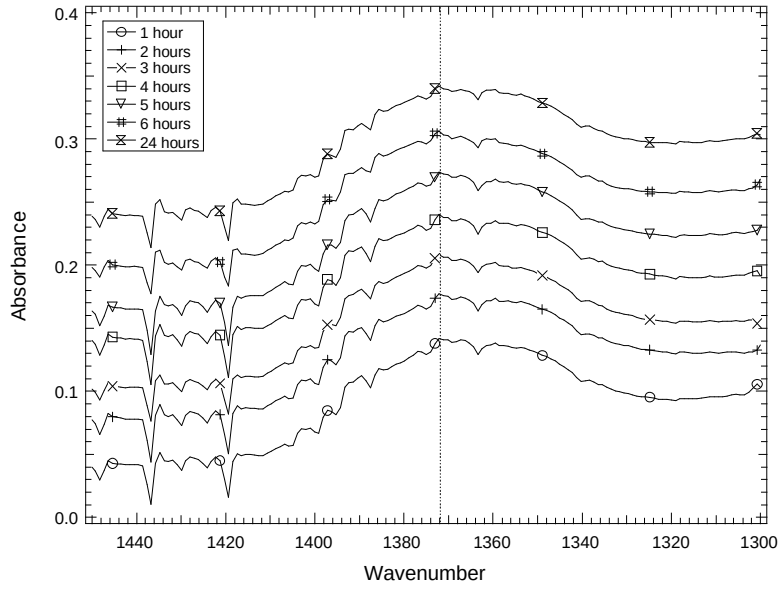

Figure 43 ***In situ*** **IR spectra of wet sulfation on 5% V_2O_5/TiO_2. (VTHF)**

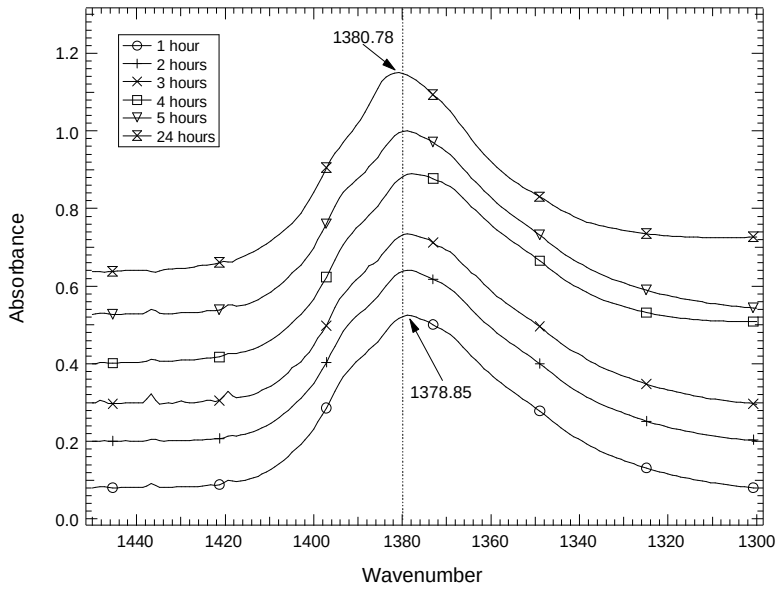

Figure 44 ***In situ*** **IR spectra of wet sulfation on 2% V_2O_5/TiO_2. (VTHG)**

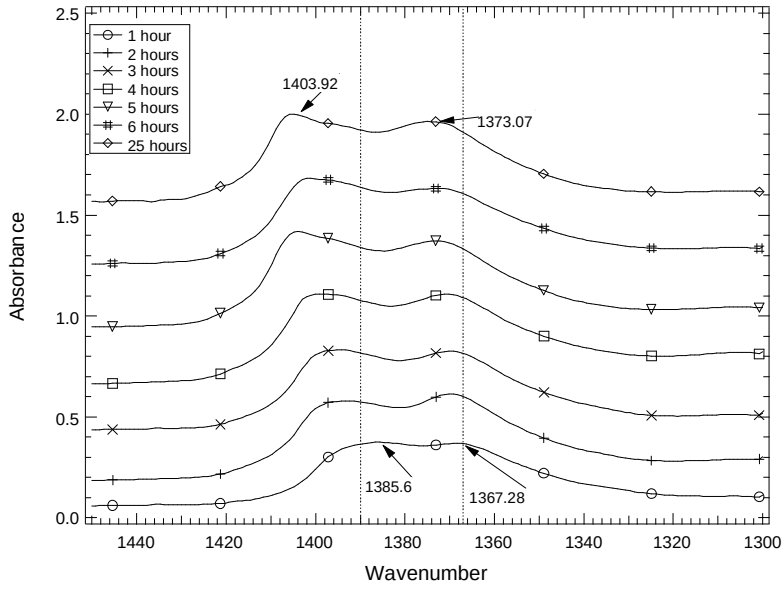

Figure 45 ***In situ*** **IR spectra of wet sulfation on TiO_2 (TiO5)**

d. Sulfated peak intensities vary with various vanadium contents on the catalyst surface

Comparing the sulfate peaks collected during dry and wet sulfation on all samples, the peak intensities in the IR spectra increase with decreasing vanadia content. Figure 46 illustrates the comparison of sulfate peak areas after 24 hour sulfation, which provides more quantitative observations, which is that generally the sulfate peak area decreases with increasing vanadia content on the catalyst surface, except the last point, which represents the sulfate peak area of the wet sulfated 5% V_2O_5/TiO_2. This observation indicates that the presence of vanadia species does not favor the sulfation species formation on the catalyst surface. Therefore, the sulfate species may not form on the vanadia sites, but instead on the titania sites.

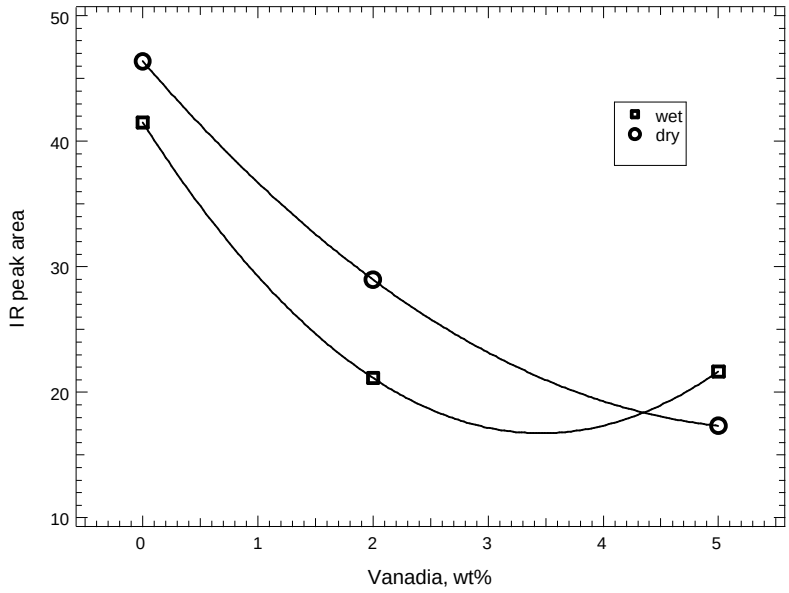

Figure 46 Sulfate peak area comparison

Moreover, this indication also provides a possible explanation for the larger sulfate peak area of wet sulfated 5% V_2O_5/TiO_2 than that of dry sulfated 5% V_2O_5/TiO_2, which is that water may assist the vanadia species migration on the catalyst surface during the sulfation. Vanadia is a highly mobile species on the catalyst surface, it exists as a liquid phase at high temperatures, such as 400 ˚C during the catalysis of sulfuric acid production. And the vanadia species should exhibits a highly mobility at the sulfation temperature of 380 ˚C, this mobility should be higher in wet conditions than in dry conditions. Therefore, with a relatively higher vanadia concentration on the catalyst surface, it may be easy to for the vanadia species to agglomerate, and more surface sites are exposed and available for the sulfate species interact with, if sulfate species does not interact with surface vanadia species but with the titania support.

e. Water effect on sulfate IR peak

On the other hand, the IR sulfate peak areas of wet sulfated samples are smaller than those of the dry sulfated samples for both TiO_2 and 2 % V_2O_5/TiO_2, it seems water decrease the sulfate peak intensity. Moreover, water is observed to be able to remove the 1375 cm^{-1} sulfate peak at 375 ˚C, and this peak appears after dehydration. Therefore, water definitely diminishes the IR activity of this sulfate peak.

This maybe due to the fact that water changes the sulfate structure, thus change the vibration mode of hydrated sulfate, resulting in the decrease of sulfate IR peak area. R.T. Yang *et al.*[23] and O. Saur *et al.* [43] suggested that the structure of sulfate on the titania surface is $(M\text{-}O)_3S{=}O$ under dry conditions, while they change to bridge bidentate $(M_2SO_4)H$ under wet conditions based on their isotope exchange and IR results. This well explained the 1375 cm^{-1} sulfate peak in IR spectra, which is designated to S=O vibration, are diminished to some degree after water introduction, as S=O bond is changed to $S\text{-}O_2H$, as shown in Figure 47.

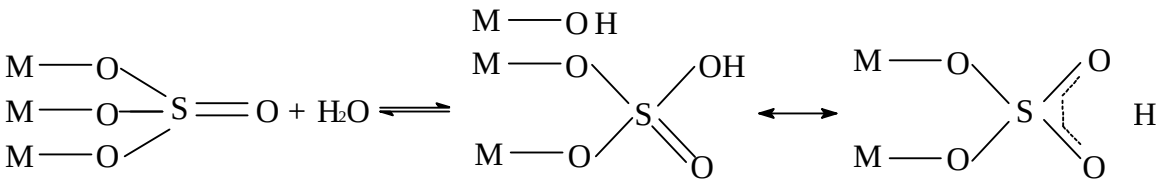

Figure 47 Sulfate transformation between dry and wet conditions

f. Doublet sulfate peak from TiO_2.

Doublet sulfate IR peak signals appear on sulfated titania samples under both dry and wet sulfation conditions, and this sulfate peak increases gradually with time. A doublet peak is also reported in Yang et al.'s work, although their IR peak around 1380 cm^{-1} is more intense than the one around 1401 cm^{-1} [33]. Our results, on the other hand, showed the IR peak around 1401 cm^{-1} to be more intense. Moreover, the peak positions shifted to higher frequencies with increasing time during the sulfation test, indicating increasing sulfate acidity with time/surface coverage.

II.B.2. XPS analysis comparison

The XPS technique measures composition of surface and near-surface layers on the exterior of catalyst particles. Results of XPS analyses for all six samples after 24-hour exposure to dilute SO_2 are summarized in Table 15. The third column of the table identifies the element and its electronic orbital analyzed by XPS.

The sulfur binding energies of all the six samples are around 168.5~169.5eV. As the change in the backscatter energies (BE) of sulfur in the XPS analysis is insignificant, which could be introduced by the instrument error during the measurement, therefore, sulfur in all three samples should be in the same oxidation state. Moreover, the binding energy around 168.5~169.5eV indicates that the sulfur species on the catalyst surface should be sulfate, which forms during the sulfation on both titanium dioxide and vanadia catalyst surface under either dry or wet conditions, no other sulfur compounds form. This conclusion agrees with the *in situ* FTIR results that also indicate only one sulfate species which more related to titanium dioxide than vanadia is produced on the surface of samples during sulfation test.

Table 15 XPS results

Sample	Elements	B.E.	Atom %	Sample	Element	B.E.	Atom %
5VTO 5% V, sulfation without water	C1s	285.00	24.2	5VTH 5% V, sulfation with water	C 1s	285.00	5.3
	O1s	533.99	56		O 1s	533.39	65.8
	S2p	168.46	1.5		S 2p	168.55	2.8
	Ti2p	458.19	16.5		Ti 2p	458.14	20.2
	V 2p3/2	516.72	3.3		V 2p3/2	516.68	3.3
2VTO 2% V, sulfation without water	C 1s	285.00	8.3	2VTH 2% V, sulfation with water	C 1s	285.00	10.1
	O 1s	533.74	67.7		O 1s	530.63	65.2
	S 2p	168.97	2.1		S 2p	169.25	2.4
	Ti 2p	458.16	20.9		Ti 2p	458.72	20.2
	V 2p3/2	516.36	1.9		V 2p3/2	517.24	2.1
TiO_2-O Titanium dioxide, sulfation without water	C 1s	285.00	8.7	TiO_2-H Titanium dioxide, sulfation with water	C 1s	285.00	10.2
	O 1s	529.48	66.4		O 1s	530.48	70.7
	S 2p	168.47	2.8		S 2p	169.50	3.4
	Ti 2p	458.42	23.2		Ti 2p	459.50	15.6

Sulfur content versus vanadia concentration on the catalyst surface from XPS analyses was plotted in **Figure 48**.

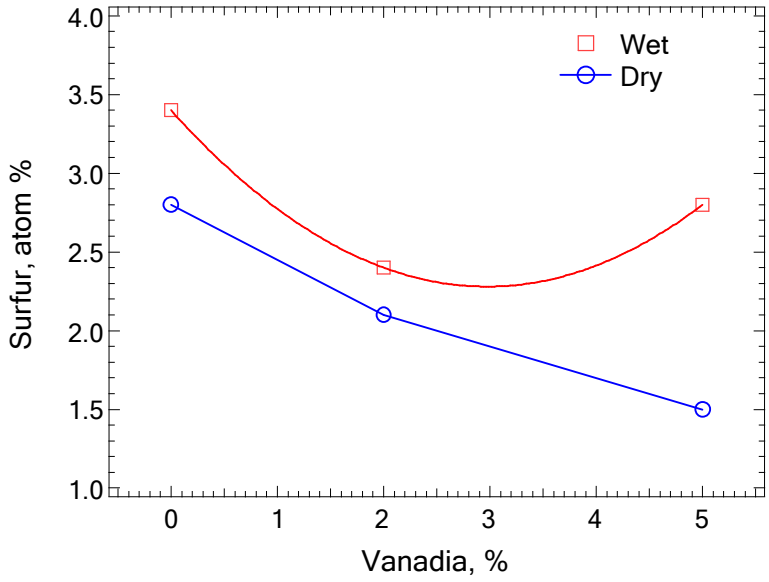

Figure 48 Sulfur content on TiO_2 and V_2O_5/TiO_2 as determined by XPS

The XPS results show that the sulfur content decreases with increasing vanadia concentration on the catalyst surface. This result agrees with the observation from *in situ* FTIR analyses, where the peak featured at 1370-1375 cm^{-1} in the FTIR spectra, decreased with increasing vanadia content on the catalyst surface. This peak is essentially not present on 5% vanadia catalyst during and after the sulfation moist test. Therefore, XPS results also indicate that vanadia species do not favor the sulfation.

Water apparently enhances accumulation of sulfur on both the titanium dioxide support and vanadia catalysts, especially above 2% percent vanadia content. For either dry or wet sulfation, the highest sulfur content was obtained on titanium dioxide. Vanadia catalyst sulfur

content is smaller relative to that of sulfated titanium dioxide; but it is still a major constituent on the surface. Noticeably, in the absence of water vapor, sulfur content decreases linearly with increasing vanadia content on the catalyst surface, although different trend obtained in wet sulfation. The sulfur content decreases on 2% vanadia catalyst compared to that on titanium dioxide, but it increases a little on 5% vanadia catalyst surface while is still lower than that on titanium dioxide in case of wet sulfation.

It is interesting to notice that in case of dry sulfation, both sulfate IR peak areas and surface atomic sulfur contents decrease almost linearly with increasing surface vanadia content. Under wet sulfation conditions, the sulfate IR peak areas and surface atomic sulfur contents decrease first then increase with increasing surface vanadia content. It could be due to the same reason mentioned before that with relative high vanadia content under wet conditions, vanadia species on the catalyst is more ready to agglomerate and provides more surface sites for sulfation. No matter it is from wet or dry sulfation, the largest sulfate peak area or sulfur content was obtained in pure titanium dioxide.

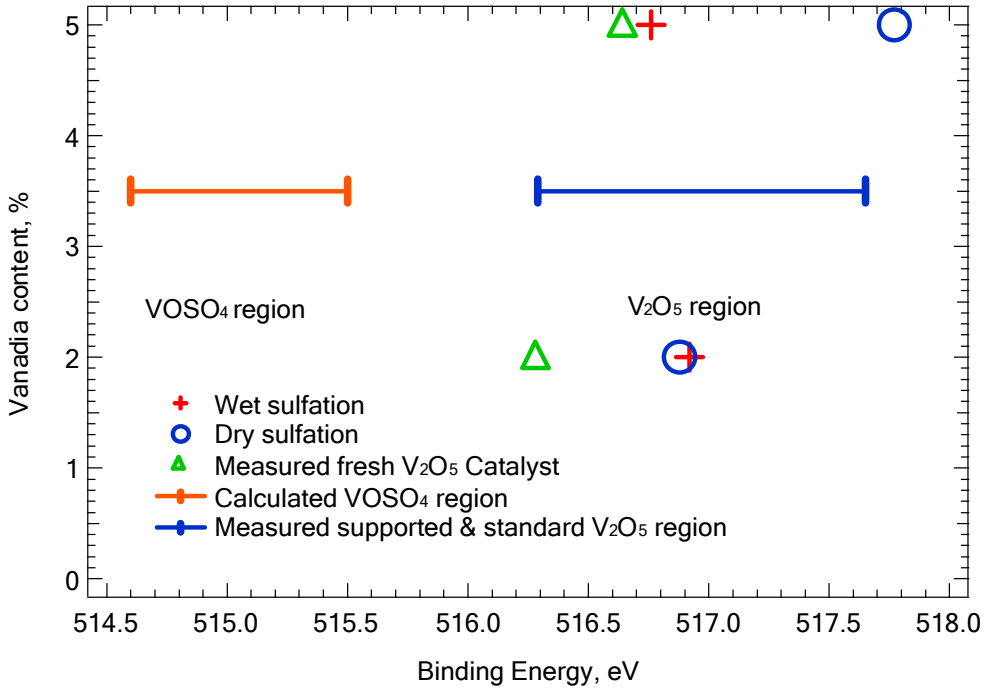

Figure 49 XPS binding energies for wet and dry sulfated vanadia catalysts

Vanadium in an unsulfated SCR catalyst exists as vanadia, or vanadium pentoxide (V2O5) with vanadium in a +5 oxidation state. Thermochemical equilibrium predictions suggest that vanadium in the presence of gas-phase SO2 forms vanadyl sulfate (VOSO4) in which the oxidation state of vanadium is +4. Vanadium sulfate (V(SO4)2), predicted to exist at higher temperatures in the presence of gas-phase SO2 also includes vanadium in the +4 oxidation state. Therefore, all reasonably expected sulfation products of vanadium pentoxide reduce the vanadium oxidation state from +5 to +4.

X-ray photon spectroscopy (XPS) measures surface composition and oxidation state, the latter being measured in terms of binding energy. XPS results (Figure 49) from catalysts exposed to SO2 under commercially relevant conditions indicate that both 2 and 5% vanadia catalysts, whether sulfated under dry or wet conditions, include vanadium in a +5 oxidation

state, consistent with the spectroscopy-based conclusion that sulfate does not sulfate reported last quarter.

The existence of the surface vanadium in a non-equilibrium state is not surprising for several reasons. These include; (1) the system is actively reacting and therefore clearly not in equilibrium, although it could possible be in local equilibrium; (2) the thermochemical properties used to predict the equilibrium condition are based on bulk samples – small surface grains introduce forces on the compounds that can and commonly do shift equilibrium from the bulk condition; and (3) the accuracy of the predictions does not include non-ideal interactions or other features that could compromise its accuracy.

Subsequent NH3 and NO adsorption tests were conducted to study the effects of sulfation and poisons on the catalysts acidity and surface chemistry.

II.C NH_3 adsorption comparison

II.C.1. NH3 adsorption comparison with various V%

1000ppm ammonia is ready to adsorb on fresh titania, 1 and 2 % V2O5/TiO2 at room temperature. Figure 50 compares ammonia adsorption on the catalyst surface vanadia content varying from 0 to 2%. Ammonia adsorbed on Lewis acid sites appears at 1602 and 1301 cm-1, while NH3 adsorbed on Brønsted acid sites appears at 1444 cm-1. Adsorption on Lewis acid sites occurs most prominently for the fresh TiO2 and to significantly lower extent on 1% V2O5/TiO2 catalysts. There is no indication of adsorption on Lewis sites in the 2% sample. However, all three samples show substantial adsorption on Brønsted sites and the adsorption intensity increase upon addition of more vanadia species on the catalyst surface. Therefore, the results indicate that the addition of vanadia decreases the amount of Lewis acid sites, and increases the amount of Brønsted acid sites. Moreover, an adsorption peak at 1568.8 cm-1, which is assigned to amide (–NH2) species, was observed on titania, but not on 1% and 2% vanadia catalysts.

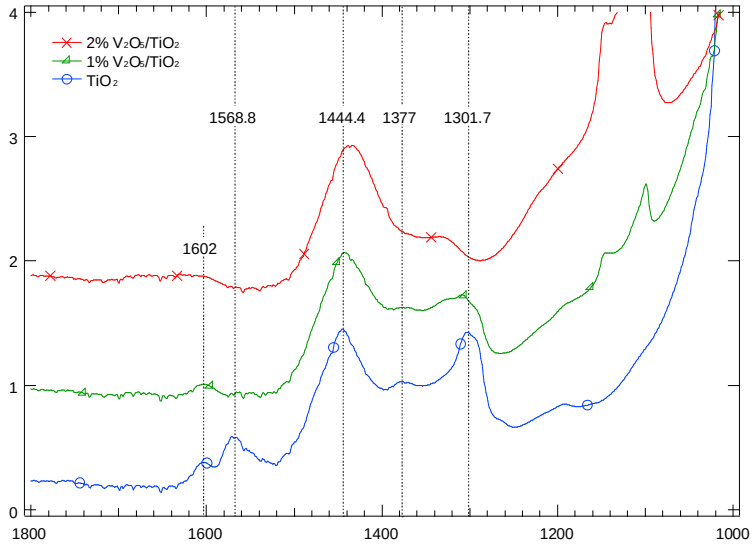

Figure 50 from QR 16

These results illustrate that commercial, non-sulfated catalysts (typically about 1% vanadia) exhibit primarily Brønsted acid activity with respect to ammonia adsorption.

II.C.2. With different S%

1000ppm ammonia adsorption was also compared on fresh and sulfated samples, as shown in Figure 51~Figure 54.

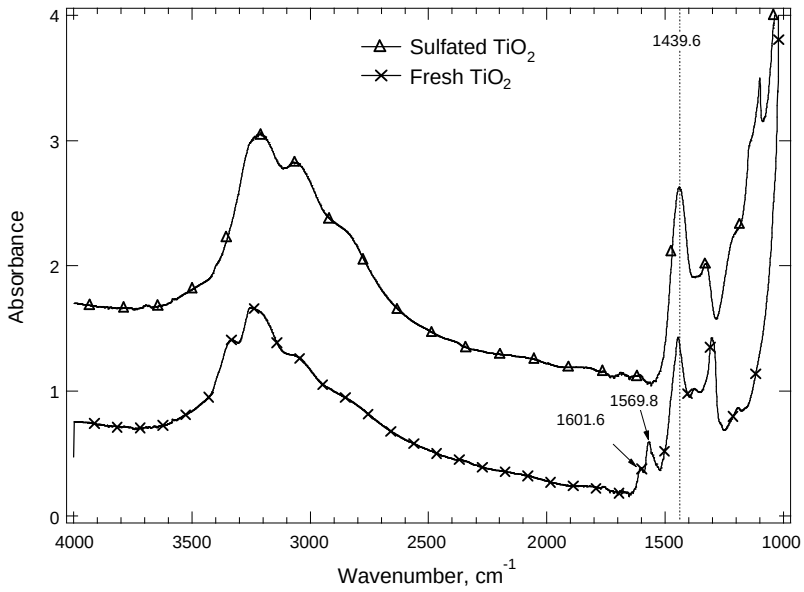

Figure 51 TiOA

On fresh titania, as shown in Figure 51, four major ammonia adsorption peaks appear. Peaks at 1601 and 1302.7 cm-1 correspond to coordinately adsorbed ammonia on Lewis acid sites, the peak at 1440 cm-1 is due to ammonia chemisorbed on Brønsted acid sites, and the peak at 1569.8 is from amide (–NH2) species. On 24-hour sulfated titania, only chemisorbed ammonia on Brønsted acid sites at 1440 cm-1 can be observed, and is more intense than that

from fresh titania. Therefore, sulfation reduces the number of Lewis acid sites and increases the number of Brønsted acid sites on the titania surface. It is possible that sulfate species transform Lewis acid sites into Brønsted acid sites on the titania surface.

Similar results were observed by comparing ammonia adsorption on fresh and sulfated 1, 2 and 5% V2O5/TiO2, as shown in Figure 52, Figure 53, and Figure 54 correspondingly. Weakly coordinated adsorbed ammonia on Lewis acid site appears on fresh 1% V2O5/TiO2, while only chemisorbed ammonia on Brønsted acid sites appears on the same catalyst sulfated for 24 hours. And only chemisorbed ammonia on Brønsted acid sites for 2 and 5% catalyst was detectable, and this adsorption was intensified after sulfation on each sample, therefore, the above results further confirmed that sulfates reduce the amount of Lewis acid sites and increase the amount of Brønsted acid sites, but not the acid sites acidity because the ammonia adsorption peaks remain at the same wavenumber before and after sulfation.

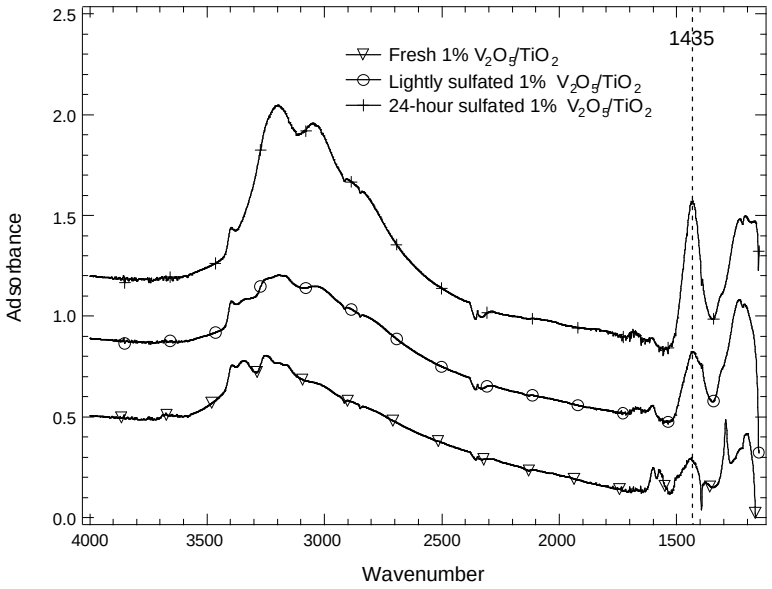

Figure 52 VTOP2

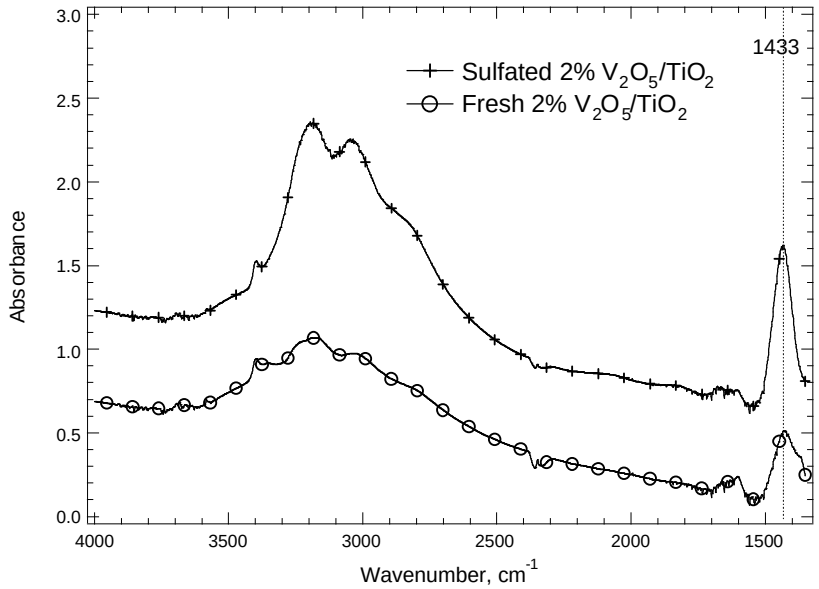

Figure 53 VTOM

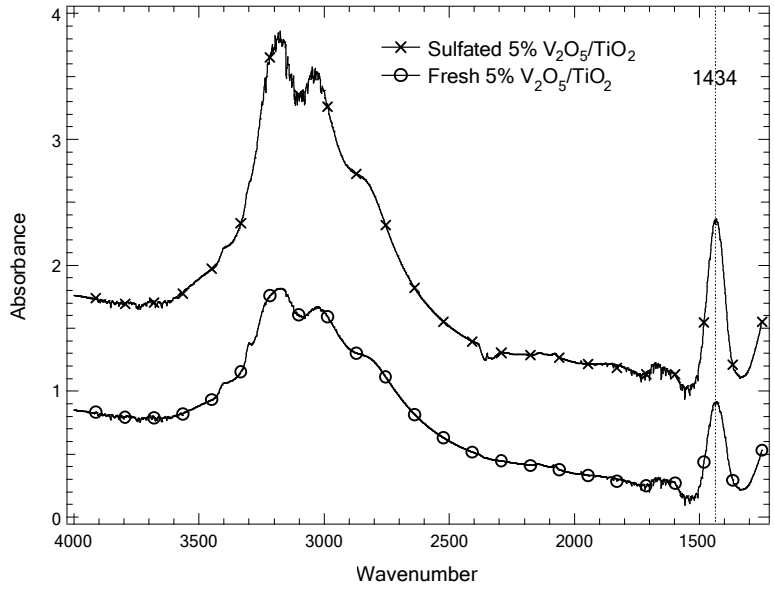

Figure 54 NH_3 ads on 5V

Previous results indicate that vanadia does not sulfate. Those results, combined with these results, indicate that surface sulfation decreases Lewis acid site concentrations for all catalysts thus far studied, confirming that catalytic activity under commercial coal-based SCR conditions occurs primarily on Brønsted acid sites and would be susceptible to decrease by basic impurities such as alkali and alkaline earth oxides, chlorides, and sulfates.

II.C.3. At different T----desorbs completely at 300 ˚C

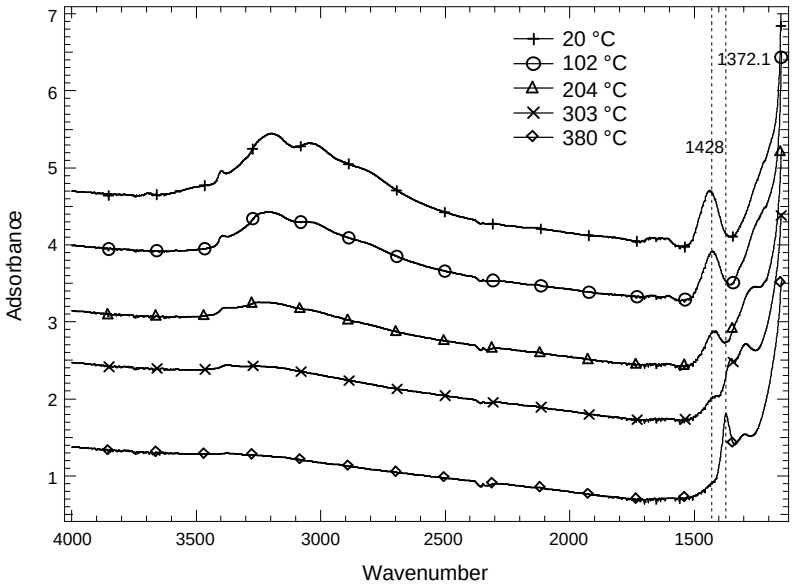

Figure 55 VTOO

Figure 55 shows 1000 ppm ammonia (helium balance) adsorption on sulfated 1% V2O5/TiO2 at different temperatures from 20-380 ˚C. The intensity of the ammonia adsorption peak decreases with increasing temperature, which indicates that ammonia gradually desorbs from the catalyst surface as the temperature slowly increases at a ramp rate of 5 ˚C/min. After the temperature reached 300 ˚C, ammonia desorbs from the surface completely, finally when temperature was 380 ˚C, sulfated peak (1372 cm-1) appears again.

II.C.4. Tungsten (W) effect

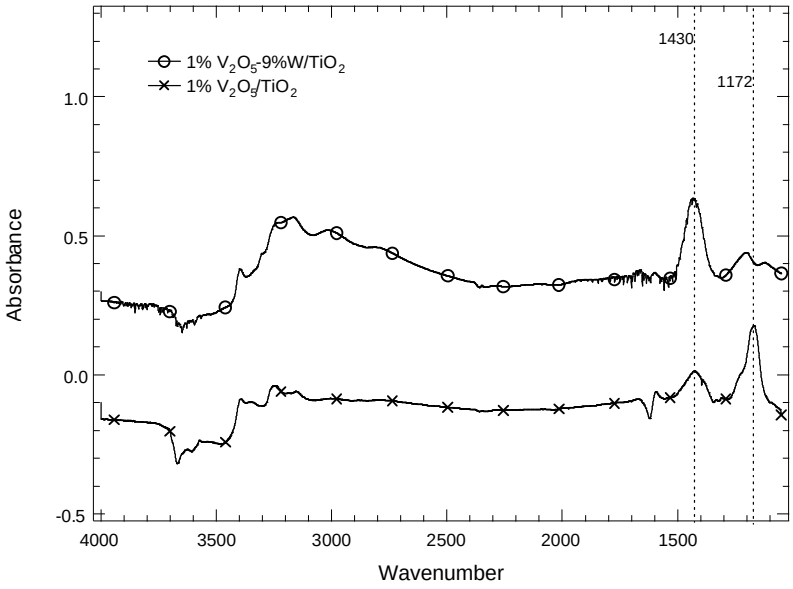

Figure 56 VWTA

In the above figure, the ammonia adsorption peak at 1172 cm-1 represents ammonia adsorption on Lewis acid sites, and the adsorption peak at 1430 cm-1 is from ammonia adsorption on the Brønsted acid sties. The tungsten addition or existence apparently decreases the ammonia adsorption on Lewis acid sites, probably because tungsten consumes the Lewis acid sites, and increases ammonia adsorption on Brønsted acid sites, and probably more Brønsted acid sites was created. Therefore tungsten may remove or occupy some Lewis acid sites, and create more or some new Brønsted acid sites on the catalyst surface.

II.C.5. Fresh vs. Contaminated samples

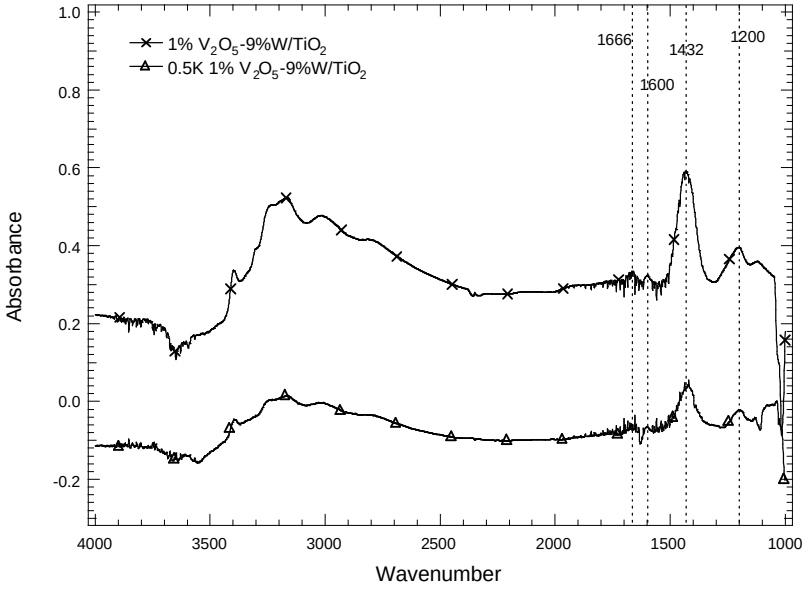

Figure 57 VWTA

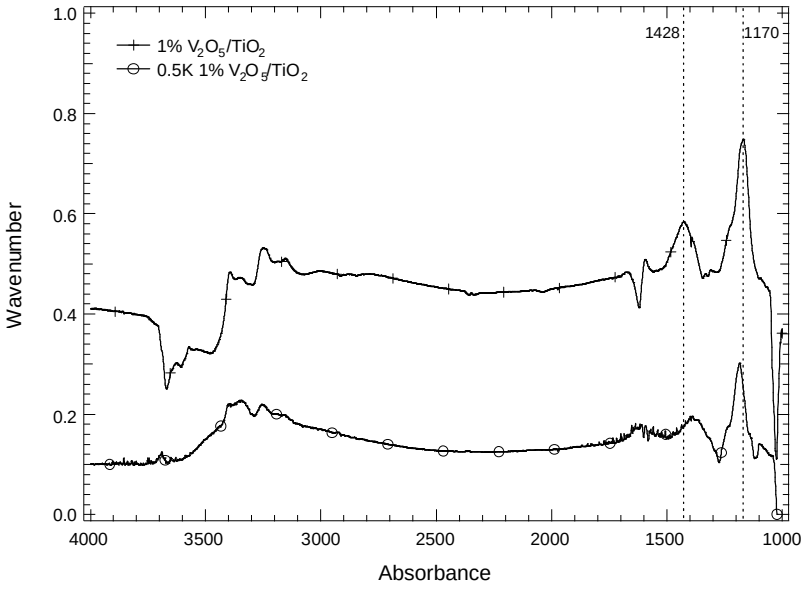

Figure 58 VWTA

In Figure 57 and Figure 58, the top line represents IR peak of ammonia adsorbed on fresh catalysts, and the bottom line is from NH3 adsorption on 0.5 K doped catalysts. It is obvious

that the addition of potassium to the vanadia catalyst decreases the intensities of ammonia adsorption on both the Brønsted and Lewis acid sites. Table 16 summarizes how the ammonia adsorption intensity, which is reflected by IR peak area, decreases by about 20% on Brønsted acid sites, 40% on Lewis acid sites on 1% V2O5/TiO2, and 56% on both Brønsted and Lewis acid sites on 1% V2O5 -9%W/TiO2 upon potassium addition. Moreover, the 1424 cm-1 IR peak, which stands for ammonia adsorption on the Brønsted acid site, shifts down to a low wave number on the 1% V2O5/TiO2 catalyst, but remains at the same position on the 1% V2O5 -9%W/TiO2. This phenomenon indicates that K addition decreases the Brønsted acid site acidity on the 1% V2O5/TiO2 catalyst surface, but has little effect on the Brønsted acid site acidity on the 1% V2O5 -9%W/TiO2, probably because tungsten helps to protect Brønsted acid site on the vanadia catalyst. On the other hand, potassium has a negligible effect on the Lewis acid site acidity because the IR peak at 1170 cm-1 remains at almost the same before and after K addition.

Table 16 NH_3 adsorption IR peak area comparison

Catalysts	IR Peak Area	
	1424 cm^{-1}	1170 cm^{-1}
1% V_2O_5/TiO_2	10.3	22
0.5 K doped 1% V_2O_5/TiO_2	8.6	13.3
1% V_2O_5 -9%WO_3/TiO_2	24.54	4.482
0.5 K doped 1% V_2O_5 -9%WO_3/TiO_2	10.8	1.964

II.C.6. NO adsorption comparison

During the NO adsorption experiment, 1000ppm NO in argon was introduced to the sample at room temperature (20 ˚C). It is found that NO adsorption is only observable with the oxygen presence.

II.C.7. With different V%

NO adsorption IR bands appear at room temperature on non-sulfated V2O5/TiO2 catalysts with vanadia content ranging from 0-5 %, as illustrated in Figure 59. The NO adsorption bands appear at the same frequencies for all catalysts, suggesting that the same adsorbed NO species form on all samples. These bands correspond to surface nitrate species[44].

Most researchers have observed NO adsorption on pure TiO2 and on reduced vanadia catalysts, but not on fully oxidized vanadia catalysts [12, 18, 23]. The V2O5/TiO2 used in this experiment had been preoxidized at 400 ˚C for 4 hours before NO adsorption; therefore,

the vanadia valence should be 5+. Thus, NO adsorption was observed on fresh vanadia catalysts.

The amount of adsorbed NO, which is proportional to the NO adsorption peak area, decreases with increasing vanadia content on the titania surface, as shown in Table 17. It seems that addition of vanadia species suppresses NO adsorption. The strongest NO adsorption happens on the fresh titania support surface, whereas the NO adsorb weakly on the 5% vanadia catalyst. One possible explanation for this observation is that vanadia species occupy the same surface site that NO interact with, which could be surface OH- group on the titania support.

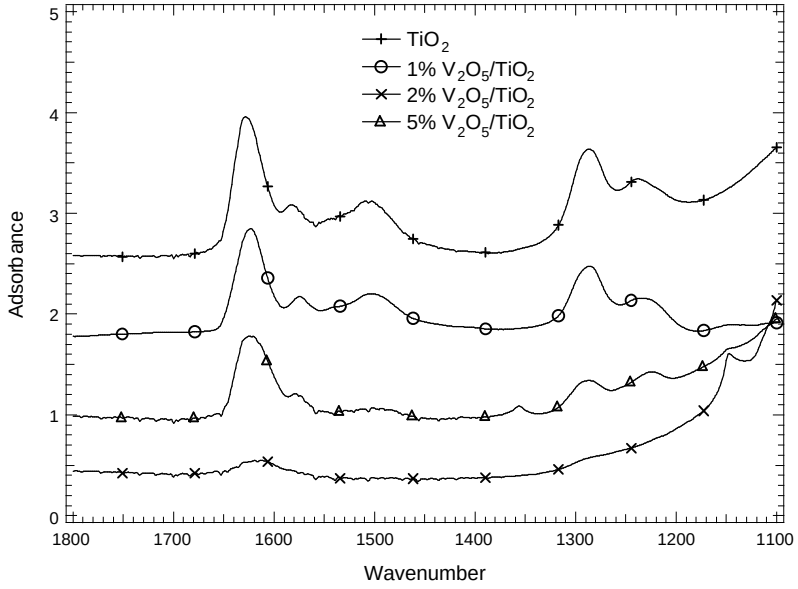

Figure 59 NO adsorption comparison

Table 17 Room-temperature NO adsorption peak area comparison on fresh TiO_2 and vanadia catalysts

	1630-1570 cm^{-1}	~1500 cm^{-1}	1285-1220 cm^{-1}
Pure TiO_2	45.41	15.19	48.14
Fresh 1% V_2O_5/TiO_2	43.29	9.78	24.23
Fresh 2% V_2O_5/TiO_2	43.64	2.46	17.3
Fresh 5% V_2O_5/TiO_2	8.07		

II.C.8. With different S%

Figure 60 shows the NO adsorption on 1% V2O5/TiO2 with various sulfation degrees. NO adsorption peaks on the fresh 1% V2O5/TiO2 catalyst are intense, but decrease with

increasing sulfation time. It seems sulfate species inhibits NO adsorption, or sulfate species may occupy the surface sites for the NO adsorption.

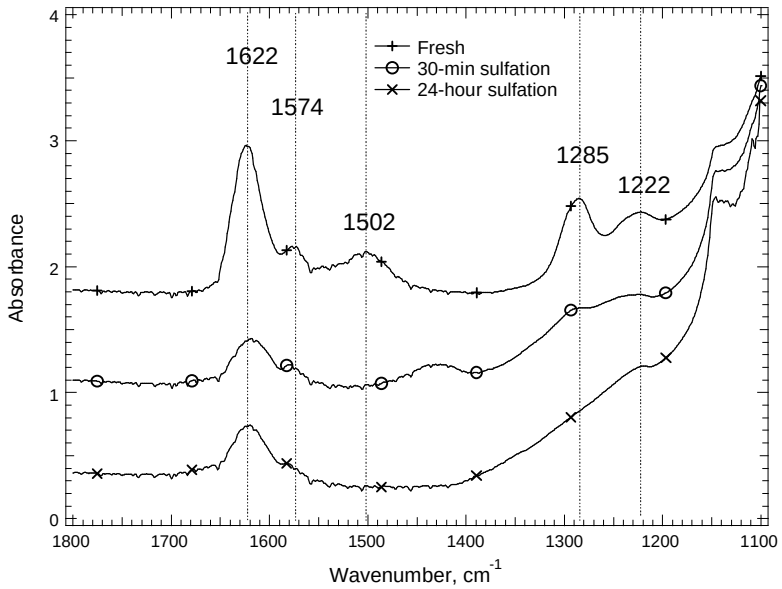

Figure 60 NO adsorption comparison on 1% V_2O5/TiO_2 with various sulfation degrees (VTOL)

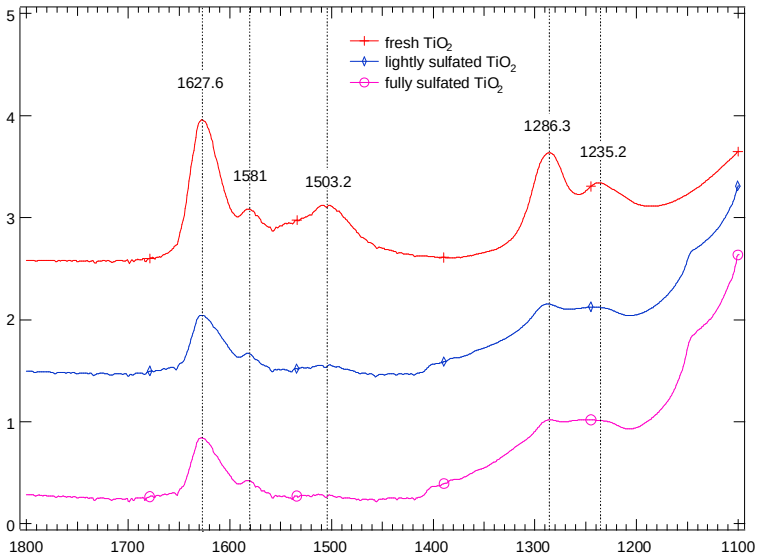

Figure 61 NO adsorption comparison on TiO_2 with various sulfation degrees (TiOA)

Similar tendency was observed for NO adsorption on TiO2 (Figure 61) with various sulfation degrees. As the sulfate species content increases, NO adsorption intensity decreases.

II.C.9. At different temperatures

Figure 62 illustrates the effect of temperature on NO adsorption of fresh 1% V2O5/TiO2. During the test, the NO adsorption peaks at 1626.7, 1582.3, and 1286.3 cm-1 gradually

decreased when the temperature gradually increased from 25 to 380 ˚C. In the case of fresh 1% V2O5/TiO2, NO adsorption bands at 1623 and 1575 cm-1 disappeared from the IR spectrum at 300 ˚C, while no band 1285 cm-1 could be observed after the temperature reached 200 ˚C. The NO adsorption on the vanadia catalyst is stable till 300 ˚C further confirming the adsorption species formed on vanadia catalyst surface is nitrate.

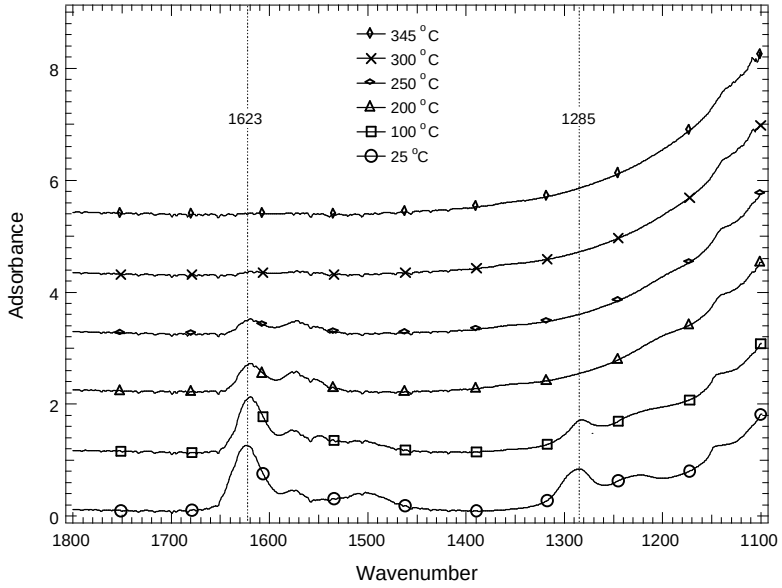

Figure 62 NO adsorption on fresh 1% V_2O_5/TiO_2 at different temperatures. (VTOL)

II.C.10. NO adsorption comparison between fresh and Contaminated samples

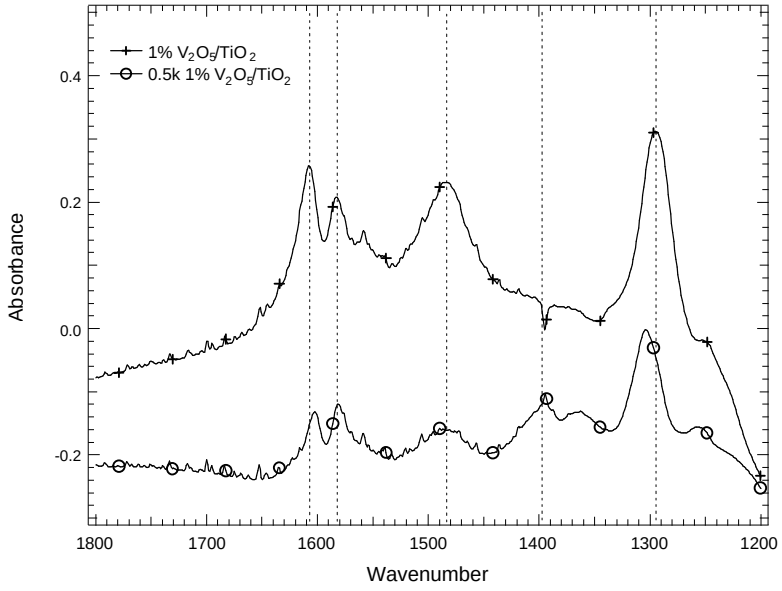

Figure 63 VWTA2

NO adsorption was also compared on fresh and potassium doped 1% vanadia catalyst. Apparently potassium on the vanadia catalyst surface weakens the NO adsorption, as shown in Figure 63.

II.D Mechanism interpretation

Figure64 shows the IR spectra were collected on pure TiO2, 1 and 2% V2O5/TiO2 catalyst wafers run in helium and O2 at room temperature after pretreatment. During the pretreatment, all the wafers were heated in 5% O2 and helium (balance) for 4 hours at 380 ˚C. Three major peaks on the spectra located at 3700-3600, 3550-3000, and ~1625 cm-1 appear in the spectra, which correspond to a free or non-bonded OH- stretch group (3700-3600 cm-1), an H-bonded OH- stretch group (3000-3500 cm-1), and an OH- bend group (~1625 cm-1) [45]. Quantitative comparisons of these spectra are difficult in this form. Integration of the peaks determines areas that indicate surface OH group concentration and that provide more meaningful quantitative results, as tabulated in Table 18. The surface OH- concentration decreases upon introduction of vanadia to the titania surface over the range of vanadia concentrations studied (0-2%). This agrees with the suggestion by Topsøe that vanadia interacts with OH- groups present on the titania surface.

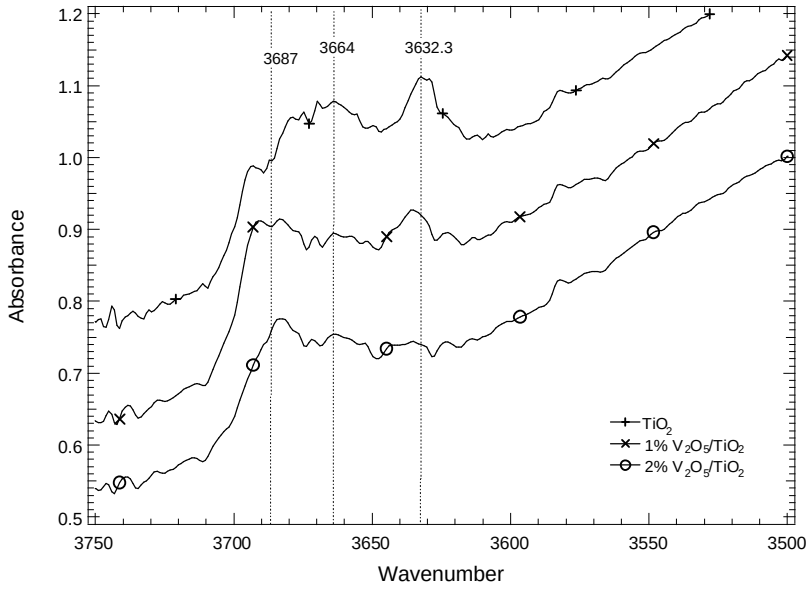

Figure64 Fresh catalyst comparison

Table 18 Surface OH^- group peak area comparison on fresh TiO_2 and vanadia catalysts

	3720-3600 cm^{-1}	3550-3000 cm^{-1}	~1625 cm^{-1}
	Free OH stretching	H bonded OH stretching	OH bending
Pure TiO_2	10.62	372.40	21.02
Fresh 1% V_2O_5/TiO_2	8.73	314.06	20.68
Fresh 2% V_2O_5/TiO_2	4.31	256.02	16.34

The effect of sulfation on OH- group concentration was also compared on titania surface, as shown in Figure 65. The OH adsorption peak almost disappeared on both lightly and 24 hour

sulfated TiO2, which indicates the sulfate species may occupy the surface hydroxyl group on the titania surface.

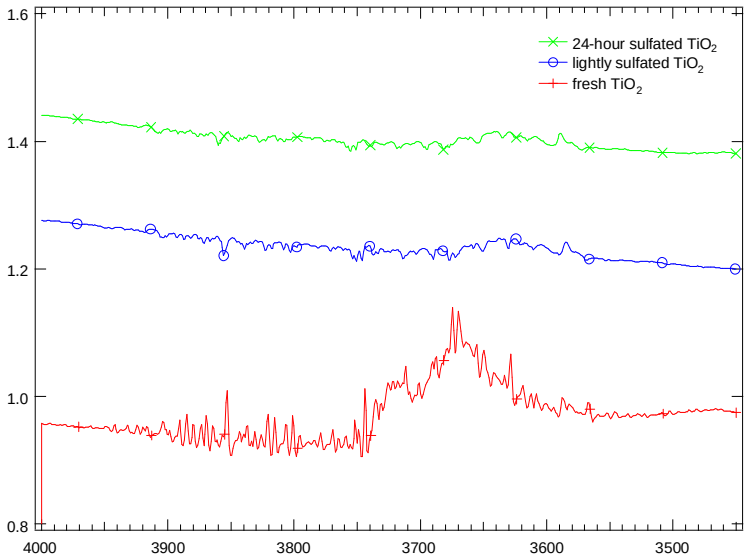

Figure 65 TiOA

Upon NO adsorption on TiO2, 1 and 2% V2O5/TiO2 catalyst, the band intensities of the free surface OH- stretch groups (3720 – 3600 cm-1) significantly decreased for all samples. The largest OH group loss appears on TiO2, which also possesses strongest NO adsorption. It seems the intensity of NO adsorption is proportional to the loss of OH group, which indicates that NO occupy surface OH group on both titania surface and vanadia catalysts. Since titania possess the most abundant OH group, therefore the NO adsorption is the strongest also.

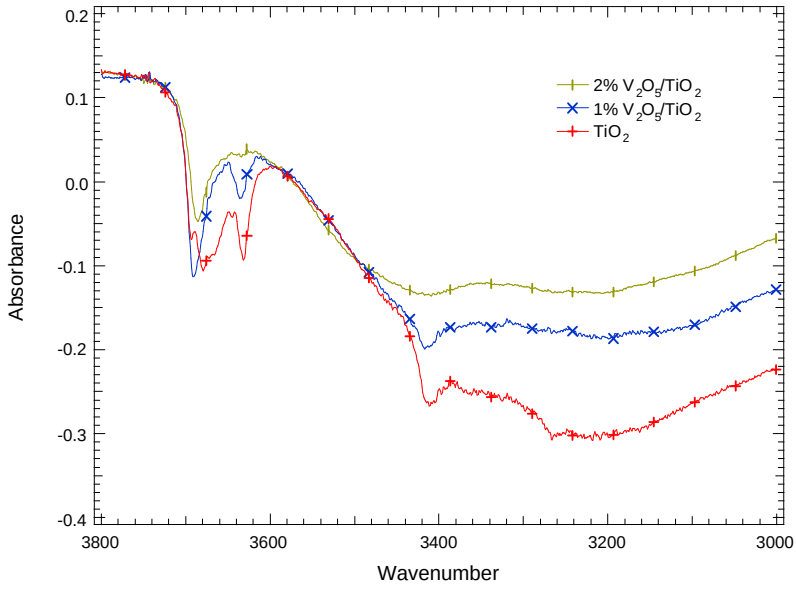

Figure 66 NO adsorption comparison

Therefore, both vanadia species and sulfate species occupy hydroxyl group on the titania surface, and NO adsorbs on titania and vandia catalyst surface through interaction with

surface OH group as well, besides, vanadia and sulfate species both inhibit NO adsorption. NO is one of the two reactant gases, vanaida provides the active sites, and sulfate species apparent increase the activity from the kinetic study. Therefore, all of the above three species, NO, V, and S are involve the SCR reaction, and they do not favor each other but inhibit each other. One explanation for the observation is that instead of vanadia species being the active center, the edge between the vanadia and titania could be the active center.

II.E BET analysis

BET surface area analyses for pore size distribution were conducted on three homemade samples: densified TiO2, 2% w/w V2O5/TiO2, and 5% w/w V2O5/TiO2. The results were shown in Table 19.

Table 19 BET surface area and pore size distribution

	Pure TiO_2	2% w/w V_2O_5/TiO_2	5% w/w V_2O_5/TiO_2
BET surface area	27.9	15.4 m^2/g	18.6 m^2/g
Surface area of pores	37.19 m^2/g	16.98 m^2/g	19.25 m^2/g
Mean pore size	39.30 nm	32.41 nm	26.61 nm

The mean pore size changes reasonably, it decreases with increasing vanadia content on the catalyst surface. This is due to pores filled or blocked with vanadia particles. However, the surface area of 2% w/w V_2O_5/TiO_2 is less than that of 5% w/w V_2O_5/TiO_2. This is in the same trend with the surface area of pores, where 5% w/w V_2O_5/TiO_2 has a larger pore area than that of 2% w/w V_2O_5/TiO_2. From the pore size distribution it is observed that small pores still exist on 5% w/w V_2O_5/TiO_2, where for 2% w/w V_2O_5/TiO_2, there are almost no small pores exits on this catalyst, thus it has smaller surface area.

II.F SCR kinetic study

II.F.1. Pore diffusion limitation

NO reduction was tested on 1% V2O5/TiO_2 at 18% conversion with temperatures of about 250 ˚C and a 30% conversion at temperatures of 300 ˚C. These conditions correspond to MTs of about 0.25 (250 ˚C) and 0.34 (300 ˚C), respectively. Both are smaller than 0.4. Therefore the pore diffusion effects can be neglected. These investigations follow.

II.F.2. Film diffusion limitation

Both calculation and experiment show that film diffusion can be neglected during SCR tests on 1% V_2O_5/TiO_2.

Film diffusion resistance is determined according to

$$K_c = \frac{1-\phi}{\phi}\left(\frac{D_{AB290}}{d_p}\right)Sh' \qquad (1)$$

ø = void fraction of packed bed

D_{AB} = gas-phase diffusivity, m^2/s

d_p = particle diameter, m

Sh' =Sherwood number

The calculated result indicates that the film resistance accounts for about 0.3% of the total resistance (combined resistance of film diffusion and kinetic resistance).

Experimentally, film diffusion investigations on SCR catalysts (1% V_2O_5/TiO_2) involved three different flow rates (93, 121, 187 ml/min). This range of space velocities in the catalyst provides significant variation in the boundary layer thickness along the catalyst surface and therefore should result in different conversions if film resistance plays a significant role in NO reduction. Similar NO conversions (17.6% at 93.3 ml/min, 18% at 121 ml/min, and 17.4% at 187ml/min at 250 ˚C) resulted from each experiment, consistent with the mathematical expectation of negligible impact of film resistance. Therefore, the following SCR reactions are investigated on 1% V_2O_5/TiO_2 catalysts with 700 ppm NH_3 and NO, 5% O_2, helium (balance) with a total flow rate of 187 ml/min at a temperature range of 250-350 ˚C, where both film diffusion and pore diffusion resistance can be neglected. This investigation involved catalyst reacting in the intrinsic kinetic range.

During NO reduction activity tests, the NO conversion is measured by comparing the changes of NO^{30}/Ar^{38} ratio of MS signal intensity before and after reaction. NO conversion increased with time, frustrating attempts to collect repeatable data. Improved normalization of the data with one of MS measurement parameters that measures background intensity improved the results.

II.F.3. Kinetic parameter calculation

Since NO reduction experiments did not involve film or pore diffusion, kinetic parameters depend directly on NO conversion based on following equation:

$$K = -\frac{Q_0}{W_{cat}} \ln(1 - X) \qquad (2)$$

K = reaction rate coefficient

Q_0 = total gas flow rate, ml/min

W_{cat} = catalyst weight

X = NO conversion

And also

$$K = A \exp\left(-\frac{E_a}{RT}\right) \qquad (3)$$

A = pre-exponential factor

E_a = activation energy

R = gas constant 8.314 J/mol·K

T = temperature, K

A matrix of reaction rate coefficient (K) values and temperatures result from measuring NO reduction as a function of temperature. Non-linear least-squares fits of these data determine the parameters A and E_a and their confidence intervals. **Fout! Verwijzingsbron niet**

gevonden. shows the estimated results of A and E_a for fresh, lightly sulfated, and fully sulfated samples.

II.F.4. Sulfation effect on 1% V C

In Figure 67, the indicated symbols represent measured NO conversion data from fully (24-hour exposure) sulfated, lightly sulfated, and fresh 1% V_2O_5/TiO_2 SCR catalysts. The solid lines represent the curve fits based on the non-linear least squares algorithm for each conversion data set. The upper and lower dotted lines indicate the 95% confidence interval for activity (K) at a given temperature. The results indicate that differences observed among the samples are statistically significant. Typically, sulfation increases intrinsic activity by about 40% in these tests. Furthermore, although K increases significantly upon catalyst sulfation, the activation energy E_a remains statistically unchanged for sulfated and non-sulfated samples, with E_a = 44921~52566 J/mol. The differences in the rate coefficient arise from the pre-exponential factor, A. Results of curve fitting show that sulfated samples have larger pre-exponential factors (A = 1716400 and 300888 cm^3/g s) than fresh samples (A = 182000 cm^3/g s). This is consistent with the *in situ* spectral results that indicate sulfation does not impact the vanadia grains on the catalyst. As indicated by the spectra, surface sulfation impacts the ammonia absorption on the surface, providing more opportunities for NH_3-NO interaction thus increase the interacting frequency, which is related to A.

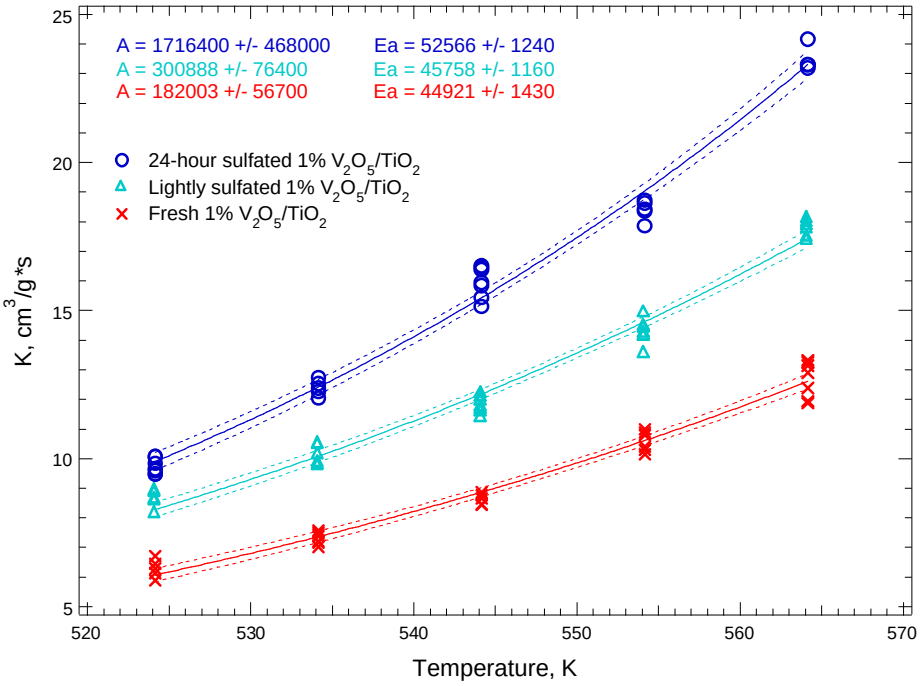

Figure 67 **Kinetic parameter (A, Ea) estimations with confidence intervals of fresh, lightly sulfated, and 24-hour sulfated 1% V_2O_5/TiO_2**

II.F.5. W effect on SCR kinetics

SCR of NO with NH_3 was also conducted on 1% V_2O_5 – 9%W/TiO_2, in order to keep the kinetic in the intrinsic regime, the reaction temperature was kept in a lower temperature range of 200-250 ˚C. The non-linear least squares fit results was compared in Figure 68. The 1% V_2O_5 – 9%W/TiO_2 catalyst exhibits about 3 times higher NO reduction activity than 1% V_2O_5/TiO_2, and possesses higher activity even than 24 hour sulfated 1% V_2O_5/TiO_2 catalyst by about 80%. Thus, tungsten appearance on the vanadia catalyst surface greatly increasees

the catalyst NO reduction ability. The enhancement, by comparing the analyzed results of A and Ea, is due to a larger A, the pre-exponential factor, which is an indication of the amount of active site. The activation energy, on the other hand, remains unchanged, indicating the reaction mechanism should remain the same. Therefore, the addition of tungsten to the vanadia catalyst increases the amount of active sites, with little impact on reaction mechanism, on the other hand, in situ IR spectra indicates that tungsten creates more Brønsted acid sites without change the acidity. The correlation between kinetic study and IR results suggests that Brønsted acid sites are the active sites on the catalyst surface.

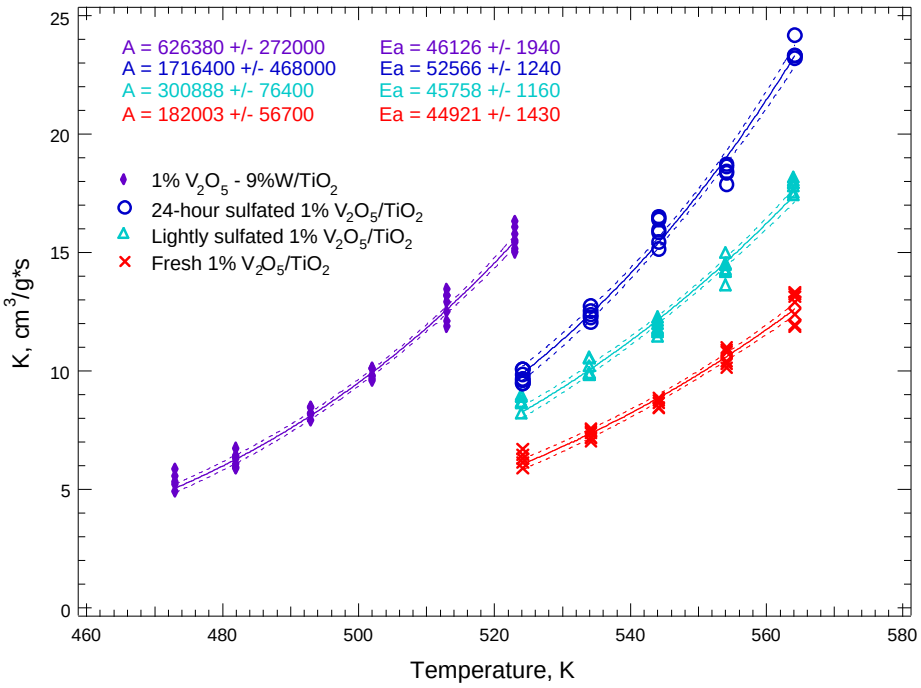

Figure 68 **Kinetic parameter (A, Ea) estimations with confidence intervals of fresh, lightly sulfated, and 24-hour sulfated 1% V_2O_5/TiO_2, and fresh** 1% V_2O_5 – 9%W/TiO_2

II.F.6. Potassium effect on NO reduction activity

SCR of NO with NH3 reaction activity was compared with two pairs of catalysts, 1% V2O5 – 9%W/TiO2 vs. 0.5 k doped 1% V2O5 – 9%W/TiO2 (Figure 69), and 1% V2O5/TiO2 vs. 0.5 k doped 1% V2O5/TiO2 (Figure 70).

The addition of potassium greatly decreases the NO reduction activity of both 1% V_2O_5 – 9%W/TiO_2 and 1% V_2O_5/TiO_2 catalysts. This decrease becomes more predominant when temperature rises higher. Comparing pre-exponential factor (A) and activation energy (E_a) before and after potassium addition, it is found that potassium introduction to the catalyst reduces values of both A and Ea, which explains why the kinetic constant decreases more intensely at high temperatures than low temperatures, because Ea was also affected, which has a exponential relationship with k (k= A*exp(-Ea/T)).

Smaller A and Ea after potassium doped onto the catalyst indicate that the amount of active sites was reduced, probably due to potassium occupied some of the active sites, and the acidity (active sites are acid sites) was also decreased as indicated by a smaller Ea. On the other hand, the IR spectra of ammonia adsorption on fresh and potassium doped vanadia catalyst illustrate that the addition of potassium decrease the ammonia adsorption intensities

on both Brønsted and Lewis acid sites, with a more predominant effect on Brønsted acid site. Therefore, the kinetic study agrees with the IR spectra investigation that potassium decreases the amount of active sites, which probably are the Brønsted acid sites.

At this point, all the kinetic studies, including fresh, sulfated, and poisoned vanadia catalyst and IR spectra investigation, agree with each other and suggest that Brønsted acid sites are the active sites, sulfate species and tungsten enhance the catalyst activity by the generation of more active sites – Brønsted acid sites without change the acidity, and potassium decrease the catalyst activity by decreasing the amount and acidity of Brønsted acid sites.

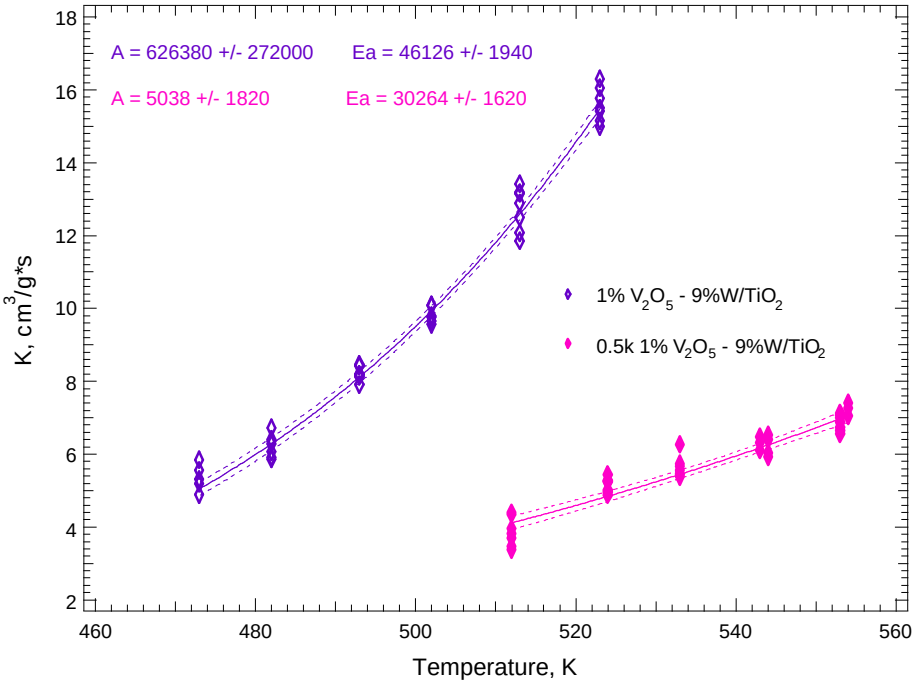

Figure 69 **Kinetic parameter (A, Ea) estimations with confidence intervals of fresh and 0.5 k doped** 1% V_2O_5 – 9%W/TiO_2

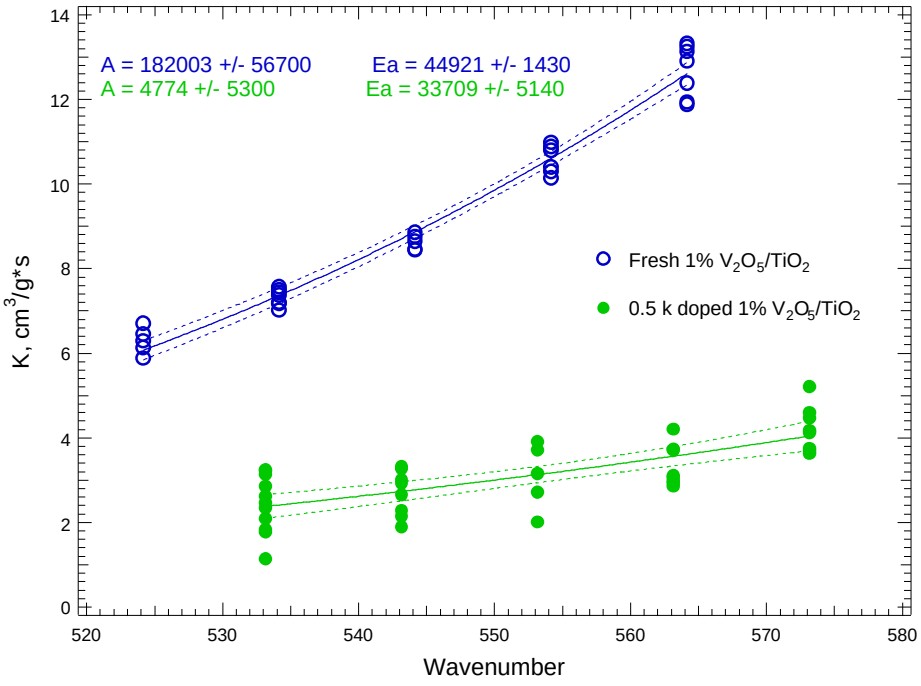

Figure 70 **Kinetic parameter (A, Ea) estimations with confidence intervals of fresh and 0.5 k doped** 1% V_2O_5 /TiO_2

Chapter 6: Conclusions

The primary conclusions from this work relative to SCR activity are as follows:

1. Brønsted acid sites appear to be the active centers for SCR activity
2. Sulfation of catalyst surfaces increases activity
3. Ammonia, NO and sulfation compete for the same sites on the catalyst surface.
4. Alkali and alkaline earth metals act as effective poisons when in intimate contact with the catalytic surface.
5. Tungsten and molybdenum, ostensibly added to catalysts to moderate conversion of SO2 to SO3, significantly decrease poisoning impacts of alkali metals.
6. Alkali metals in non-intimate contact with SCR surfaces, such as those undergoing dry deposition and residency, do not appear to significantly poison catalysts.
7. Based on field and laboratory tests, the most significant sources of catalyst deactivation during biomass-coal cofiring appear to be (in priority order) channel plugging, surface fouling, chemical poisoning, catalyst sintering. However, this conclusion is preliminary due to a lack of long-term exposure to high-alkali fly ash streams.

References

1. EPA, *Clean Air Markets-Progress and Results.* (2004).p.
2. DOE, N., *Selective Catalytic Reduction (SCR) Technology for the Control of Nitrogen Oxide Emissions from Coal-Fired Boilers*, in *Clean Coal Technoogy, Topical report number 23.* 2005 May.
3. Siemens, *PRB coal and high arsenic concentrations: catalyst specific issues and operating experience.* Workshop on selective catalytic reduction, (2000).p.
4. Pritchard, S., Kaneki, S., and Suyama, K., *Opitmizing SCR catalyst design and performance for coal-fired boilers.* report.
5. Busca, G., et al., *Chemical and mechanistic aspects of the selelctive catalytic reduction of NOx by ammonia over oxide catalysts: A Review.* Appl. Catal B: Environmental, 1-2: (1998).p. 1.
6. Bartholomew, R.J.F.a.C.H., *Fundamentals of industrial catalytic processes.* 1997: Blackie academic & professional.
7. Wachs, I.E., et al., *Selective catalytic reduction of NO with NH3 over supported vanadia catalysts.* Journal of Catalysis, 1: (1996).p. 211.
8. Forzatti, P., *Present status and perspective in de-NOx SCR analysis.* Appl. Catal A: General, (2001).p. 221.
9. Forzatii, P. and Lietti, L., *Recent Advances in De-NOxing Catalysis for Stationary Applications.* Heterogeneous Chemistry Reviews, (1996).p. 33.
10. Went, G.T., et al., *Raman-Spectroscopy and Thermal-Desorption of NH_3 Adsorbed on TiO_2 (Anatase)-Supported V_2O_5.* Journal of Physical Chemistry, 5: (1992).p. 2235.
11. Reddy, B.M., Ganesh, I., and Chowdhury, B., *Design of stable and reactive vanadium oxide catalyst supported on binary oxides.* Catal. Today, (1999).p. 115.
12. Topsoe, N.Y., Topsoe, H., and Dumesic, J.A., *Vanadia-Titania Catalysts for Selective Catalytic Reduction (Scr) of Nitric-Oxide by Ammonia .1. Combined Temperature-Programmed in-Situ Ftir and Online Mass-Spectroscopy Studies.* Journal of Catalysis, 1: (1995).p. 226.
13. Went, G.T., et al., *The Effects of Structure on the Catalytic Activity and Selectivity of V_2O_5/TiO_2 for the Reduction of NO by NH_3.* Journal of Catalysis, 2: (1992).p. 492.
14. Dunn, J.P., et al., *Oxidation of sulfur dioxide to sulfur trioxide over supported vanadia catalysts.* Appl. Catal. B-Environ., 2: (1998).p. 103.
15. Lietti, L., et al., *Chemical, structural and mechanistic aspects on NOx SCR over commercial and model oxide catalysts.* Catal. Today, 1-2: (1998).p. 101.
16. Lietti, L. and Forzatti, P., *Temperature-Programmed Desorption - Reaction of Ammonia over V2o5/Tio2 De-No(X)Ing Catalysts.* Journal of Catalysis, 1: (1994).p. 241.
17. Wachs, I.E. and Weckhuysen, B.M., *Structure and reactivity of surface vanadium oxide species on oxide supports.* Appl. Catal. A-Gen., 1-2: (1997).p. 67.
18. Ozkan, U.S., Kumthekar, M.W., and Cai, Y.P.P., *Selective Catalytic Reduction of Nitric-Oxide over Vanadia/Titania Catalysts - Temperature-Programmed Desorption and Isotopically Labeled Oxygen-Exchange Studies.* Industrial & Engineering Chemistry Research, 12: (1994).p. 2924.
19. Choo, S.T., et al., *Characteristics of V_2O_5 supported on sulfated TiO_2 for selective catalytic reduction of NO by NH_3*, in *Applied Catalysis A:General*. 2000, Elsevier Science B.V. p. 177.
20. Chen, J.P. and Yang, R.T., *Mechanism of Poisoning of the V_2O_5/TiO_2 Catalyst for the Reduction of NO by NH_3.* Journal of Catalysis, 2: (1990).p. 411.

21. Centeno, M.A., Carrizosa, I., and Odriozola, J.A., *NO-NH3 coadsorption on vanadia/titania catalysts: determination of the reduction degree of vanadium.* Appl. Catal. B-Environ., 4: (2001).p. 307.
22. Ozkan, U.S., Cai, Y., and Kumthekar, M.W., *Mechanistic studies of selective catalytic reduction of nitric oxide with ammonia over V₂O₅/TiO₂ (anatase) catalysts through transient isotopic labeling at steady state*, in *Journal of Physical Chemistry.* 1995, ACS,Washington,DC,USA. p. 2363.
23. Yang, R.T., Li, W.B., and Chen, N., *Reversible chemisorption of nitric oxide in the presence of oxygen on titania and titania modified with surface sulfate.* Appl. Catal. A-Gen., 2: (1998).p. 215.
24. Amiridis, M.D., et al., *Reactivity of V_2O_5 catalysts for the selective catalytic reduction of NO by NH_3: Influence of vanadia loading, H_2O, and SO_2.* Journal of Catalysis, 1: (1996).p. 247.
25. Khodayari, R. and Odenbrand, C.U.I., *Regeneration of commercial SCR catalysts by washing and sulphation: effect of sulphate groups on the activity.* Appl. Catal. B-Environ., 4: (2001).p. 277.
26. Topsoe, N.Y., *Characterization of the Nature of Surface Sites on Vanadia Titania Catalysts by Ftir.* Journal of Catalysis, 2: (1991).p. 499.
27. Srnak, T.Z., et al., *Temperature-Programmed Desorption Reaction and Insitu Spectroscopic Studies of Vanadia Titania for Catalytic Reduction of Nitric-Oxide.* Journal of Catalysis, 1: (1992).p. 246.
28. Topsoe, N.Y. and T.Z. Srnak, J.A.D., B.S. Clausen, E. Tornqvist, *Temperature-Programmed Desorption/Reaction and in Situ Spectruscopic Studies of Vanadia/Titania for Catalytic Reduction of Nitric Oxide.* J. Catal., (1992).p. 246.
29. Lisi, L., et al., *Single and combined deactivating effect of alkali metals and HCl on commercial SCR catalysts.* Appl. Catal. B-Environ., 4: (2004).p. 251.
30. Ramis, G., et al., *Fourier transform-infrared study of the adsorption and coadsorption of nitric oxide, nitrogen dioxide and ammonia on vanadia-titania and mechanism of selective catalytic reduction.* Applied Catalysis, 1-2 Sep: (1990).p. 259.
31. Hadjiivanov, K., *Indentification of neutral and charged N_xO_y surface species by IR spectroscopy.* Catal. Rev.-SCI.ENG., 1&2: (2000).p. 71.
32. Topsoe, N.Y., Dumesic, J.A., and Topsoe, H., *Vanadia-Titania Catalysts for Selective Catalytic Reduction of Nitric-Oxide by Ammonia .2. Studies of Active-Sites and Formulation of Catalytic Cycles.* Journal of Catalysis, 1: (1995).p. 241.
33. Chen, J.P. and Yang, R.T., *Selective catalytic reduction of NO with NH_3 on SO_4^{-2}/TiO_2 superacid catalyst.* Journal of Catalysis, (1993).p. 277.
34. Orsenigo, C., et al., *Dynamic Investigation of the Role of the Surface Sulfates in NOX Reduction and SO2 Oxidation over V2O5-WO3/TiO2 Catalysts.* Ind. Eng. Chem. Res., (1998).p. 2350.
35. Dunn, J.P., et al., *Interactions between surface vanadate and surface sulfate species on metal oxide catalysts.* Journal of Physical Chemistry B, 32 Aug 6: (1998).p. 6212.
36. Zheng, Y.J., Jensen, A.D., and Johnsson, J.E., *Laboratory investigation of selective catalytic reduction catalysts: Deactivation by potassium compounds and catalyst regeneration.* Industrial & Engineering Chemistry Research, 4: (2004).p. 941.
37. Chen, J.P., et al., *Deactivation of the vanadia catalyst in the selective catalytic reduction process.* Journal of the Air & Waste Management Association, 10 Oct: (1990).p. 1403.

38. Tokarz, M.J., S.; Persson, B. Eka Nobel AB, Surte, Swed., *Poisoning of de-NOx SCR catalyst by flue gases from a waste incineration plant.* Studies in Surface Science and Catalysis, Catal. Deact. 1991: (1991).p. 523.
39. Stuart, B.J. and Kosson, D.S., *Characterization of Municipal Waste Combustion Air-Pollution Control Residues as a Function of Particle-Size.* Combustion Science and Technology, 1-6: (1994).p. 527.
40. Khodayari, R. and Odenbrand, C.U.I., *Deactivating effects of lead on the selective catalytic reduction of nitric oxide with ammonia over a V2O5/WO3/TiO2 catalyst for waste incineration applications.* Industrial & Engineering Chemistry Research, 4: (1998).p. 1196.
41. Lin, W.Y. and Biswas, P., *Metallic Particle Formation and Growth Dynamics During Incineration.* Combustion Science and Technology, 1-6: (1994).p. 29.
42. Franklin, H.N., *The effect of fuel properties and characteristics on selective catalytic reduction systems.* ASME International Joint Power Generation Conference, (1996).p.
43. O. Saur, M.B., A.B. Mohammed Saad, J.C. Lavalley, Carl P. Tripp, B.A. Morrow, *The Structure and Stability of Sulfated Alumina and Titania.* Journal of Catalysis, (1986).p. 104.
44. Ramis, G. and Busca, G., *Fourier Transform Infrared Study of the Adsorption and Coadsorption of Nitric oxide, Nitrogen Dioxide and Ammonia on TiO_2 anatase.* Appl. Catal, (1990).p. 243.
45. Coates, J., *Interpretation of infrared spectra, a practical approach.* Encyclopedia of analytical chemistry, (2000).p. 10815.

Appendix

I BYU monolith catalyst preparation procedure

Brigham Young University prepared the M4 catalyst where the active catalyst has been wash-coated onto a cordierite monolith support.

The primary obstacle in preparation of the wash-coated monolithic involved development of robust surfaces. Aqueous slurries of titania crack as they dry, resulting in thin films that do not adhere to the monolith. After many consultations with experts and a search of the literature, a combination of additives and procedures produced a stable titania washcoat suitable for the basis of an SCR catalyst.

I.A.1. Materials

The following raw materials were used in the preparation of the BYU SCR catalyst.

Monolith

1 19 pieces of cordierite monolith each approximately 2 1/8" x 2 1/8" x 6", containing ¼" square channels

Ingredients used in Titania washcoat

1 P25 Titania from Degussa
2 Ludox® AS-40 colloidal silica from Grace Davison
3 Certified A.C.S Barium Nitrate (crystal)
4 Reagent Grade Sulfuric Acid

Ingredients used during Impregnation of Active Metals

1 Laboratory Grade Ammonium Metavanadate
2 Anhydrous Crystal, Reagent Oxalic Acid
3 AMT-1 Grade Ammonium Metatungstate

I.A.2. Procedure

The monolith pieces were immersed in an aqueous 1 M nitric acid solution for 30 min at 80 °C.

The acid bath roughens the surface of the cordierite and improves washcoat adhesion. Following the acid treatment, the monolith pieces were rinsed with distilled water and dried at 120 °C overnight.

The P25 Titania from Degussa was treated with a densification procedure similar to the one of Baiker et al. The titania was mixed with distilled water at a ratio of 1:1.75 by weight. The paste that was produced was dried at 120 °C for 24 hours. After drying, the titanium dioxide

was crushed with a mortar and pestle. The crushed titanium dioxide was calcined at 600 °C for 4h.

The calcined titanium dioxide was then mixed with distilled water at a 1:1 ratio by weight and poured into a ball mill. The resulting slurry was ball milled at 45 rpm for 90 min. The ball-milled slurry product had a bimodal particle size distribution with major peaks at 2 microns and 20 microns. This particle sizing produces a tough, non-cracking coating.

Ludox® AS-40 was added to the ball milled slurry. Ludox® AS-40 contains 40 weight percent silica. Enough of this colloidal silica was added to create a 9:1 ratio of titanium dioxide to silica by weight.

Barium sulfate can be added to the SCR catalyst support as a binder according to U.S. Patent 4,975,256.

Enough barium nitrate was dissolved into the balled-milled titania slurry that the resulting ratio of barium sulfate to titanium dioxide will be 1:9 by weight. Reagent-grade sulfuric acid was then added at 5% excess to precipitate virtually all of the barium, to barium sulfate.

The resulting slurry was thinned with a small amount of distilled water so that the dry coating would account for 20% of the total mass of the coated monolith. The monolith pieces were dipped in the titania slurry and compressed air was used to blow out the passages of the monolith. The coated monoliths were then dried for 15 hours at 120 °C followed by calcining at 600°C for 4 hours. Table 20 below shows the change in mass due to the addition of the titania washcoat.

Table 20 Monolith and Washcoat Weights

	Monolith alone (g)	with TiO2 coat (g)	wt% TiO2
	191	231	17.3%
	193	238	18.9%
	193	245	21.2%
	195	247	21.1%
	197	248	20.6%
	198	251	21.1%
	200	255	21.6%
	201	255	21.2%
	203	263	22.8%
	203	263	22.8%
	205	264	22.3%
	205	265	22.6%
	207	268	22.8%
	208	271	23.2%
	211	275	23.3%
	213	275	22.5%
	218	282	22.7%
	220	289	23.9%
	224	294	23.8%
Average	204.47	262.05	21.9%
Standard deviation	9.5	16.8	1.7%

The pore volume of the coated monoliths needs to be known before an appropriate impregnation solution can be prepared. The coated monolith pieces were dipped into distilled water. The excess water was blown off with compressed air, and the monolith pieces were weighed to determine the water uptake. On average, a coated monolith piece had an uptake of 45 grams of water.

The desired amount of active metal for one monolith piece needs to be dissolved in 45 mL of solution. The impregnation solution was prepared by dissolving the ammonium metavanadate and oxalic acid in warm water, dissolving the ammonium metatungstate in the solution, and finally adding enough water to dilute to the desired concentration.

After the impregnation solution was prepared, each titania-coated piece of monolith was immersed in the solution, the excess was blown off with compressed air. The impregnated monoliths were then dried at 120° for 15 hours followed by calcination at 550° for 5 hours.

Table 21 below shows the weights and approximate composition of the catalyst.

Table 21 Weight and composition of final catalyst

	monolith (g)	w/ TiO_2 coat (g)	wt% TiO_2	w/ W and V	wt% W & V wrt Ti
	191	231	17.3%	235	12.5%
	193	238	18.9%	241	8.3%
	193	245	21.2%	250	12.0%
	195	247	21.1%	251	9.6%
	197	248	20.6%	252	9.8%
	198	251	21.1%	255	9.4%
	200	255	21.6%	261	13.6%
	201	255	21.2%	260	11.6%
	203	263	22.8%	268	10.4%
	203	263	22.8%	268	10.4%
	205	264	22.3%	269	10.6%
	205	265	22.6%	269	8.3%
	207	268	22.8%	273	10.2%
	208	271	23.2%	276	9.9%
	211	275	23.3%	279	7.8%
	213	275	22.5%	280	10.1%
	218	282	22.7%	288	11.7%
	220	289	23.9%	295	10.9%
	224	294	23.8%	299	8.9%
average	204.4736842	262.0526316	21.9%	267	10.3%
standard deviation	9.5	16.8	1.7%	17.3	1.5%

This procedure yields a suitable V2O5/WO3/TiO2 catalyst washcoated on a cordierite monolith.

II CCS Test Runs

It was decided that the test conditions of the monolith and plate samples would be at a flow rate of 1000 sccm comprised of 2% O2, 10 % H2O, 900 ppm NH3, 900 ppm NO, and the balance He over the temperature range 250 0C to 325 0C. Flow conditions and temperature

range were chosen as such to be similar to research from literature (Chen). This temperature range was also selected so that NO conversion, and thus activity could be adequately compared. Higher temperatures would cause conversion to be too high to be comparable, and would likely cause the catalyst activity to be controlled more by bulk flow diffusion rather than kinetic activity of the catalyst.

SO_2 was not used for these tests to avoid side reactions and salt formation (ammonium sulfate). SO_2 was used in a preliminary run, which resulted in a white layer forming along much of the tubing and in the reactor chambers.

To ensure that the equipment or materials of the MTR itself would not initiate reactions on it's own under these conditions, a run was conducted with an empty MTR. The results from this run show that the concentration of NO from the reactor outlet didn't change with temperature, indicating that no NO conversion took place (Table 22).

Table 22 Results from Empty Reactor.

Temperature (^{0}C)	NO (ppm)
257	971
282	971
310	969
331	966

Test samples from M1 and M2 were wrapped in insulation around the sides, but not covering the ends and placed in the MTR aluminum inserts before placing in samples the MTR (Figure 71). This forced all the gas to flow through the four channels and prevented gas from flowing around the sample. M3 samples were set in the aluminum insert and put into the MTR. P1 and P2 samples were run by setting one plate sample vertically in the middle grooves of the aluminum insert.

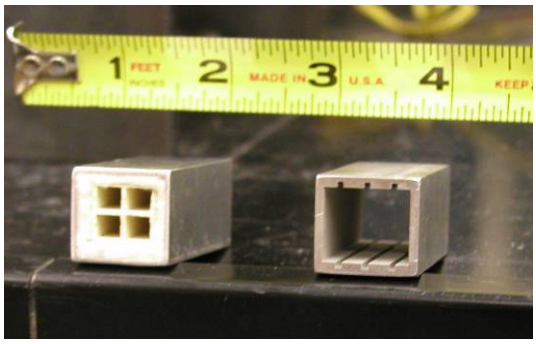

Figure 71 Monolith piece inside sample holder (left) and empty slotted plate catalyst sample holder (right).

A sample run procedure was as follows. First the MTR inside temperature was set to a temperature within the range of 250 to 325 0C and flow conditions were set as stated above.

The reactor outlet was sent to the analytical train and data was recorded. The system was left at these conditions for at least two and a half hours, which allowed the system to reach near steady state. The feed stream was then sampled and recorded. Then the temperature was changed and set at a new temperature within the range, and the reactor outlet stream was again sampled and recorded. For this second temperature and subsequent temperatures, the system was left for 40 minutes, which allowed the system to reach near steady state. The sample was tested at approximately 250, 275, 300, and 325 °C. In each run, a different order of temperatures was used.

The term near steady state is used, because although steady state was probably never quite reached, each run came close enough to retrieve useful data. Steady state was nearly impossible to reach due to the fact that the temperature is adjusted and set by manually controlling the variable power transformer. Tests were run to insure that our data would be useful, and taken at near enough to steady state conditions. Figure 72 shows data from a run in which the temperature was set at about 325 °C, then 300 °C, then 275 °C, then 250 °C and finally 225 °C. The areas where the NH_3 and NO levels spike are where sample stream was switch from the outlet to the feed and then back to the outlet. As seen, when different temperatures were set, the temperature, NH_3 and NO levels never flattened out. However, the data was analyzed to show that although NO level was changing, it was changing consistently with the change in temperature. Figure 73 indicates that for the second through fifth temperature change, the NO Conversion reaches the same curve (curve drawn as best fit second order polynomial) as the results (data taken at least 40 minutes after temperature change) after 15 to 20 minutes. For runs, data is taken after at least 40 minutes for every change after the first to be sure that this near steady state condition is reached. Figure 74 indicates that for the first step, this curve is reached two hours after the run started. These analyses were verified by running the same sample on three separate days, varying the order of the temperatures. Figure 75 indicates that the data is reproducible.

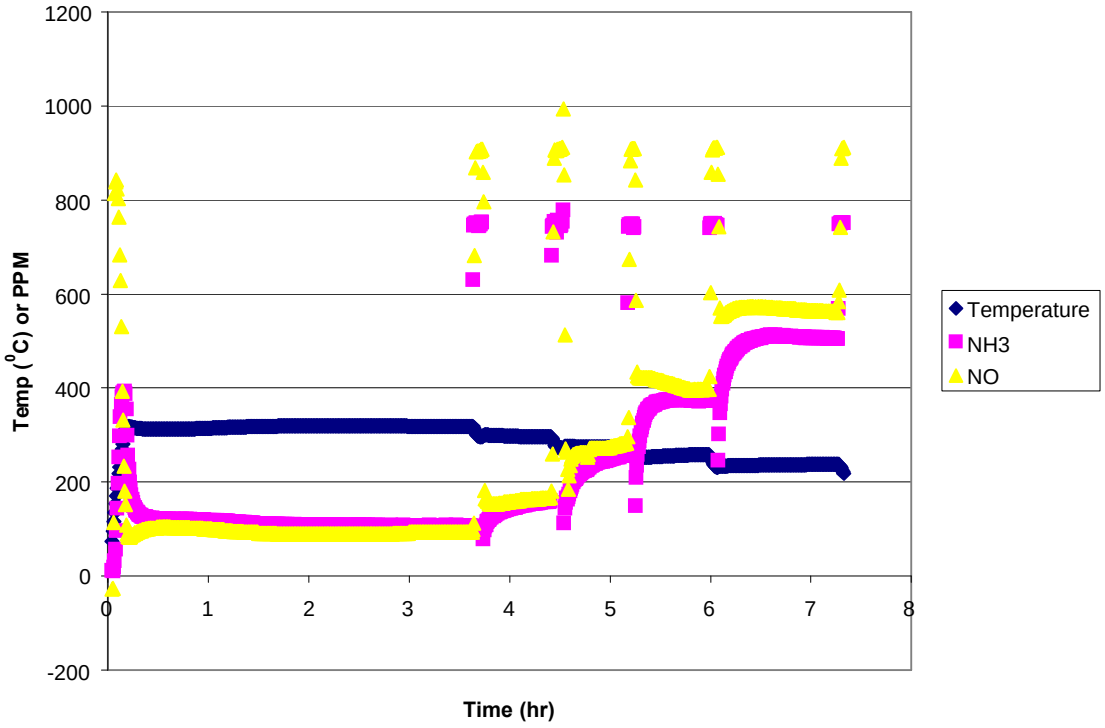

Figure 72 **Data From a Run that Shows Near Steady State Conditions**

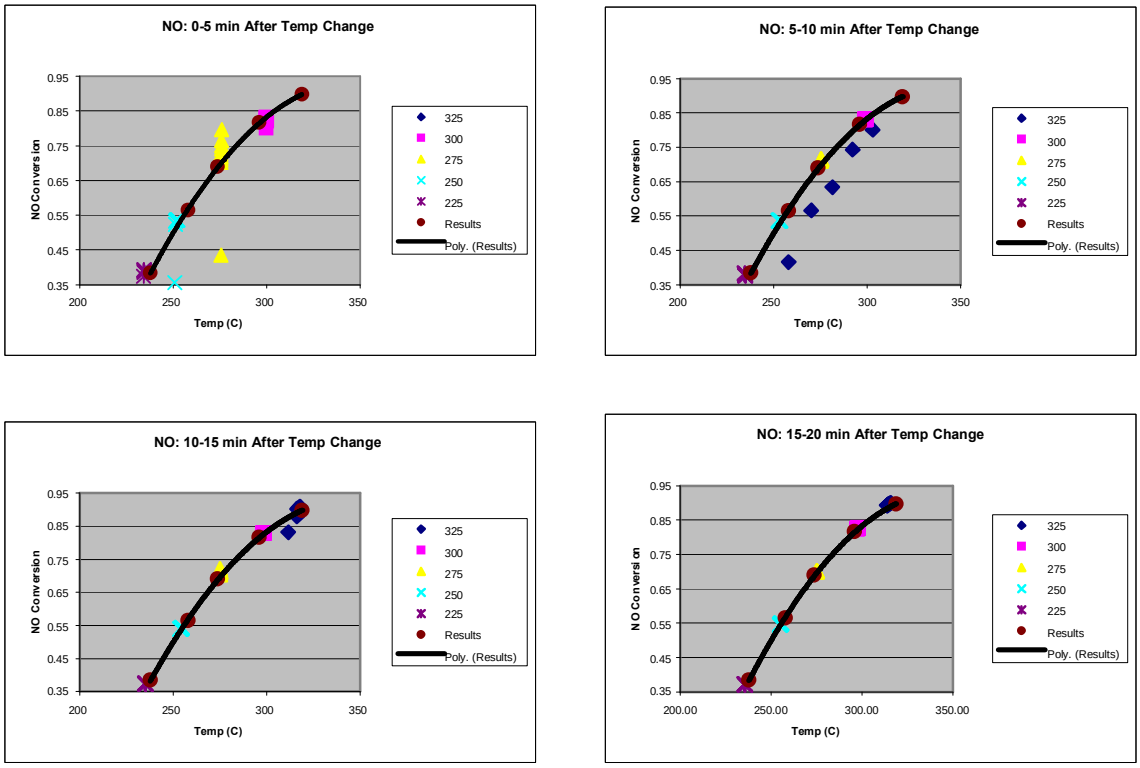

Figure 73 **Graphs Showing NO Conversion Changing with Respect to Amount of Time After Temperature Change.**

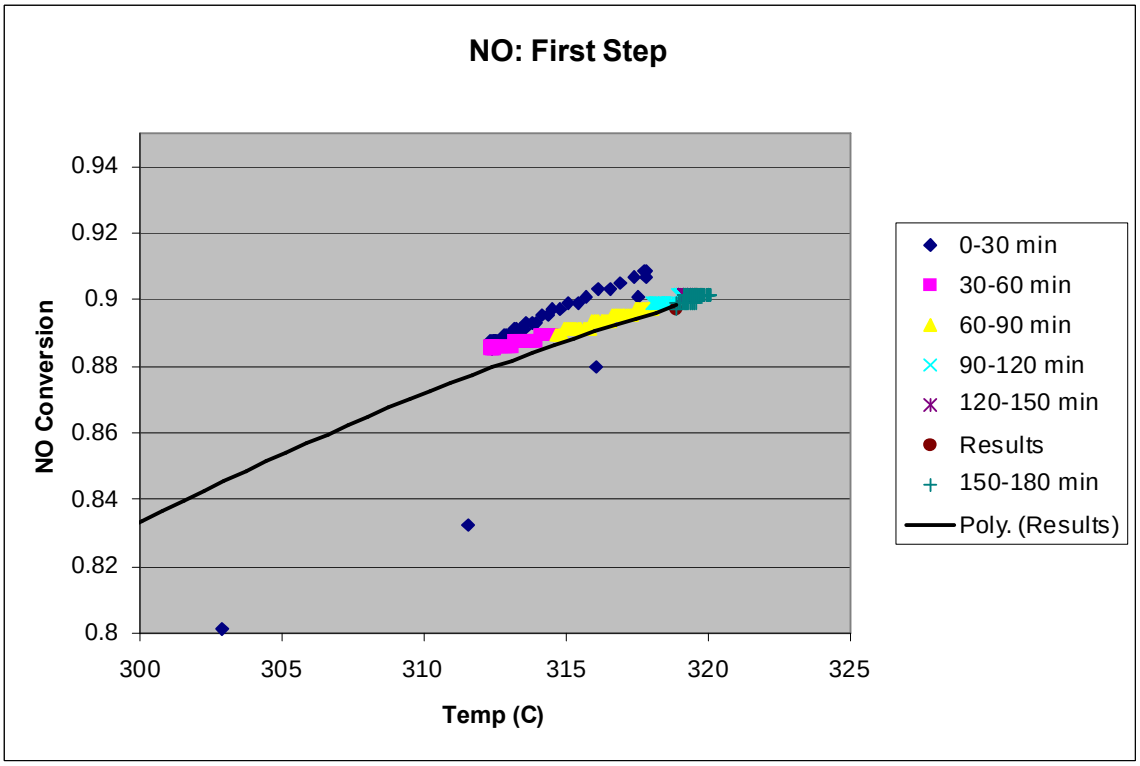

Figure 74 **Graph Showing NO Conversion Changing with Respect to Result Curve for the First Temperature of the Run.**

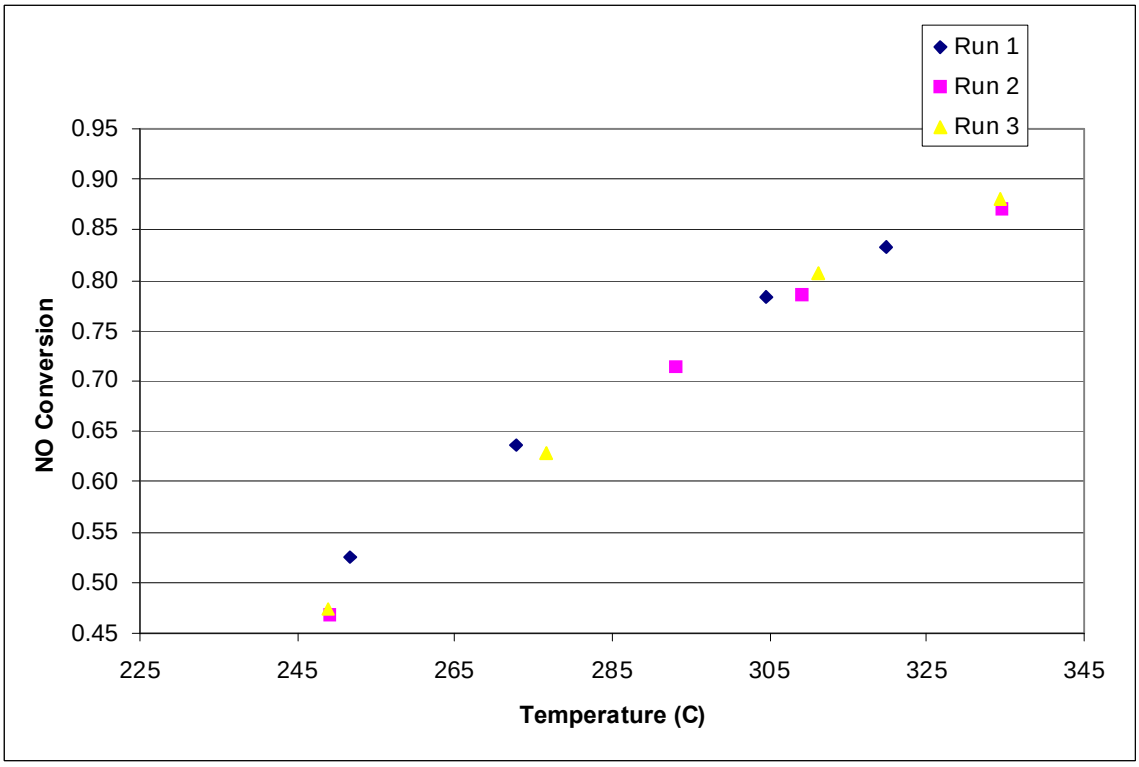

Figure 75 **NO Conversion Calculated from Data for Three Separate Runs on the Same Sample (M1 Fresh b)**

III Derivation of the Chen model

Figure 76 schematically illustrates a two-dimensional reactor in which a reactant from the bulk flow is transported to a porous wall containing catalyst. The dimension in the direction of flow is z and the dimension perpendicular to the low is x. The origin is taken from the reactor entrance at the center of the porous catalyst. If we assume Fickian diffusion, that the catalyst is isothermal and homogeneous and that the surface reaction is first order in reactant, that the flux in the flow direction is negligible compared to the flux in the direction perpendicular to the flow, and that bulk diffusion does not influence the conversion rate, then the flux at any point in the catalyst can be equated to the rate of reaction in the catalyst as follows, where the dependence of the mole fraction of reactant on both coordinate directions is emphasized.

$$cD_e \frac{d^2 y}{dx^2} = h^2 k a c\, y(x,z)$$

where c represents gas concentration, De represents the diffusivity of the reactant in the porous media, and a represents a time-dependent and dimensionless activity factor, defined as the ratio of the chemical activity in the catalyst at arbitrary time divided by its initial value. The value of a generally decreases from unity with chemical deactivation but could exceed unity because of catalyst activity increases caused, for example, by catalyst sulfation.

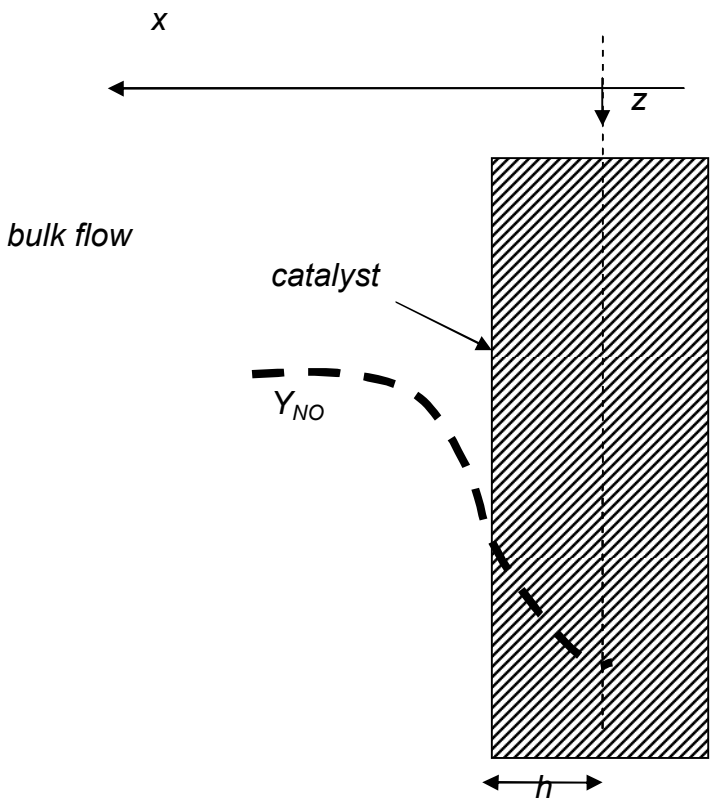

Figure 76 Schematic diagram of a two-dimensional reactor.

This equation can be written in dimensionless form as follows:

$$\frac{d^2y'}{dx'^2} = \frac{h^2kay'}{D_e}$$

where

$$x' = \frac{x}{h}$$

and

$$y' = \frac{y_{NO}}{y_{NO}^{\infty}}$$

are based on the half-thickness of the wall (h) and the bulk mole fraction in the cell (y∞NO). The boundary conditions are:

$$y'\Big|_{x'=0} = 1 + Bi^{-1}\frac{dy'}{dx'}$$

$$\left.\frac{dy'}{dx'}\right|_{x'=1} = 0$$

The solution gives the concentration profile within the wall:

$$y' = \frac{e^{\phi(x'-2)} + e^{-\phi x'}}{1 - e^{-2\phi} - \frac{\phi}{Bi}\left(e^{-2\phi} - 1\right)}$$

where

$$\phi^2 = \frac{h^2 ka}{D_e}$$

and

$$Bi = \frac{k_m h}{D_e}$$

This equation describes the relative impacts of film mass transfer, pore diffusion and surface reaction on conversion.

Considering the reactor, the mass balance along the axial direction of the reactor, z, is:

$$\frac{dy_{NO}^{\infty}}{dz} + \frac{k_m \sigma}{uA}\left(y_{NO}^{\infty} - y_{NO}^{s}\right) = 0$$

where u is the linear gas velocity in the cell which is assumed to be constant, □ is the perimeter length of a cell in the monolith and A is the cross-sectional area of a cell. The boundary condition is:

$$y_{NO}^{\infty}\Big|_{z=0} = y_{NO}^{\infty,0}$$

and the bulk and surface NO concentrations are related by:

$$y_{NO}^{\infty} = y_{NO}^{s}\left(1 - \frac{\phi}{Bi}\frac{e^{-2\phi} - 1}{e^{-2\phi} + 1}\right)$$

The overall conversion, X, of NO in the reactor at axial position L is given by:

$$X = \frac{y_{NO}^{\infty,0} - y_{NO}^{NO,L}}{y_{NO}^{\infty,0}}$$

Combining these results, the NO conversion is given by:

$$X = 1 - \exp\left[-\frac{\sigma L}{uA\left(\frac{1}{k_m} - \frac{1}{\sqrt{D_e ka}}\frac{e^{-2\phi} + 1}{e^{-2\phi} - 1}\right)}\right]$$